

THESIS
2
2101

This is to certify that the

dissertation entitled

**Design, Synthesis and Catalytic Applications
of Mesoporous Silica Molecular Sieves**

presented by

Wenzhong Zhang

has been accepted towards fulfillment
of the requirements for

Ph.D. degree in Chemistry


Major professor

Date 5/7/99

**LIBRARY
Michigan State
University**

PLACE IN RETURN BOX to remove this checkout from your record.
TO AVOID FINES return on or before date due.
MAY BE RECALLED with earlier due date if requested.

DATE DUE	DATE DUE	DATE DUE

**DESIGN, SYNTHESIS AND CATALYTIC APPLICATIONS OF
MESOPOROUS SILICA MOLECULAR SIEVES**

BY

Wenzhong Zhang

A DISSERTATION

**Submitted to
Michigan State University
In partial fulfillment of the requirements
For the degree of**

DOCTOR OF PHILOSOPHY

Department of Chemistry

1999

DESIGN, S
MI

The disc
stimulated great
mesopores in the
of large substrate
much larger pore
sites in the frac
reactions. Hexag
pore-connectivity
pore branching.
and scientifically
catalytic sites in
in mesostructure
and shape of the
promising strateg
specific pore con
formation and hy

In additio
extremely importa

ABSTRACT

DESIGN, SYNTHESIS AND CATALYTIC APPLICATIONS OF MESOPOROUS SILICA MOLECULAR SIEVES

BY

Wenzhong Zhang

The discovery of the Mobil M41S family of mesoporous molecular sieves has stimulated great interest in surfactant-directed assembly of inorganic mesostructures. The mesopores in these molecular sieves provide new opportunities for catalytic conversion of large substrates in the liquid phase. Even though mesoporous molecular sieves exhibit much larger pore sizes than conventional zeolites, accessibility to the catalytically active sites in the framework of the mesopores is still very crucial for diffusion limited reactions. Hexagonal and cubic mesostructures with uni-dimensional and 3-dimensional pore-connectivity, respectively, show similar catalytic reactivities, despite differences in pore branching, most likely both are diffusion limited. Therefore, it is practically useful and scientifically significant to find some ways to improve the accessibility to the active catalytic sites inside the mesopores. Regardless of the type of inorganic precursors used in mesostructure synthesis, the pore size and connectivity of the framework take the size and shape of the surfactant micelles filling in the structural channels. Therefore, an promising strategy for the design and synthesis of mesoporous molecular sieves with specific pore connectivity and accessibility would be to control the surfactant micelle formation and hydrolysis of the inorganic precursors.

In addition to framework mesopores, complementary textural mesopores are extremely important for enhancing the accessibility in catalysis. Our first objective was to

tailor both t

electrically

polarity, also

nucleation r

faster hydro

led to meso-

was to use o

tailor the f

exhibiting a

the flaky sur

meso-scaled

the comple

accessibility

peroxidation

the catalysts.

using Al-sub

enhanced cat

complementa

the pore chan

Variat

and concentra

altering the as

surfactant head

tailor both the framework and the textural porosity of HMS silicas assembled through an electrically neutral $S^{\circ}T^{\circ}$ mechanism. The approach involved control of the solvent polarity, along with the use of organic auxiliary agent (i.e. mesitylene) to control particle nucleation rates and pore size. Increasing the polarity of the synthesis medium caused faster hydrolysis of silicon alkoxide in the presence of the alkyl amine surfactant, which led to meso-scaled fundamental particles and high textural porosity. Our second objective was to use organic assembly modifiers such as tartaric, oxalic, gluconic and citric acids to tailor the formation of MCM-41 through a S^+T pathway. Well-ordered MCM-41 exhibiting a flake-shaped particle morphology with pore channels running orthogonal to the flaky surface was obtained. Also, MCM-41 with textural pores in association with meso-scaled fundamental particles was prepared under careful control. The importance of the complementary meso-scaled inter-particle (textural) pores for improving the accessibility of the framework pores in catalysis was demonstrated for the liquid phase peroxidation of 2,6-di-tert-butyl phenol in the presence of Ti-substituted derivatives as the catalysts. Also, liquid phase alkylation of 2,4-di-tert-butyl phenol was carried out using Al-substituted derivatives as the catalysts. By facilitating accessibility, significantly enhanced catalytic activity was observed for both Al-HMS and Al-MCM-41 with complementary textural mesopores and meso-scaled fundamental particles comparable to the pore channel lengths.

Variation of surfactant packing parameter $g (= V/a_0l)$ by changing the structure and concentration of surfactant has been reported in literature as an effective approach to altering the assembled mesostructures. Little is known about chemical modification of surfactant head group using simple chemicals rather than co-surfactants to ultimately

tailor the r

molecular

successful

dimensional

hydrotherm

ammonium

relatively

incorporati

introductio

micelles a

Mesoporous

dimensional

hexagonal

polyethylen

mediated

mesostruct

hydroxyl c

polyethylen

surfactant

group-area

mesostruct

tailor the molecular sieves. The concept of altering the structures of mesoporous silica molecular sieves by organic promoters in electrostatic S⁺T assembly has been successfully illustrated. Mesoporous silica molecular sieves with well ordered 3-dimensional hexagonal, cubic, and uni-dimensional hexagonal phases were hydrothermally assembled in the presence of organic modifiers using cetyltrimethyl ammonium bromide as the structure director and sodium silicate as the silicon source at a relatively low surfactant to silicon ratio (i.e. 0.11). In addition, the concept of incorporating structural order into mesoporous silica molecular sieves through the introduction of electrostatic interactions at the interfaces of electrically neutral surfactant micelles and neutral inorganic precursors has also been successfully demonstrated. Mesoporous silica molecular sieves with well ordered hybrid domains consisted of 3-dimensional hexagonal and spherical cubic (3-d-hex-cubic) phases, an uni-dimensional hexagonal phase, and wormhole structural motifs were assembled using alkyl polyethylene oxide surfactants and tetraethyl orthosilicate through a new counterion mediated (N^oM⁺X⁻)I^o pathway. Our approach explicitly illustrates that silica mesostructures can be altered using both organic and inorganic modifiers such as hydroxyl carboxylic acids for quaternary ammonium surfactant and metal salts for alkyl polyethylene oxide surfactants, respectively. The modifiers most likely bind to the surfactant head group to cause a significant change in the effective-surfactant-head-group-area, which alters the packing parameter g and, ultimately, the inorganic mesostructure.

To my grandparent and parants, my wife and my son.

I w
support and
seriousness
example for
over the ye
J.F. Harris
committee.

I am
the kindness
Wang, Dr. Y
Pauly for the

I am
obtain XAN
assistance fro
and SEM ima

My de
patience for y
son, Dejjia, w
than play with

ACKNOWLEDGMENT

I would like to thank Professor Thomas J. Pinnavaia for his continuously solid support and invaluable advice over the years in both sciences and life. His attitude and seriousness toward the pursuing of the truth and beauty of chemistry set a perfect example for me. I strongly believe that I will greatly benefit from my experiences gained over the years in his lab. I would also like to thank Professor M.G. Kanatzidis, Professor J.F. Harrison and Professor S. Garrett for their guidance in serving on my program committee.

I am so lucky to be a member in such a nice research group. I am very grateful for the kindness and help from my colleagues. I would especially thank my friends Dr. Zhen Wang, Dr. Yu Liu, Dr. Seong-Su Kim, Dr. Jiali Wang, Dr. Tie Lan, and Mr. Thomas Pauly for their generous help.

I am also very grateful for Dr. J. Wong and Dr. M. Froba for their measurement to obtain XANES spectra of Ti-substituted mesoporous molecular sieves. Very helpful assistance from Dr. J. Heckman Jr. and Dr. S.L. Flegler to obtain many attractive TEM and SEM images is greatly appreciated.

My deepest gratitude goes to my parent, my wife and son for their inspiration and patience for years to allow me work during weekends and holidays. I am obligated to my son, DeJia, who sacrificed his enjoyable kid's time to allow me to stay in the lab rather than play with him.

LIST OF TABLES

LIST OF FIGURES

CHAPTER 1

1.1

1.2

1.3

1.4

1.5

CHAPTER 2

Abstract

TABLE OF CONTENTS

LIST OF TABLES	iv
LIST OF FIGURES.....	v
CHAPTER 1 SUPRAMOLECULAR ASSEMBLY OF MESOPOROUS MOLECULAR SIEVES AND THEIR APPLICATION IN CATALYSIS.....	1
1.1 Introduction	1
1.2 Structural Characteristics of Mesoporous Silica Molecular Sieves Assembled through Neutral and Electrostatic Pathways.....	5
1.3 Synthesis of Mesoporous Silica Molecular Sieves Using Primary Amine Surfactant as the Structure Directors.....	9
1.4 Catalysis	12
1.4.1 General Application of Mesoporous Molecular Sieves	12
1.4.2 Peroxide Oxidation.....	13
1.4.3 Ring Opening Polymerization.....	17
1.4.4 Selective Catalytic Reduction (SCR) of NO	19
1.4.5 Acid Catalysis.....	20
1.5 References	24
CHAPTER 2 MESOPOROUS TITANOSILICATE MOLECULAR SIEVES PREPARED AT AMBIENT TEMPERATURE BY ELECTROSTATIC (S ⁺ T, S ⁺ X ⁺ T ⁺) AND NEUTRAL (S ⁰ T ⁰) ASSEMBLY PATHWAYS : A COMPARISON OF PHYSICAL PROPERTIES AND CATALYTIC ACTIVITY FOR PEROXIDE OXIDATIONS	27
Abstract	27

1

2

2.3

2.4

2.5

CHAPTER 3 T.A.
OF
NE

Abstract ...

3.1 Intr

3.2 Exp

3.3 Re

3.4 Dis

3.5 Ref

CHAPTER 4 IN-
SIE

Abstract ...

4.1 Intr

4.2 Exp

4.3 Re

4.3.

4.3.

2.1	Introduction	28
2.2	Experimental	29
2.2.1	Materials	29
2.2.2	Characterization	31
2.2.3	Catalytic experiments	33
2.3	Results and Discussion	34
2.3.1	Synthesis	34
2.3.2	Characterization	35
2.3.3	Catalytic results	48
2.4	Conclusions	52
2.5	References	54
CHAPTER 3 TAILORING THE FRAMEWORK AND TEXTURAL MESOPORES OF HMS MOLECULAR SIEVES THROUGH AN ELECTRICALLY NEUTRAL (S⁰I⁰) ASSEMBLY PATHWAY.....		57
	Abstract	57
3.1	Introduction	59
3.2	Experiment	61
3.3	Results	63
3.4	Discussion	74
3.5	References	81
CHAPTER 4 IN-SITU ALUMINATION OF MESOPOROUS HMS MOLECULAR SIEVES SILICA FOR USE AS ALKYLATION CATALYSTS		82
	Abstract	82
4.1	Introduction	83
4.2	Experimental	85
4.3	Results and Discussion	88
4.3.1	Catalyst Synthesis	88
4.3.2	Catalyst Characterization	89

4.4

4.5

CHAPTER 5

Abstract

5.1

5.2

5.3

5.4

5.5

CHAPTER 6

Abstract ...

6.1

6.2

6.3

6.4

6.5

4.3.3	Catalytic Results for 2,4-Di-tert-phenol Alkylation.....	104
4.4	Conclusions	107
4.5	References	109
CHAPTER 5 TOWARD MCM-41 WITH MESO-SCALED CHANNEL LENGTHS AND TEXTURAL PORES FOR CATALYSIS		111
	Abstract	111
5.1	Introduction	113
5.2	Experimental	116
5.3	Results and Discussion.....	120
5.3.1	Effect of Organic Acid Addition on Silica Mesostructure Formation	120
5.3.2	Siliceous MCM-41 Type Meso-structure Formation	123
5.3.3	Catalyst Preparation	133
5.3.4	Catalytic Alkylation of 2,4-di-tert-butylphenol with Cinnamyl Alcohol.....	141
5.4	Conclusions	145
5.5	References	147
CHAPTER 6 INCORPORATION OF STRUCTURE ORDER INTO MESOPOROUS SILICA MOLECULAR SIEVES ASSEMBLED VIA A METAL SALT MEDIATED $N^{\circ}(M^{\ast}X)I^{\circ}$ PATHWAY		149
	Abstract	149
6.1	Introduction	150
6.2	Experimental	152
6.3	Results and Discussion.....	153
6.3.1	Materials Characterization	153
6.3.2	Discussion	168
6.4	Conclusion.....	173
6.5	References	174

Table 1.1

Table 1.2

Table 1.3

Table 1.4

Table 2.1

Table 2.2

Table 2.3

Table 3.1

Table 4.1

Table 4.2

Table 5.1.

Table 5.2.

LIST OF TABLES

Table 1.1	Catalytic Peroxidation Activity of Ti-substituted (2 mol%) Mesoporous Molecular Sieve Silica.....	14
Table 1.2	Lactide polymerization over heterogeneous catalysts.....	18
Table 1.3	Comparison of the apparent and intrinsic first-order rate constants and the over all diffusivity for NO SCR reaction over Fe ³⁺ exchanged Al-HMS and Al-MCM-41	20
Table 1.4	Cumene Conversions (%) at 300 °C.....	23
Table 2.1	Properties of Ti-substituted Mesoporous Silicas Prepared by Ambient Temperature Synthesis Using Different Templating Pathways	35
Table 2.2	Ti K-edge XANES Results for Ti-Containing Materials	45
Table 2.3	Catalytic Activity of Ti-Substituted (2 Mol %) Molecular Sieves Prepared by Ambient Temperature Synthesis Using Different Templating Pathways	49
Table 3.1	Physical Parameters for Calcined (650 °C) HMS Molecular Sieve Silica Prepared by S ⁰ I ⁰ Assembly in H ₂ O-rich and EtOH-rich Medium ..	75
Table 4.1	Physical and Chemical Properties for Al-substituted Mesoporous Molecular Sieves	102
Table 4.2	Alkylation of 2,4-di-tert-butylphenol with Cinnamyl Alcohol Catalyzed by Al-substituted Mesoporous Molecular Sieves.....	105
Table 5.1.	Physical and chemical properties of Al-MCM-41 mesoporous molecular sieves	140
Table 5.2.	Alkylation of 2,4-di-tert-butylphenol with cinnamyl alcohol catalyzed by Al-substituted mesoporous molecular sieves	143

Figure 1.1

Figure 1.2

Figure 1.3

Figure 1.4

Figure 1.5

Figure 1.6

Figure 2.1

Figure 2.2

Figure 2.3

Figure 2.4

Figure 2.5

LIST OF FIGURES

Figure 1.1	Schematic showing of interfacial interactions for surfactant micelles in cooperatively assembly	2
Figure 1.2	X-ray diffraction patterns for mesoporous molecular sieves assembled via electrostatic (S^+I^-) and neutral (S^0I^0) pathways ...	6
Figure 1.3	N_2 adsorption and desorption isotherms for mesostructured molecular sieves assembled via S^+I^- and S^0I^0 pathways.....	7
Figure 1.4	TEM images showing regular order of mesopores for (a) MCM-41 and (c) MCM-48, but wormhole like channels for (b) KIT-1 and (d) HMS	8
Figure 1.5	TEM image showing wormhole-like framework mesopores and meso-scaled textural pores indicated by the arrows.....	10
Figure 1.6	N_2 adsorption and desorption isotherms for HMS prepared in (A) EtOH-rich medium ($H_2O : EtOH = 35 : 65$ by vol.); (B) H_2O -rich medium ($H_2O : EtOH = 90 : 10$ by vol.)	11
Figure 2.1	Powder XRD patterns for calcined pure and Ti-substituted (2 mol %) silica molecular sieves. (A) MCM-41 and Ti-MCM-41 prepared by $S^+X^-I^+$ assembly and (B) MCM-41 and Ti-MCM-41 prepared by S^+I^- assembly, and (C) HMS and Ti-HMS prepared by S^0I^0 assembly	37
Figure 2.2	^{29}Si -MAS NMR spectra of as-synthesized pure and Ti-substituted (2 mol %) silica molecular sieves: (A) MCM-41 and Ti-MCM-41 prepared by $S^+X^-I^+$ assembly, (B) MCM-41 and Ti-MCM-41 prepared by S^+I^- assembly, and (C) HMS and Ti-HMS prepared by S^0I^0 assembly	39
Figure 2.3	UV-VIS spectra of calcined Ti-containing materials.....	41
Figure 2.4	Ti K-edge XANES spectra of reference compounds containing Ti in tetrahedral and octahedral oxygen environments: (a) anatase, (b) rutile, (c) $MgTiO_3$, (d) neptunite, and (e) spirotitanate.....	44
Figure 2.5	Ti K-edge XANES spectra of calcined (a) Ti-HMS prepared by S^0I^0 assembly, (b) Ti-MCM-41 prepared by $S^+X^-I^+$ assembly, (c) Ti-MCM-41 prepared by S^+I^- assembly, and (d) TS-1.....	47

Figure 3.1

Figure 3.2

Figure 3.3

Figure 3.4

Figure 3.5

Figure 3.6

Figure 3.7

Figure 4.1

Figure 3.1	N₂ adsorption-desorption isotherms for HMS silicas assembled at ambient temperatures from dodecylamine and TEOS: Curves A and B are for derivatives obtained from a water-rich (water : ethanol = 90 : 20 (v/v)) and ethanol-rich solution (water : ethanol = 35 : 65 (v/v)); curves C and D are for derivatives prepared from the same water-rich and ethanol-rich solutions, but in the presence of mesitylene (Mes/S° = of 1.0). The HK values are the Horvath-Kawazoe pore diameters.	64
Figure 3.2	N₂ adsorption-desorption isotherms for HMS silicas prepared from tetradecylamine and TEOS in water-rich and ethanol-rich solution. The labeling of the isotherms is the same as in Figure 3.1	65
Figure 3.3	N₂ adsorption-desorption isotherms for a HMS silica prepared from dodecylamine in water-rich solution in the presence of mesitylene (Mes/S = 4.5): (A) after calcination at 650 °C with retention of framework and textural mesopores and (B) after calcination at 1000 °C with collapse of framework pores but with retention of textural pores. Insert: Horvath-Kawazoe pore size distribution after calcination at 650 °C	67
Figure 3.4	TEM images of calcined (650 °C) HMS molecular sieve silicas assembled from dodecylamine : a. mesoscale fundamental particles obtained from water-rich solution; b. the spheroid fundamental particles and macroscale beads-on-a-string texture obtained from ethanol-rich solution.....	69
Figure 3.5	TEM images of HMS silica prepared from dodecylamine in water-rich solution in the presence of mesitylene (Mes/S = 4.5) and calcined at 1000 °C to collapse the framework pore structure.; (a) Low magnification image showing the retention of the textural mesopores and, (b) High magnification image showing the absence of framework pores	71
Figure 3.6	X-ray powder diffraction pattern of calcined (650 °C) HMS silicas assembled from dodecylamine amine in water-rich and ethanol-rich solution with or without mesitylene as an auxiliary structure director	72
Figure 3.7	Schematic representation of the structure-directing effects of mesitylene on HMS assembly. In the water-rich media, the mesitylene “dissolves” in the hydrophobic central core of the micelle leading to pore expansion. In the ethanol-rich environment, mesitylene preferentially “adsorbs” to interfacial head groups, thus increasing effective head group size and subsequently decreasing the pore size.....	77
Figure 4.1	N₂ adsorption and desorption isotherms for calcined (650 °C) Al-HMS molecular sieves with different textural porosity. Each sample was	

Figure 4.2

Figure 4.3

Figure 4.4

Figure 4.5

Figure 4.6

Figure 4.7

Figure 4.8

Figure 5.1

	prepared at ambient temperature using dodecylamine as the structure director, TEOS as the silicon source, and using Al(sec-OBu) ₃ as the alumination agent, but the alumination agent was added to the reaction mixture 0, 0.33, and 20 hrs after mixing the TEOS and the surfactant. The aluminum content in each case is 2.0 mole%. The Horvath-Kawazoe (H-K) framework pore size, and the ratio of textural to framework mesoporosity (V_{tx}/V_{fr}) is provided for each sample 90
Figure 4.2	N ₂ adsorption-desorption isotherms for calcined (650 °C) Al-HMS molecular sieves prepared as described in the caption to Figure 4.1, except that the alumination agent was sodium aluminate 91
Figure 4.3	N ₂ adsorption-desorption isotherms for calcined (650 °C) 2% Al-HMS and calcined (540 °C) Al-MCM-41 with zero-textural porosity. The inset shows Harvath-Kawazoe pore size distributions for these two samples. This Al-HMS was prepared using aluminum sec-butoxide as the alumination agent, which was added to the reaction mixture 20 minutes after mixing the TEOS and the surfactant solution 93
Figure 4.4	XRD patterns of calcined 2% Al-HMS molecular sieves prepared as described in the caption to Figure 4.1 95
Figure 4.5	XRD patterns of 2% Al-HMS prepared as described in the caption to Figure 4.1, except that NaAlO ₂ was the Al-source 96
Figure 4.6	XRD patterns of calcined 2% Al-HMS and Al-MCM-41 with zero-textural porosity as described in the caption to Figure 4.3..... 97
Figure 4.7	TEM images showing meso-scaled textural pores as well as worm-hole like framework mesopores for calcined 1.5-tex-Al-HMS and 0-tex-Al-HMS..... 99
Figure 4.8	²⁷ Al-NMR spectra showing predominantly tetrahedral Al-sites (63 ppm) and a small amount (~10%) of octahedral Al-sites (18 ppm) in as-made Al-HMS prepared using Al(sec-OBu) ₃ as the alumination agent. Calcined forms of Al-HMS, as well as calcined Al-MCM-41, show 70% tetrahedral and 30% octahedral Al-sites..... 100
Figure 5.1	X-ray diffraction patterns for calcined (540 °C) cubic silica meso-structures formed at 150°C with a reaction composition of 1.0Si : 0.11CTAB : 0.39Na ₂ O : 0.28H ⁺ : 130H ₂ O. The diffraction patterns for MCM-48 prepared by following Landry's method as well as the diffraction patterns for a sample prepared in the absence of both EtOH and salicylic acid are included..... 121

Figure 5.2

Figure 5.3

Figure 5.4

Figure 5.5

Figure 5.6

Figure 5.7

Figure 5.8

Figure 5.9

Figure 5.2	X-ray diffraction patterns for calcined (540 °C) 3-d hexagonal silica meso-structures formed under the same conditions as noted in Figure 5.1 with the promotion of citric, oxalic and tartaric acids.....	122
Figure 5.3	N ₂ adsorption and desorption isotherms for calcined (540 °C) siliceous MCM-41 prepared under the promotion of gluconic, lactic, oxalic, and citric acids with a H ⁺ /NaOH ratio of 0.75 showing framework mesoporosity as well as clay-like textural porosity similar to that of montmorillonite. The Mobil MCM-41 sample was prepared using sulfuric acid to adjust the pH (i.e. ~10.5) at the very beginning of the synthesis by control the over-all H ⁺ /NaOH ratio to 0.625	124
Figure 5.4	TEM images showing (A and B) interwoven tubular MCM-41 formed upon use of sulfuric acid; (C and D) thin sheet MCM-41 (formed upon use of citric acid) with pore channels running orthogonal to sheet surface (the thickness of the sheet estimated to be ~100nm according to the penetration depth of electron beam accelerated at 120 kV); Both samples were prepared with an over all H ⁺ /NaOH ratio of 0.75.....	127
Figure 5.5	X-ray diffraction patterns for MCM-41 molecular sieves as noted in Figure 5.3.....	128
Figure 5.6	N ₂ adsorption and desorption isotherms for MCM-41 molecular sieves prepared using tartaric acid as the structure promoter under various conditions showing the controlled formation of significant amount of HMS-like textural pores as well as clay-like textural pores. Horvath-Kawazoe pore size distribution plots are included in the inset	130
Figure 5.7	X-ray powder diffraction patterns for MCM-41 molecular sieves as noted in Figure 5.6. Notably, the MCM-41 with high textural porosity exhibits well resolved (100), (110) and (200) reflections	131
Figure 5.8	TEM image of MCM-41 showing meso-scaled fundamental particles with inter particle voids as textural pores and regular hexagonal framework mesopores running orthogonal to thin sheet surfaces exemplified by a sample prepared using tartaric acid as the structure promoter	132
Figure 5.9	N ₂ adsorption and desorption isotherms for 8.8mol%Al-substituted MCM-41 molecular sieves (calcined at 540 °C) with clay-like and HMS-like textural porosity prepared using tartaric acid as the structure promoter and aluminum nitrate as the follow-up in situ alumination reagent in the presence of surfactant micelles in the pores. (The inset is the corresponding Horvath-Kawazoe plots showing sharp narrow distribution of framework mesopores)	133

Figure 5.10

Figure 5.11

Figure 6.1

Figure 6.2

Figure 6.3

Figure 6.4

Figure 5.10	²⁷ Al-NMR spectra for as-made and calcined Al-MCM-41 molecular sieves prepared using tartaric acid as the structure promoter with HMS-like and clay-like flaky textural pores 136
Figure 5.11	Temperature programmed desorption (TPD) of pyridine pre-adsorbed on Al-MCM-41 catalysts and purged at 150 °C in N ₂ stream for 1 h before the TPD started. This TPD profile was carried out on a thermal gravity analyzer 138
Figure 6.1	TEM images of calcined (600 °C) mesoporous silica molecular sieves prepared in water using the alkyl polyethylene oxide type surfactant Brij 56 (C ₁₆ H ₃₃ (EO) ₁₀ H) as the structure director and TEOS as the silicon source in the presence of CoCl ₂ salt as the structure promoter under the same reaction conditions (45 °C, 40 h reaction time) except that the surfactant to Co ²⁺ ratios are different. The surfactant to silicon ratio was 1 to 24 for both samples, but the surfactant to metal ratio was 8.5 for the sample denoted as MSU-C (top photo) and 2.0 for the sample denoted as MSU-H (bottom photo). These images are provided as negatives for easier viewing of the pores as black spots. Pore to pore distance is constantly ~13.7 nm through the specimen for MSU-C. The insets are the electron diffraction patterns for areas imaged. 154
Figure 6.2	(a). Selected area TEM image of MSU-C; (b). Electron diffraction pattern of MSU-C; (c). Optic diffraction pattern obtained from the Fourier-transformation of image (a); (d). Image obtained by reverse-Fourier-transformation of the center tetragonal pattern in the optic diffraction pattern (c); (e). Image obtained from the total reverse-Fourier-transformation of optic diffraction pattern (c); (f). Image obtained from the reverse-Fourier-transformation of 7 diffraction spots selected from pattern (c) in such a way that these 7 spots resembling 7 spots in the real electron diffraction pattern (b). 155
Figure 6.3	A TEM segment for MSU-C showing a different orientation of the structure. The optic diffraction pattern (obtained by Fourier-transformation of arrow indicated area in the image) is attributable to both a (01-10)-3-d-hexagonal orientation and a (210) cubic orientation. These patterns are very similar to the diffraction pattern for meso-structured silica films with pores running orthogonal to the film surface, as reported by Brinker et al. Notably, the pore to pore distance is ~13.7 nm. 156
Figure 6.4	X-ray diffraction patterns for the calcined MSU-C and MSU-H samples that were used to obtain the TEM images shown in Figure 6.1. Both d-spacings, observed and calculated according to an uni-

Figure 6.5

Figure 6.6

Figure 6.7

Figure 6.8

Figure 6.9

Figure 6.10.

N
s
d
o
t
N
sil
m
fo
sil
dir
hy
X-
me
sur
dir
con
rat
pro
spa
N
sie
por
stru

	dimensional hexagonal phase for MSU-H, are provided for comparison.	159
Figure 6.5	N ₂ adsorption and desorption isotherms for calcined MSU-C and MSU-H. Pore necking hysteresis loop for MSU-C is indicated by the step at desorption branch, which is ~0.2 unit of relative pressure behind the adsorption branch. MSU-H exhibits almost identical adsorption and desorption branches signify the uniformity of unidimensional pores.....	160
Figure 6.6	TEM images showing the wormhole (top) and 3-d-hex-cubic (lower) meso-structures assembled at Co ²⁺ : Brij56 molar ratios of 1:13 and 1 : 8.5 respectively. TEOS was the silicon source and the silicon to surfactant ratio was 17 to 1.....	161
Figure 6.7	X-ray diffraction pattern of the calcined (600 °C) meso-structured silica molecular sieves assembled using Brij 56 as the structure director and TEOS as the silicon source at a silicon to surfactant ratio of 15 to 1 under the same reaction conditions (45 °C, 40 h reaction time), except that the surfactant to Li ⁺ ratio was varied as shown.	163
Figure 6.8	N ₂ adsorption and desorption isotherms of as-made meso-structured silica molecular sieves as described in Figure 6.7. The surfactant in the mesopores was removed by ethanol extraction (i.e. refluxing in ethanol for 2 h) prior to the adsorption measurement. Again, the hexagonal silica exhibits no hysteresis loop, as expected for uniform unidimensional pores, whereas the wormhole silicas show pore necking hysteresis loops.	164
Figure 6.9	X-ray diffraction patterns for calcined (600 °C) mesoporous silica molecular sieves prepared using the mixed alkyl polyethylene oxide surfactant Tergitol 15-S-12 (C ₁₂₋₁₆ H ₂₅₋₃₃ (EO) ₈₋₁₀ H) as the structure director and TEOS as the silicon source under the same reaction conditions (45 °C, 40 h reaction time and a surfactant to metal cation ratio of approximately 24 to 1), but different cation valences for the promotional metal salts. The X-ray patterns show a decrease of d-spacing from 6.4 to 4.65 nm upon replacing Co ²⁺ and Mn ²⁺ with Cr ³⁺ . .	165
Figure 6.10.	N ₂ adsorption and desorption isotherms for mesoporous molecular sieves described in Figure 6.9. The Cr ³⁺ mediated structure shows a pore size 2.0 nm in comparison with a pore size of 3.3 nm for the structures mediated by Co ²⁺ and Mn ²⁺ ..	166

Figure 6.11.

Figure 6.12.

Scheme 1

Figure 6.11.	SEM (top) and TEM (bottom) images of mesoporous silica prepared using Tergitol 15-S-12 in the presence of Cr^{3+} as a structure promoter, showing micrometer sized intergrown spherical particles with flatten surfaces on the spheres.....	167
Figure 6.12.	^{29}Si NMR spectra for as-made HMS($\text{S}^{\text{0T}^{\text{0}}}$), MSU-H, MCM-41($\text{S}^{\text{+X}^{\text{T}^{\text{+}}}$) and MCM-41($\text{S}^{\text{+T}}$). MSU-H was synthesized using Brij 56 as the structure director in the presence of CoCl_2 . HMS and MCM-41s were prepared as reported.	169
Scheme 1	Metal salt mediated formation of mesostructured silicas	170

Supramole

1.1. Introducti

A major

Mobil researche

of M4IS materi

Kuroda and his

quaternary ammo

more versatile M

surfactants (S^+) a

extended the S^+

assembly mechan

$X = Cl, Br$ and

further extended

substrate.⁴ It w

mesoporous silica

Another

molecular sieves

(F) in the presen

directing agent. T

molecular sieve an

Chapter 1

Supramolecular Assembly of Mesoporous Molecular Sieves and Their Application in Catalysis

1.1. Introduction

A major advance in the design of mesoporous molecular sieves was provided by Mobil researchers in reporting ¹ the supramolecular surfactant assembly of a broad family of M41S materials with uniform pore sizes in the mesopore range 2.0-10.0 nm. Also, Kuroda and his co-workers ² described a structurally related mesoporous silica by quaternary ammonium surfactant rearrangement of a layered precursor (kanemite). The more versatile Mobil approach was based on the supramolecular assembly of cationic surfactants (S^+) and anionic inorganic precursors (I^-). Stucky and his co-workers ³ greatly extended the S^+I^- electrostatic pathway of Mobil to include a charge-reversed S^-I^+ assembly mechanism, as well as counterion-mediated $S^+X^-I^+$ and $S^-M^+I^-$ pathways, where $X^- = Cl^-, Br^-$ and $M^+ = Na^+, K^+$. More recently, counterion-mediated $S^+X^-I^+$ pathway was further extended to prepare well ordered cubic mesoporous silica films on glass substrate.⁴ It was also extended to protonated nonionic surfactants to synthesis mesoporous silica with pore size up to 30 nm.⁵

Another pathway has been developed for the preparation of mesoporous molecular sieves based on the hydrolysis of an electrically neutral inorganic precursor (I^0) in the presence of a neutral amine (S^0) surfactant as the predominate structure directing agent. This S^0I^0 pathway was first used to prepare a mesoporous silica molecular sieve and a Ti-substituted analog. A small amount of protonated amine was

used as a co-
protonated co-
Electrostatic fo
forces at the
An equivalent
nonionic polye
in electrically n
mesoporous

S

Figure 1.1 Sch

used as a co-surfactant in the original synthesis,⁶ but subsequent studies⁷ showed that the protonated co-surfactant component was not needed to achieve framework assembly. Electrostatic forces do not play an important role in S^oI^o assembly. Instead, the assembly forces at the surfactant-inorganic precursor interfaces are based on hydrogen bonding. An equivalent H-bonding pathway, denoted N^oI^o has also been demonstrated for nonionic polyethylene oxide surfactants and I^o precursors.⁸ The most recent development in electrically neutral assembly was a preparation of an entire family of ultrastable vesicle mesoporous

Supramolecular Assembly Pathways to Mesoporous Molecular Sieves

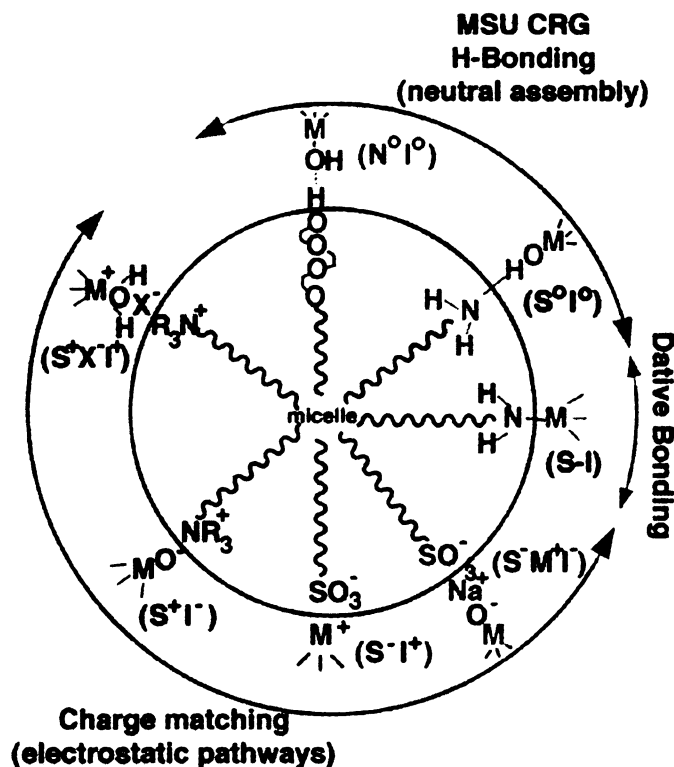


Figure 1.1 Schematic showing of interfacial interactions for surfactant micelles in cooperatively assembly

molecular sie

N₂ pathway

pathways also

workers for the

a coordinate co

metal center. A

structures conta

schematically il

Other t

templating mec

not intrinsicall

pre-formed liq

concentration o

of the surfacta

altering of the

products. How

difficulty in

precursors lim

Surfact

extensively ex

structures. in

surfactant liqu

a good strateg

molecular sieves using neutral gemini surfactants as the structure director.⁹ The S°I° and N°I° pathways are complementary to those electrostatic templating pathways. These pathways also are distinguishable from the S-I pathway developed by Ying and her co-workers for the synthesis of meso-structured transition metal oxides.¹⁰ In the S-I pathway a coordinate covalent bond is formed between the surfactant (usually, an amine) and the metal center. All aforementioned cooperative assembly pathways afford as-made meso-structures contain liquid crystal micelles in the framework pores. All the pathways were schematically illustrated in Figure 1.1.

Other than the cooperative assembly mechanisms, surfactant liquid crystal templating mechanism have been proposed too.^{1,11} Although this templating pathway is not intrinsically different from cooperative assembly pathways, it relies very much on pre-formed liquid crystal phases to form meso-structured molecular sieves under a high concentration of surfactant. Diffusion of inorganic precursor molecules to the interfaces of the surfactant head groups and water molecules in the liquid crystal micelles without altering of the liquid crystal phase is crucial for obtaining structural order in the final products. However, the inefficient use of relatively expensive surfactants and the difficulty in maintaining the liquid crystal phases upon addition of the inorganic precursors limits the wide-spread use of this templating pathway.

Surfactant-directed assembly of mesostructures by sol-gel methods has been extensively exploited. Regardless of the type of inorganic precursors used to form meso-structures, in general, the pore size and connectivity take the size and shape of the surfactant liquid crystal phase in the structural channels of as-made materials. Therefore, a good strategy for the design and synthesis of meso-structures would be the over-all

control of m

framework po

In ad

alumina, s¹²

molecular sie

metal oxides

mesostructure

primary am

zirconia was

between sur

could not be

structured tu

nonionic pl

structurally s

metal oxides

removal of s

Unlik

mesoporous s

has been inve

walls are stil

toward synthe

limited X-ray

quasi-crystall

consequence o

control of micelle formation that determines the final liquid crystal phases in the framework pores.

In addition to mesoporous silica molecular sieves, structurally stable mesoporous alumina,^{8,12} niobia,¹⁰ titania,^{13,14} many other metal oxides and metallic platinum molecular sieves¹⁵ have been reported. Interestingly, most of these stable mesoporous metal oxides have made use of electrically neutral or nonionic surfactants. For example, mesostructured zirconium oxide¹⁶ and niobium oxide¹⁰ have been prepared using primary amine surfactants as structure directors. The surfactant in mesostructured zirconia was easily removed by ethanol extraction because of weak hydrogen bonding between surfactant molecules and framework walls, however the surfactant in niobia could not be simply extracted by ethanol because of the presence of dative bonds. Mesostructured tungsten and iron oxide, as well as other metal oxides were assembled using nonionic pluronic surfactants.¹⁴ Nevertheless, neutral surfactants produced more structurally stable mesoporous transition metal oxides. In contrast, most mesostructured metal oxides prepared using charged surfactants as the structure directors collapsed upon removal of surfactants.^{17,18}

Unlike crystalline microporous zeolites, it has been recognized that the mesoporous silica molecular sieves are built of amorphous silica walls.¹⁹ Although, effort has been invested in the synthesis of crystalline walled mesoporous molecular sieves, the walls are still amorphous for most of the mesoporous molecular sieves. An advance toward synthesis of fully crystalline mesoporous materials was claimed for materials with limited X-ray order, as indicated by limited number of reflections.¹⁴ Intrinsically, the quasi-crystalline walls of these materials is alike of a mesostructured SnO₂, which is a consequence of particle assembly rather than a surfactant directed assembly.²⁰ Actually,

the assembly
relative or
relatively
worm-hole
patterns. T
ordered m
characterist
neutral pat

1.2. Structure through N

Four
one is an o
(CTAB) as
precursor (D
(i.e. surfacta
4) prepared
as the silic
concentration
worm-hole-l
as the struct
disordered K
EDTA as the
sieves were ch

the assembly forces at the surfactant-inorganic precursor interfaces greatly determines the relative order of meso-structures. Longer range electrostatic interaction force affords relatively higher structural order. The shorter range H-bond interaction force affords worm-hole-like structural motifs that usually exhibit single-line X-ray diffraction patterns. The key-role of longer range electrostatic interaction in the formation of higher ordered meso-structures is illustrated in the following section comparing four characteristic mesoporous silica molecular sieves assembled through electrostatic and neutral pathways.

1.2. Structural Characteristics of Mesoporous Silica Molecular Sieves Assembled through Neutral and Electrostatic Pathways

Four characteristic mesoporous molecular sieves are compared below. The first one is an ordered cubic MCM-48 assembled using cetyltrimethyl ammonium bromide (CTAB) as the structure director (S^+) and tetraethyl orthosilicate (TEOS) as the inorganic precursor (I) under basic conditions at relatively high concentrations of the surfactant (i.e. surfactant to silicon ratio at 0.5).^{21,22} The second one is an ordered hexagonal MCM-41 prepared using cetyltrimethyl ammonium as the structure director and sodium silicate as the silicon precursor through typical S^+I assembly pathway at relatively low concentration of the surfactant (i.e. surfactant to silicon ratio at 0.25).¹⁷ The third one is a worm-hole-like HMS formed by a supramolecular assembly pathway with dodecylamine as the structure director that is predominately $S^{\circ}I^{\circ}$ in character.⁷ The fourth one is a disordered KIT-1 silica assembled via the S^+I pathway using CTAB, sodium silicate and EDTA as the reagents as reported by Ryoo et al.²³ These four mesoporous molecular sieves were chosen because they are structurally distinctive.

Figure

order reflecti

Cubic order is

reflections. w

(200) reflecti

smearred hump

intrinsic short-

KIT-1, electro

precursor migh

density caused b

EDTA salts.

conditions. st

inevitably o

electrostatic in

shortened.

Apparen

mesoporous

prepared via an

pathway exhibi

mesoporosity, a

N_2 pore-filling

pressure of 0.2

The isotherm for

Figure 1.2 shows the X-ray diffraction patterns of these four samples. Higher order reflections for hexagonal MCM-41 and cubic MCM-48 are unambiguously shown. Cubic order is indicated by the presence of (211), (220), (321), (400), (420), and (332) reflections, whereas hexagonal order is indicated by the presence of (100), (110) and (200) reflections. In contrast, HMS and KIT-1 both show broad first reflection with smeared humps at higher 2θ angles. The Lack of structural order for HMS indicates the intrinsic short- range interaction property of H-bonding in the assembly mechanism. For KIT-1, electrostatic interactions between the surfactant head group and the inorganic precursor might be weakened due to a decrease in the surfactant head group charge density caused by association with

EDTA salts. Under these conditions, structural disorder inevitably occurs as the electrostatic interaction range is shortened.

Apparently, those three mesoporous molecular sieves prepared via an electrostatic S^+T pathway exhibit only framework mesoporosity, as indicated by the N_2 pore-filling step at a relative pressure of 0.2 to 0.4. (Fig. 1.3)

The isotherm for HMS

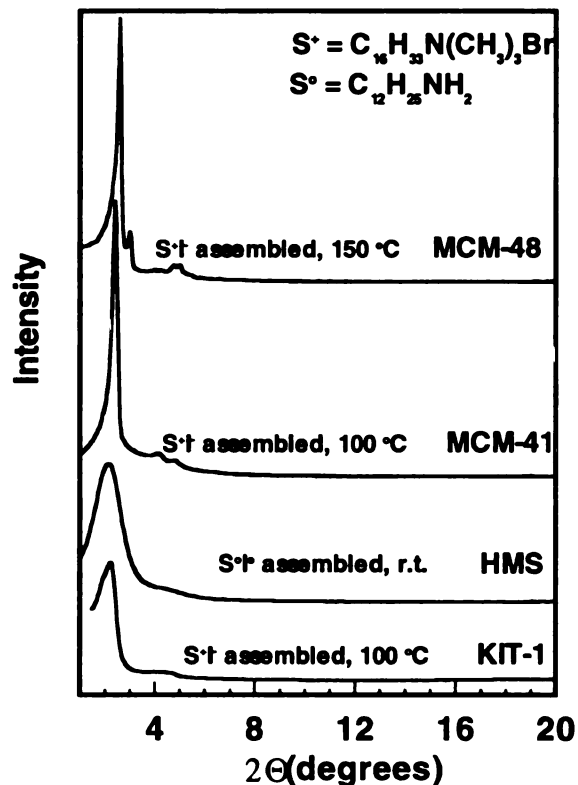


Figure 1.2 X-ray diffraction patterns for mesoporous molecular sieves assembled via electrostatic (S^+T) and neutral (S^0T^0) pathways.

characteristic

significant N

Figure 1.3, the

and 33 Å, re

differences ar

size for MC

structurally si

is reported to

sizes for MC

N Volume Adapted (2014)

Figure 1.

characteristically exhibits both framework and textural mesoporosity with two significant N₂ uptake steps at relative pressures of 0.3 and 0.7. As shown by the inset in Figure 1.3, the average pore sizes of HMS, MCM-41 and KIT-1 molecular sieves (29, 30, and 33 Å, respectively) are significantly larger than that of MCM-48 (26 Å). Structural differences are associated with differences in framework pore size. The similarity in pore size for MCM-41 and KIT-1 may indicate that MCM-41 and KIT-1 tend to be structurally similar, but different from bi-continuous cubic MCM-48, even though KIT-1 is reported to possess interconnected pore channels analogous to MCM-48. Larger pore sizes for MCM-48 (Ia3d) so far have not been reported. Although the X-ray diffraction

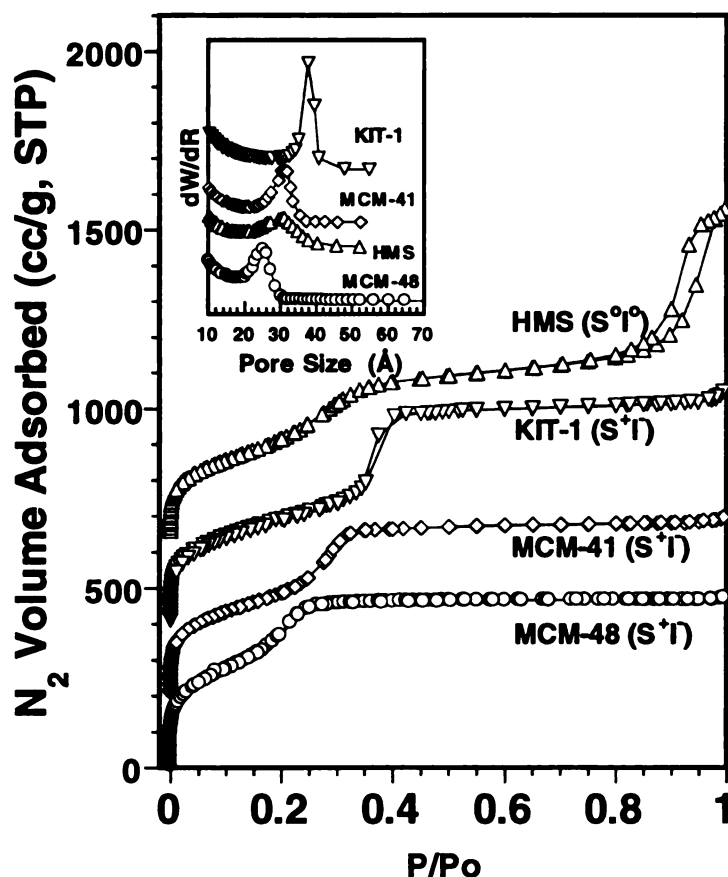


Figure 1.3 N₂ adsorption and desorption isotherms for mesostructured molecular sieves assembled via S⁺I and S⁰I⁰ pathways.

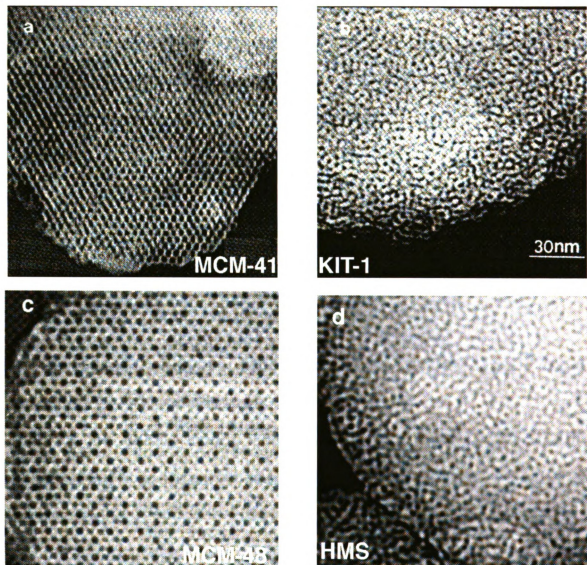


Figure 1.4 TEM images showing regular order of mesopores for (a) MCM-41 and (c) MCM-48, but wormhole like channels for (b) KIT-1 and (d) HMS.

pattern does

pore size dist

fundamental

TEM

(Figure 1.4).

of uni-dimens

pore channels

pore channels.

structural diff

electrostatic as

structures asse

limited to the

materials.

1.3. Synthesis

Surfactant as

The fir

presence of a

structure direct

exhibited only

range structure

occasional occ

majority of the

structure.

pattern does not explicitly shown higher order reflections, KIT-1 exhibits a quite narrow pore size distribution which is about 3 times narrower than that of HMS. This verifies the fundamental differences in assembly mechanisms for HMS and KIT-1.

TEM images show the structural versatility for these four molecular sieves. (Figure 1.4). The image for MCM-41 explicitly shows a typical hexagonal arrangement of uni-dimensional pores. The image for MCM-48 shows triangle arrangement of the pore channels running along the cubic (111) direction. Instead of very regularly arranged pore channels, HMS and KIT-1 both exhibit worm-hole-like channels. It is hard to tell the structural difference by TEM for HMS and KIT-1. Nevertheless, the long range electrostatic assembly affords meso-structures with relatively higher order than meso-structures assembled from electrically neutral surfactants. However, the order is still limited to the order of pore channels, which is far from the atomic order in crystalline materials.

1.3. Synthesis of Mesoporous Silica Molecular Sieves Using Primary Amine Surfactant as the Structure Directors

The first example of HMS silica was prepared at ambient temperature in the presence of a 13.5:1 molar mixture of dodecylamine and dodecylammonium ion as the structure directing co-surfactants.⁶ The product formed under these reaction conditions exhibited only one resolved XRD reflection, which precluded the assignment of a long range structure. Selected area electron diffraction studies provided evidence for the occasional occurrence of very small domains of hexagonal symmetry, but the vast majority of the sample was highly disordered and lacking in a long range regular structure.

St
omitting t
structure
pore sizes
using a m

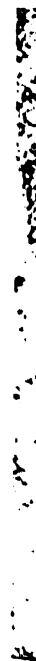


Figure 1

hexagonal
when proto
scaled inter
up to 15%
protonic ac
replacement
protonated a

Subsequent studies revealed that equivalent HMS silicas could be prepared by omitting the onium ion from the reaction mixture and using only the neutral amine as the structure director.⁷ This $S^{\circ}I^{\circ}$ pathway afforded silicas with N_2 adsorption properties, pore sizes, and XRD patterns virtually identical to the original HMS products formed using a mixture of S° and S^+ surfactants. Also, the sparsely occurring small domains of

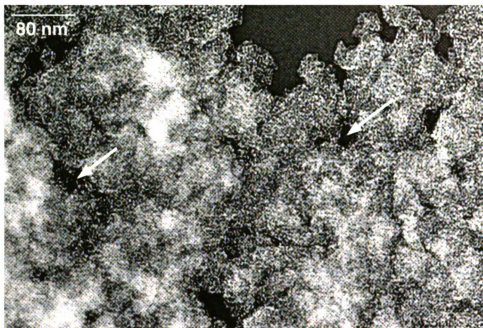


Figure 1.5 TEM image showing wormhole-like framework mesopores and meso-scaled textural pores indicated by the arrows

hexagonal order were absent. In fact, hexagonal regions are very rarely formed even when protonated surfactant is present. Instead, the wormhole channel motif with meso-scaled inter particle voids shown in Figure 1.5 is formed almost exclusively²⁴ even when up to 15% of the amine is protonated. The onium ion can be introduced by adding a protonic acid. Alternatively, the introduction of certain Lewis acid centers, as in the replacement of some Si^{4+} sites by Al^{3+} , Fe^{3+} or B^{3+} , will result in the formation of some protonated amine surfactant during the assembly process in order to balance the resulting

framework.

structurally

meso-scaled

**Figure 1.6 N₂
rich medium**

Recent

can be judicia

polarity water-

like to sponge

significant amo

framework. However, this small electrostatic participation of the surfactant is structurally inconsequential, and neither it alter the wormhole channel motif, nor the meso-scaled textural pores.

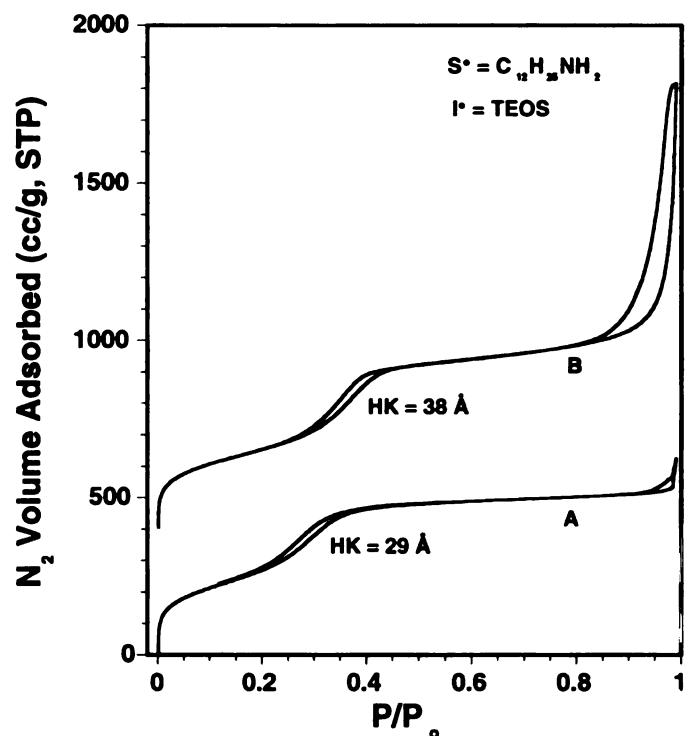


Figure 1.6 N₂ adsorption and desorption isotherms for HMS prepared in (A) EtOH-rich medium (H₂O : EtOH = 35 : 65 by vol.); (B) H₂O-rich medium (H₂O : EtOH = 90 : 10 by vol.)

Recent studies have shown that particle morphology and textural porosity of HMS can be judiciously controlled by choice of solvent polarity.²³ HMS prepared in higher polarity water-rich media (i.e. 90:10 H₂O : EtOH medium by volume) shows wormhole-like to sponge-like channels with fractal-like particle texture. This HMS exhibits a significant amount of textural mesopores in the range of 150 Å to 500 Å, built from inter-

growth of r
from the vo
ethanol medi
with beads o
Therefore, te
but a property

1.4 Catalysis

1.4.1 Genera

As po
have received
framework p
grafting chem
complex to th
also afforded
an exceptiona
groups of MC
has been stud
the mesopore

Mesop
uniform. A re
utilization of
encounter dif

growth of meso-scaled fundamental particles. These textural mesopores are different from the voids formed by the physical packing of particles. HMS prepared in high ethanol medium ($\text{H}_2\text{O} : \text{EtOH} = 35 : 65$) exhibits much larger fundamental particle size, with beads on string type of morphology and very little textural porosity. (Figure 1.6) Therefore, textural porosity is not an intrinsic property of electrically neutral assembly, but a property generated by the kinetics of the assembly process.

1.4 Catalysis

1.4.1 General Application of Mesoporous Molecular Sieves

As potential sorbents, catalyst supports or catalysts, mesoporous molecular sieves have received considerable attention. A high density silanol groups on the walls of the framework provide unique capability for meso-structured silica molecular sieves for grafting chemistry. A very active Ti-MCM-41 was prepared by grafting of a titanocene complex to the meso-structured walls of MCM-41.²⁵ A grafted Ru-complex on MCM-41 also afforded a super active oxidation catalyst.^{26,27} Pd supported on MCM-41 generated an exceptionally active catalyst for Heck reactions.²⁸ Grafting chelating ligand to silanol groups of MCM-41 achieved excellent adsorbent for heavy metals in waste water.^{29,30} It has been studied that most of hazardous heavy metals could be remedied by trapping into the mesopores.

Mesoporous molecular sieves are catalytically useful as long as their pores are uniform. A relatively high X-ray order is not necessarily beneficial for the catalytic utilization of mesoporous molecular sieves. Actually, mesoporous molecular sieves still encounter diffusion limitations, particularly for reactions in condensed media. The

accessibility

extremely in

The u

silicas, prep

chemical con

polymerizat

be discussed

prepared thro

mesopores, a

facilitate acce

1.4.2. Peroxi

Metal

for the pero

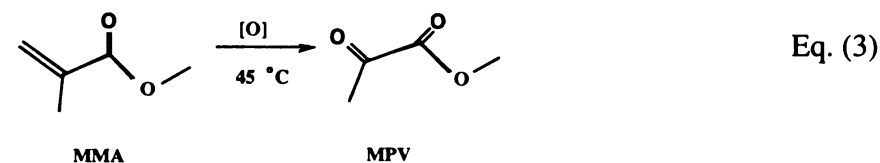
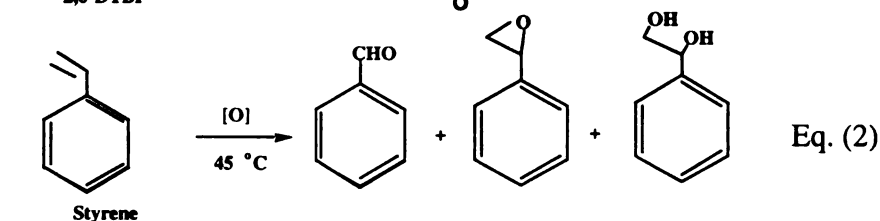
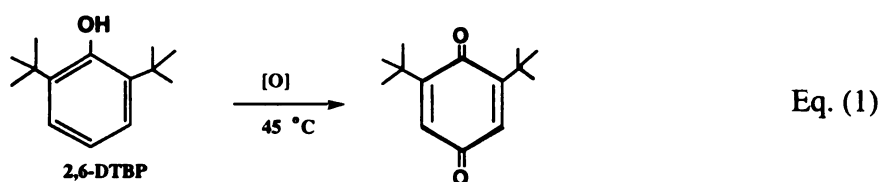
epoxides and

accessibility to the catalytically active centers located in the mesoporous framework is extremely important for diffusion controlled reactions.

The uses of chemically modified derivatives of mesoporous HMS molecular sieve silicas, prepared by neutral surfactant assembly pathways, as catalysts for a variety of chemical conversions, including peroxide oxidations of olefins and phenols, ring opening polymerization of lactide dimers, selective reduction of NO_x , and cumene cracking will be discussed below. These HMS catalysts are often more active than analogous catalysts prepared through electrostatic assembly mechanisms. The wormhole-like framework mesopores, along with the presence of complementary textural mesopores, most likely facilitate access to the catalytic active centers in the framework.

1.4.2. Peroxide Oxidation

Metal-substituted HMS silicas have received considerable attention as catalysts for the peroxide oxidation of aromatics to phenols and quinones and of alkenes to epoxides and diols (see equation 1-3). One of the first reactions to be investigated was



the Ti-HM
correspondi
was of partic
1. an industr
have been in
phenol, meth
epoxide, diol

The ca
phase oxida
described in
obtained wit
consideration
for the meso
HMS cataly

Table 1.1
Molecular

MMA
Styrene
2,6-DTBP
MMA is m

prepared b
pronounce

the Ti-HMS catalyzed oxidation of 2,6-di-*tert*-butylphenol (2,6-DTBP) to the corresponding mono- and dinuclear quinones using H₂O₂ as the oxidant.⁶ This substrate was of particular interest, because it was too large to access the framework Ti sites of TS-1, an industrial microporous molecular sieve catalyst.³¹ Other oxidation reactions that have been investigated using Ti-HMS as a catalyst includes the conversion of benzene to phenol, methyl methacrylate to methyl pyruvate and styrene to the corresponding epoxide, diol and benzaldehyde.³²

The catalytic properties of mesoporous Ti-HMS and of Ti-MCM-41 for the liquid phase oxidations of methylmethacrylate, styrene and 2,6-di-*tert*-butylphenol are described in Table 1.1.³² Included in the Table for comparison are the conversions obtained with microporous TS-1 as the catalyst. As expected based on pore size considerations, the conversions observed for all three substrates are substantially larger for the mesoporous catalysts than for the microporous catalyst. The S[°]T[°]-assembled Ti-HMS catalyst exhibited consistently greater reactivity than the two Ti-MCM-41 catalysts

Table 1.1 Catalytic Peroxidation Activity of Ti-substituted (2 mol%) Mesoporous Molecular Sieve Silica

Catalyst		TS-1	Ti-MCM-41 (S ⁺ T)	Ti-MCM-41 (S ⁺ X ⁺ T ⁺)	Ti-HMS (S [°] T [°])
MMA	Conv. (mol%)	2.5	4.0	6.2	6.8
Styrene	Conv. (mol%)	8.4	10	23	28
2,6-DTBP	Conv. (mol%)	5.0	39	22	55

MMA is methylmethacrylate.

prepared by electrostatic assembly. The superior performance of Ti-HMS is especially pronounced in the case of the large 2,6-di-*tert*-butylphenol substrate.

be attri

titanium

coordin

similar

segrega

centers.

superior

availabi

inaccess

Ti-MCM

1.5). Th

to the a

efficienc

S

silicas as

verify tha

MCM-41

active site

number of

not take p

HMS. All

redox pote

these fram

The differences in catalytic reactivity between Ti-HMS and Ti-MCM-41 cannot be attributed to differences in Ti siting. XANES and EXAFS studies showed that the titanium center adopt primarily tetrahedral coordination in all three catalysts.³² Also, the coordination environment is very similar for the three catalysts, as judged from the similarities in the EXAFS features. Also, UV-VIS adsorption spectra showed no phase segregation of titania, the spectral features being consistent with site-isolated titanium centers. Because the framework walls of HMS tend to be thicker than MCM-41, the superior reactivity of Ti-HMS cannot be due to an enhancement in the fraction of Ti available for reaction on the pore walls. Thicker walls should bury more titanium at inaccessible sites within the walls. The most distinguishing feature between Ti-HMS and Ti-MCM-41 is the greater textural (inter particle) mesoporosity for Ti-HMS (cf. Figure 1.5). This complementary textural mesoporosity facilitates substrate transport and access to the active sites in the framework-confined mesopores, thus enhancing catalytic efficiency compared to MCM-41 meso-structures with little or no textural porosity.

Sayari and his co-workers³³⁻³⁶ have investigated Ti- and V-substituted HMS silicas as liquid phase oxidation catalysts for large organic molecules. Their results verify that the activity of HMS derivatives is typically higher than the corresponding MCM-41 analogs. He also has emphasized the importance of the accessibility of Ti-active sites in determining reactivity toward large molecules. He further noted that a number of oxidation reactions which occurred readily over small pore TS-1 catalysts, did not take place in the presence of larger pore Ti- β or ultra large pore Ti-MCM-41 and Ti-HMS. All these observations suggest that differences in surface hydrophilicity and Ti redox potential also play a role in determining the reactivity of tetrahedral Ti sites in these frameworks. On the other hand, TS-1 is not known to catalyze the oxidation of

acetone at

acetone ox

Kali

HMS and

butylhydrop

than Ti-MCM

^{39,40} prepared

temperature.

air were po

subsequently f

Ti-MCM-41 f

Tuel suggest

textural poros

textural mesop

N₂ adsorption

HMS and HM

for framework

process is car

textural poros

catalysts can

comparable in

acetone at rates that are competitive with benzene hydroxylation, yet Ti-HMS catalyzes acetone oxidation readily.³⁷

Kaliaguine and his co-workers³⁸ have compared the catalytic reactivity of Ti-HMS and Ti-MCM-41 silicas for the epoxidation of α -pinene with tert-butylhydroperoxide as the oxidant. The conversions over Ti-HMS were somewhat lower than Ti-MCM-41, although epoxide selectivities were similar. Also, Gontier and Tuel^{39,40} prepared a series of Ti-HMS using reaction times as short as 15 min at ambient temperature. Tetrahedral Ti loadings up to 2 wt % and thermal stabilities up to 650°C in air were possible without forming extra-framework titania.³⁹ However, they subsequently found no substantial difference in catalytic reactivity between Ti-HMS and Ti-MCM-41 for the oxidation of aniline.⁴⁰ These results of Kaliaguine and Gontier and Tuel suggest that the Ti-HMS derivatives used in these studies not possess the high textural porosity needed for facile access to framework Ti sites. In fact, the absence of textural mesoporosity in the Ti-HMS catalyst used by Gontier and Tuel was confirmed by N₂ adsorption studies.⁴¹ These reports verify that the interparticle mesoporosity of Ti-HMS and HMS molecular sieves, in general, is dependent on the reaction conditions used for framework assembly. In general, textural porosity is formed when the assembly process is carried out in a water-rich solvent. Alcohol-rich solvents tend to eliminate textural porosity. Enhanced reactivity for large molecule conversions over HMS catalysts can be expected only when the textural and framework mesoporosities are comparable in magnitude.

1.4.3 Ri

achieved

promotin

the cataly

potential

Sn(IV)-st

lactide di

low polyc

Sr

assembly

Sn(II)-C₃

directing s

indicated

a textural

Ta

equation -

a Sn-dope

prepared

those usec

Th

conversion

and a low

1.4.3 Ring Opening Polymerization

The small crystallite domain sizes and high textural mesoporosity that can be achieved for HMS derivatives through S^oI^o assembly may be especially beneficial in promoting polymerizations and other bulky conversions where diffusion effects can limit the catalytic effectiveness of larger particle mesostructures. In order to demonstrate the potential utility of mesostructures for polymerization reactions, it has been shown⁴² that Sn(IV)-substituted HMS is remarkably effective for the ring opening polymerization of *l*-lactide dimer to poly (*l*-lactic acid), abbreviated PLA, with a high molecular weight and low polydispersity.

Sn-HMS containing 1 mol % tin(IV) was prepared at ambient temperature by S^oI^o assembly in ethanol:water (3:1v/v) using a 100:1 molar mixture of Si(OC₂H₅)₄ and Sn(*iso*-C₃H₇)₄ as the inorganic precursors and dodecylamine as the structure directing surfactant. The N₂ adsorption isotherm for the calcined (550 °C) mesostructure indicated a BET surface area of 886 m²/g, an average framework pore size of 2.7 nm, and a textural (inter-particle) mesoporosity in excess of the framework mesoporosity.

Table 1.2 reports the conversions of *L*-lactide dimer to PLA at 130 °C (see equation 4). Included for comparison purposes are the conversions for pure HMS silica, a Sn-doped silica gel (1.0 mol% Sn) and pure SnO₂. The latter two catalysts were prepared by hydrolysis of the corresponding alkoxides under condition analogous to those used to form Sn-HMS.

The polymerization product obtained from Sn-HMS exhibited the highest conversion as determined by ¹HNMR (82%), the largest average molecular mass (36000) and a low polydispersity (1.1). In the case of pure tin oxide as the catalyst, the

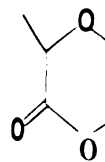
conversion

lower mole

case of Sn-d

centers in t

Lewis-acid



Lactide

Table 1.2

Catalyst

Sn-HMS

HMS

Sn-doped S

SnO₂

^aReaction c

where 0.00

550 °C prio

with a rea

ordered po

comparison

PLA chain

reactions.

conversion was substantial (73%), but the polymerization product had a much lower molecular mass (17800) and a high polydispersity (1.7). The low activity in the case of Sn-doped silica gel may indicate the lack of a suitable dispersion of active metal centers in the host silica. Sn-HMS, however, clearly combines the reactivity of tin Lewis-acid sites with the selectivity of a regular mesopore structure in affording PLA

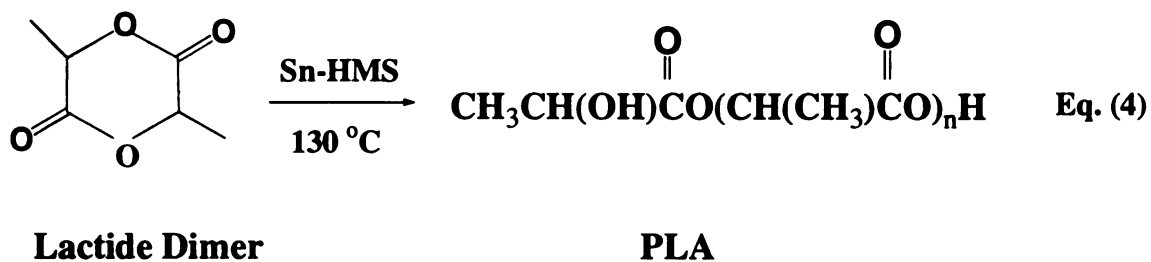


Table 1.2 Lactide polymerization over heterogeneous catalysts^a

Catalyst	Conversion (%)	PLA Molecular mass
Sn-HMS	82	36 000
HMS	0	--
Sn-doped Silica	22	3 200
SnO ₂	73	17 800

^aReaction conditions: 2.00 g (13.9 mmol) lactide dimer; 0.1 g catalyst (except for SnO₂, where 0.001 g was used); $T = 130\text{ }^{\circ}\text{C}$; reaction time 72 h. All catalysts were calcined at $550\text{ }^{\circ}\text{C}$ prior to use.

with a reasonably high molecular mass and low polydispersity. It appears that the ordered pore structure improves average molecular mass and polydispersity values in comparison to homogeneous catalysts by imposing steric constraints on the propagating PLA chains and minimizing ‘back-biting’ and intermolecular transesterification reactions.

1.4.4.9

MCM-

equati

differe

conten

distrib

were in

0.75 d

mesop

or no t

surface

Fe/Al-

domain

was of

as judg

Table 1

pore di

HMS w

'C. An

1.4.4. Selective Catalytic Reduction (SCR) of NO

Yang et al.,⁴³ recently investigated the activity of Fe³⁺ exchanged forms of Al-MCM-41 and Al-HMS for the selective catalytic reduction (SCR) of NO by NH₃ (see equation 5). In order to minimize the number of factors that may cause significant differences in the catalytic properties between Al-MCM-41 and Al-HMS, the aluminum contents of both molecular sieves were controlled to around 8%. Also, the pore size distribution for the two supports was controlled to around 28 Å, the BET surface areas were in the range 800-850 m²/g, and the framework pore volumes were similar (0.62 and 0.75 cm³/g for Al-HMS and Al-MCM-41, respectively). However, the textural mesoporosity of Al-HMS was comparable to the framework mesoporosity, whereas little or no textural porosity was present for Al-MCM-41.

Although HMS and MCM-41 are similar both in terms of chemical composition, surface area, and pore volume, Fe/Al-HMS showed considerably higher activities than Fe/Al-MCM-41. The main differences between HMS and MCM-41 are the crystal domain sizes and the unique textural porosity of HMS. The crystal domain size for HMS was of the order 150 Å, whereas that of MCM-41 was larger by two orders of magnitude, as judged by XRD line widths and TEM.

The comparison of the estimated apparent and intrinsic rate constants given in Table 1.3 show that the reaction for the Fe/Al-MCM-41 sample was severely limited by pore diffusion, but not for HMS molecular sieve. The Thiele effectiveness factor for the HMS was nearly 1.0, whereas that for the MCM-41 were 0.53 at 350 °C and 0.44 at 400 °C. An overall activation energy of 6.5 kcal/mol for Fe-HMS was in the range for SCR

without

attribu

Thus, t

Al-HM

Table

the ove

MCM-

Catalys

Fe/Al-F

Fe/Al-N

^aThe in

mesopo

1.4.5. A

investig

catalytic

electros

calcinat

with NH

been rep

without diffusion limitation. The high effectiveness factor for the HMS catalyst is attributable to the small domain size and short diffusion path in the framework channels. Thus, the advantage for the Fe³⁺ exchanged mesoporous molecular sieves, in particular Al-HMS, for the SCR reaction is clearly demonstrated.

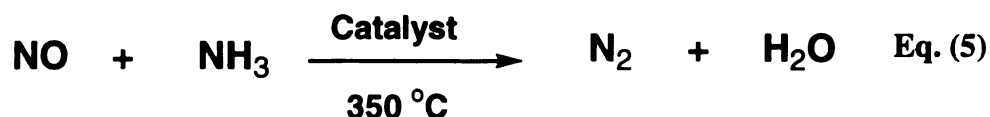


Table 1.3 Comparison of the apparent and intrinsic first-order rate constants and the over all diffusivity for NO SCR reaction over Fe³⁺ exchanged Al-HMS and Al-MCM-41*

Catalyst	Apparent k (s ⁻¹)		Intrinsic k (s ⁻¹) ^a		Diffusivity (cm ² /s) ^a	
	350 °C	400 °C	350 °C	400 °C	350 °C	400 °C
Fe/Al-HMS	56.5	87.5	56.6	87.6	3.95x10 ⁻⁷	4.0x10 ⁻⁷
Fe/Al-MCM-41	30.0	38.5				

^aThe intrinsic rate constant and diffusivity are assumed to be the same for both mesoporous catalysts.

1.4.5. Acid Catalysis

The replacement of silicon by trivalent elements in HMS materials has been investigated by several groups in an effort to improve Bronsted and Lewis acidity for catalytic applications.⁴⁴⁻⁴⁸ Although Al-MCM-41 derivatives can be prepared directly by electrostatic assembly pathways, the as-synthesized materials are structurally sensitive to calcination.⁴⁹ Also, if sodium silicate is used in the synthesis, a post-synthesis treatment with NH₄NO₃ is needed to remove residual Na⁺ ions from the exchange sites.⁵⁰ It has been reported by Corma and his co-workers⁵¹ that Al-MCM-41 undergoes framework

dealumin

dealumin

dealumin

proton ex

In

pathway

molecular

noted earl

of structur

framework

tetrahedral

interaction

surfactant

preserves t

Tu

pathway fo

of catalyti

incorporate

importanti

damaging

primary al

either by c

the alumin

substituted

dealumination upon calcination to remove the surfactant. Hitz and Prins⁵² verified the dealumination of surfactant-filled Al-MCM-41 upon calcination, but they showed that dealumination could be minimized by first removing up to 73% of the surfactant by proton exchange in ethanol.

In contrast to the electrostatic assembly pathways to Al-MCM-41, the S^oI^o pathway to Al-HMS derivatives offers a convenient route to acidic mesoporous molecular sieves with retention of framework aluminum and other trivalent ions. As noted earlier, the replacement of Si⁴⁺ by Al³⁺ requires the protonation of one equivalent of structure-directing amine surfactant for every equivalent of Al³⁺ incorporated into the framework. However, because only up to 15 mole % of the silicon can be replaced at tetrahedral sites, the majority of the framework is assembled through H bonding interactions of the amine surfactant with the silica framework. Consequently, most of the surfactant (>90%) can be efficiently removed by simple solvent extraction and this preserves the tetrahedral siting of aluminum centers in the framework.

Tuel and Gontier⁴⁴ have recognized the potential importance of the S^oI^o assembly pathway for the preparation of HMS derivatives containing trivalent framework elements of catalytic significance. They found that Al³⁺, Ga³⁺, Fe³⁺ and B³⁺ all could be incorporated into the framework of HMS silica at Si/M³⁺ ratios as low as 10. More importantly, the neutral amine surfactant could be removed by solvent extraction without damaging the framework. Also, the remaining small concentration of charge balancing primary alkylammonium ions associated with the aluminum sites could be removed either by calcination or by ion exchange without collapsing the framework or removing the aluminum from the framework. Similar results were obtained for other M³⁺-substituted derivatives. Thus, the structural degradation that normally occurs upon

calcining

through S

surfactant.

protonated

MoK

mesoporous

pathway. U

synthesis (i.e.

ethanol/wate

surfactant). 1

identical to F

HMS deriva

range 5-40 e

compared to

aluminum co

It is unlikely

HMS. Al-Me

walls in all t

materials ma

compared to

The short in

may well fac

may be the n

calcining M^{3+} -substituted mesostructured silicas to remove surfactant can be avoided through $S^{\circ}I^{\circ}$ assembly and the subsequent solvent extraction of the vast majority of the surfactant. The heat of combustion associated with the removal of the remaining protonated surfactant is not sufficient to significantly alter the framework structure.

Mokaya and Jones^{45,46} also have recognized the advantages of preparing mesoporous silica and aluminosilicate molecular sieves through a $S^{\circ}I^{\circ}$ assembly pathway. Using a synthetic methodology equivalent to that originally reported for HMS synthesis (i.e., alkyl amines as the surfactant, alkoxides as the inorganic precursors, ethanol/water as a solvent, ambient temperature assembly, and solvent extraction of the surfactant), they prepared a series of derivatives with XRD and textural properties identical to HMS materials. However, they designated their products as MMS rather than HMS derivatives. Interestingly, their Al^{3+} -substituted products with Si/Al ratios in the range 5-40 exhibited greater Bronsted acidity and catalytic activity for cumene cracking compared to Al-MCM-41, amorphous aluminosilicate gel and zeolite HY of similar aluminum content.⁴⁷ In addition, the Al-HMS catalysts were less prone to deactivation. It is unlikely that the siting and intrinsic acidity of tetrahedral aluminum centers in Al-HMS, Al-MCM-41, and aluminosilicate gels differ significantly, because the framework walls in all three materials are amorphous. However, *access* to the acidic sites in these materials may differ greatly. What is particularly distinctive of most Al-HMS materials compared to Al-MCM-41 and amorphous gels is the uniformity of the framework pores. The short intersecting framework pores, in addition to the small crystallite domain size, may well facilitate access to the active sites in HMS structures. This improved access may be the main reason for the superior reactivity of Al-HMS materials as acid catalysts

relative to Al-MCM-41, which have very long channel lengths, and amorphous gels with irregular, highly constrained pore-structures.

Very recently, van Bekkum and his co-workers⁴⁸ have reported modifying Al-HMS and Al-MCM-41 ($\text{Si}/\text{Al} \cong 30$) to contain entrapped unit cells of ZSM-5. These modified mesostructures were prepared by ion exchanging the aluminosilicates with tetrapropylammonium cations as MFI structure directors and subsequently digesting the mesostructures in glycerol at 120°C for 24 h. The resulting nanoporous aluminosilicate products, designated NPA-1 and NPA-2, respectively, exhibited XRD patterns

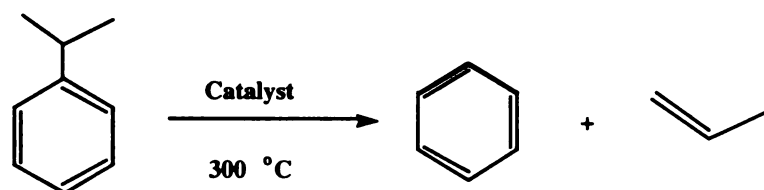


Table 1.4 Cumene Conversions (%) at 300 °C

Catalyst	Al-MCM-41	PNA-1	Al-HMS	PNA-2	ZSM-5
20 min	14.7	41.3	24.8	47.6	95.1
3 hr.	13.6	37.5	26.8	42.4	93.7

characteristic of Al-MCM-41 and Al-HMS, but reflections characteristic of ZSM-5 were absent. An FTIR band at 550-560 cm^{-1} in both products was considered to be indicative of unit cells of ZSM-5 highly dispersed in the mesostructure framework. Further evidence for the presence of entrapped ZSM-5 unit cells was provided by the acid catalytic activity of NPA-1 and NPA-2 toward cumene cracking. As can be seen from the cumene conversions listed in Table 1.4, the acid catalytic activity of the modified mesostructures is substantially greater than the parent mesostructures. It is especially

noteworthy that PNA-2, obtained by modification of Al-HMS, is more active than the PNA-1 product derived from Al-MCM-41. The superior activity of Al-HMS and NPA-2 relative to Al-MCM-41 and NPA-1 may again be attributed to the intrinsically more efficient access to framework catalytic sites for HMS derivatives.

1.5. References

1. Beck, J.S.; Vartuli, J.C.; Roth, W.J.; Leonowicz, M.E.; Kresge, C.T.; Schmit, K.D.; Chu, C.T.-W.; Olson, D.H.; Sheppard, E.W.; McCullen, S.B.; Higgins, J.B.; Schlenker, J.L. *J. Am. Chem. Soc.* **1992**, *114*, 10834.
2. Inagaki, S.; Fukushima, Y.; Kuroda, K. *Chem. Commun.* **1993**, 680.
3. Huo, Q.; Margolese, D.I.; Ciesla, U.; Feng, P.; Gier, T.E.; Sieger, P.; Leon, R.; Petroff, P.M.; Schüth, F.; Stucky, G.D. *Nature* **1994**, *368*, 317.
4. Lu, Y.; Ganguli, R.; Drewien, A.C.; Anderson, M.T.; Brinker, C.J.; Gong, W.; Guo, Y.; Soyez, H.; Dunn, B.; Huang, M.H.; Zink, J.I. *Nature* **1997**, *389*, 364.
5. Zhao, D.; Feng, J.; Huo, Q.; Melosh, N.; Fredrickson, G.H.; Chmelka, B.F.; Stucky, G.D. *Science* **1998**, *279*, 548.
6. Tanev, P.T.; Chibwe, M.; Pinnavaia, T.J. *Nature* **1994**, *368*, 321.
7. Tanev, T.P.; Pinnavaia, T.J. *Science* **1995**, *267*, 865.
8. Bagshaw, S.A.; Prouzet, E.; Pinnavaia, T.J. *Science*, **1995**, *269*, 1242.
9. Kim, S-S.; Zhang, W.; Pinnavaia, T.J. *Science* **1998**, *282*, 1302.
10. Antonelli, D.M.; Ying, J.Y. *Angew. Chem., Int. Ed. Engl.*, **1996**, *35*, 426.
11. Attard, G.S.; Glyde, J.C.; Goltner, C.G. *Nature* **1995**, *378*, 366.
12. Bagshaw, S.A.; Pinnavaia, T.J. *Angew. Chem. Int. Edn. Engl.* **1995**, *34*, 2014.
13. Antonelli, D.M.; Ying, J.Y. *Angew. Chem. Int. Edn. Engl.* **1995**, *34*, 2014.
14. Yang, P.; Zhao, D.; Margolese, D.I.; Chmelka, B.F.; Stucky, G.D. *Nature* **1998**, *396*, 152.
15. Attard, G.S.; Bartlett, P.N.; Coleman, N.R.B.; Elliott, J.M.; Owen, J.R.; Wang, J.H. *Science* **1997**, *278*, 838.
16. Huang, Y.; McCarthy, T.J.; Sachtler, W.M. *Appl. Catal. A.* **1996**, *148*, 135.

17. Huo.
P.: Fi
1176.
18. Yada.
19. Chen.
20. Sever
21. Monn
Stucky
B.F. S
22. Zhang
23. Ryoo.
24. Zhang
25. Masch
26. Kim, S
27. Liu, L.
28. Mehne
29. Mercie
30. Feng.
1997.
31. Notari
32. Zhang
Chem.
33. Reddy
34. Reddy
35. Sayari
36. Reddy
37. Zhang
1996.
38. On, T.
1997.

17. Huo, Q.; Margolese, D. I.; Ciesla, U.; Demuth, D. G.; Feng, P.; Gier, T. E.; Sieger, P.; Firouzi, A.; Chmelka, B. F.; Schüth, F.; Stucky, G. D. *Chem. Mater.* **1994**, *6*, 1176.
18. Yada, M.; Machida, M.; Kijima, T. *Chem. Commun.* **1996**, 769.
19. Chen, C.-Y.; Li, H.-X.; Davis, M.E. *Microporous Mater.* **1993**, *2*, 17.
20. Severin, K.G.; Abdel-Fattah, T.M.; Pinnavaia, T.J. *Chem. Commun.* **1998**, 1471.
21. Monnier, A.; Schuth, F.; Huo, Q.; Kumar, D.; Margolese, D.; Maxwell, R.S.; Stucky, G.D.; Krishnamurty, M.; Petroff, P.; Firouzi, A.; Janicke, M.; Chmelka, B.F. *Science* **1993**, *261*, 1299.
22. Zhang, W.; Pinnavaia, T.J. *Catal. Lett.* **1996**, *38*, 261.
23. Ryoo, R.; Kim, J.M.; Shin, C.H.; Lee, J.Y. *J. Phy. Chem.* **1996**, *100*, 17718.
24. Zhang, W.; Pauly, T.R.; Pinnavaia, T.J. *Chem. Mater.* **1997**, *9*, 2491.
25. Maschmeyer, T.; Rey, F.; Sankar, G.; Thomas, J.M. *Nature* **1995**, *378*, 159.
26. Kim, S-S.; Zhang, W.; Pinnavaia, T.J. *Catal. Lett.* **1997**, *43*, 149.
27. Liu, L.J.; Yu, W.Y.; Li, S.G.; Che, C.M. *J. Organ. Chem.* **1998**, *63*, 7364.
28. Mehnert, C.P.; Ying, J.Y. *Chem. Commun.* **1997**, 2215.
29. Mercier, L.; Pinnavaia, T.J. *Adv. Mater.* **1997**, *9*, 500.
30. Feng, X.; Fryxell, G.E.; Wang, L.-Q.; Kim, A.Y.; Liu, J.; Kemner, K.M. *Science* **1997**, *276*, 923.
31. Notari, B. *Adv. Catal.* **1996**, *41*, 253.
32. Zhang, W.; Fröba, M.; Wang, J.; Tanev, P.T.; Wong, J.; Pinnavaia, T.J. *J. Amer. Chem. Soc.* **1996**, *118*, 9164.
33. Reddy, K.M.; Moudrakovski, I.; Sayari, A. *Chem. Commun.* **1994**, 1059.
34. Reddy, J.S.; Sayari, A. *Chem. Commun.* **1995**, 2231.
35. Sayari, A. *Chem. Mater.* **1996**, *8*, 1840.
36. Reddy, J.S.; Liu, P.; Sayari, A. *Appl. Catal. A* **1996**, *148*, 7.
37. Zhang, W.; Wang, J.; Tanev, P.T.; Pinnavaia, T.J. *J. Chem. Soc., Chem. Comm.* **1996**, 979.
38. On, T.D.; Kapoor, M.P.; Joshi, P.N.; Bonneviot, L.; Kaliaguine, S. *Catal. Lett.* **1997**, *44*, 171.

39. Gontier, S.; Tuel, A. *Zeolites* **1995**, *15*, 601.
40. Gontier, S.; Tuel, A. *J. Catal.* **1995**, *157*, 124.
41. Tuel, A.; Gontier, S. *Chem. Mater.* **1996**, *8*, 114.
42. Abdel-Fattah, T.M.; Pinnavaia, T.J. *Chem. Commun.* 1996, 665.
43. Yang, R.T.; Pinnavaia, T.J.; Li, W.; Zhang, W. *J. Catal.* **1997**, *172*, 488.
44. Yue, Y.; Sun, Y.; Xu, Q.; Gao, Z. *Appl. Catal. A*: **1998**, *175*, 131.
45. Mokaya, R.; Jones, W. *Chem. Commun.* **1996**, 981.
46. Mokaya R.; Jones, W. *Chem. Commun.* **1996**, 983.
47. Mokaya, R.; Jones, W. *J. Catal.* **1997**, *172*, 211.
48. Kloetstra, K.R.; van Bekkum, H.; Jansen, J.C. *Chem. Commun.* 1997, 2281.
49. Corma, A. *Chem. Rev.* 1997, *97*, 2373.
50. Luan, Z.; Cheng, C.F.; He, H.; Klinowski, J. *J. Phys. Chem.* 1995, *99*, 10590.
51. Corma, A.; Fornés, V.; Navarro M.T.; Pérez-Pariente, J. *J. Catal.* **1994**, *148*, 569.
52. Hitz, S.; Prins, R. *J. Catal.* **1997**, *168*, 194.

Me
Temp
Pathw

Abstrac

He

textural

tempera

incorpor

and wal

anionic

S-I and

ionic sil

MAS N

(where S

degree o

for the c

isolated

along wi

independ

case of

crystallite

to framew

Chapter 2

Mesoporous Titanosilicate Molecular Sieves Prepared at Ambient Temperature by Electrostatic (S^+I^- , $S^+X^-I^+$) and Neutral (S^0I^0) Assembly Pathways : A Comparison of Physical Properties and Catalytic Activity for Peroxide Oxidations

Abstract

Hexagonal mesoporous titanosilicates with distinguishable framework charges and textural mesoporosity, namely, Ti-MCM-41 and Ti-HMS were prepared at ambient temperature by electrostatic and neutral assembly processes, respectively. Titanium incorporation at the 2 mol % level was accompanied by increases in lattice parameters and wall thickness, but the framework pore size remained unaffected. Cross-linking of anionic framework of as-synthesized Ti-substituted MCM-41 prepared by electrostatic S^+I^- and $S^+X^-I^+$ assembly pathways (where S^+ is a quaternary surfactant and I^- and I^+ are ionic silicon precursors) was enhanced significantly by Ti-substitution, as judged by ^{29}Si MAS NMR. The neutral framework of as-synthesized Ti-HMS formed by S^0I^0 assembly (where S^0 is a primary amine and I^0 is a neutral silicon precursor) exhibited the same high degree of cross-linking as the unsubstituted silica analog. UV-VIS and XANES spectra for the calcined forms of Ti-MCM-41 and Ti-HMS indicated: (i) the presence of site-isolated Ti species in the framework; (ii) predominantly tetrahedral coordination for Ti, along with some rehydrated five- and six-coordinated sites; (iii) Ti siting that was virtually independent of the framework assembly pathway. The exceptional catalytic activity in the case of Ti-HMS, especially toward larger substrates, was attributable to the small crystallite size and complementary textural mesoporosity that facilitates substrate access to framework Ti sites .

2.1 Intro

T

phase p

hydroxy

site-isol

coordin

small po

are limi

hexagon

surfacta

pore TS

MC

assembl

electros

rod-like

). The s

of the s

positive

a neutra

neutral S

orthosili

with neg

framewo

2.1 Introduction

Titanium silicalite-1 (denoted TS-1) is an effective active catalyst for the liquid phase peroxide oxidations of alcohols and alkanes ¹, the epoxidation of alkenes ² and the hydroxylation of aromatics ³. The activity of TS-1 arises from the presence of accessible, site-isolated Ti centers in the silicalite framework that are capable of undergoing a facile coordination change and forming an active peroxo-titanium complex ⁴. Because of the small pore size of the inorganic framework, the substrates that can be oxidized by TS-1 are limited to species having kinetic diameters $< 6 \text{ \AA}$. However, the recently reported hexagonal mesoporous silica molecular sieves prepared by electrostatic ^{5,6} and neutral ^{7,8} surfactant templating pathways offer promising opportunities for the preparation of large pore TS-1 analogs capable of transforming larger organic molecules.

MCM-41 silicas normally are prepared by one of two possible electrostatic assembly pathways. The S⁺I⁻ pathway originally utilized by Mobil researchers⁵ involves electrostatic interactions and charge matching between positively charged assemblies of rod-like micelles of quaternary ammonium surfactants (S⁺) and anionic silicate species (I⁻). The second pathway, the so-called counterion mediated S⁺X⁻I⁺ pathway ⁶, makes use of the same surfactant cations under strongly acidic conditions in order to assemble a positively charged silica precursors (I⁺). In contrast, HMS derivatives were prepared by a neutral S[°]I[°] assembly pathway that involves hydrogen bonding interactions between neutral S[°] primary amine surfactants and neutral I[°] inorganic precursors (e.g., tetraethyl orthosilicate) ⁷. The electrostatic assembly pathways afford as-synthesized materials with negatively charged framework walls, whereas neutral assembly yields *neutral* frameworks and walls that are characteristically thicker than those formed by electrostatic

assembly.

chemical pro

Corma

The catalyst

at 408 K. V

MCM-41 an

greater reac

reported on

the synthes

hydrotherm

concerning

assembled

In the

HMS catal

compare th

catalytic a

2.2 Exper

2.2.1 Mat

TS-1

by the me

orthotitana

assembly. These fundamental differences give rise to distinguishable physical and chemical properties for MCM-41 and HMS materials.

Corma *et al.* have reported the preparation and catalytic activity of Ti-MCM-41 ⁹. The catalyst was obtained by electrostatic S⁺I⁻ assembly under hydrothermal conditions at 408 K. We reported the *ambient temperature* preparation of S⁺X⁻I⁺ - assembled Ti-MCM-41 and S⁺I⁺ assembled Ti-HMS catalysts ¹⁰ and found preliminary evidence for greater reactivity for the Ti-HMS derivative. More recently, several other groups have reported on the preparation and catalytic properties of Ti-MCM-41. ¹¹⁻¹⁵ In all instances the syntheses were accomplished using exclusively the S⁺I⁻ assembly pathway ⁵ under hydrothermal conditions at temperatures above 373K. Thus, relatively little is known concerning the catalytic activities of titanium-substituted mesoporous molecular sieves assembled at ambient temperature by electrostatic assembly pathways.

In the present work we investigate the assembly of mesoporous Ti-MCM-41 and Ti-HMS catalysts *via* electrostatic and neutral assembly processes at *ambient temperature*, compare the physical properties of these products, and elucidate the differences in their catalytic activities for the peroxide oxidations of large organic molecules.

2.2 Experimental

2.2.1 Materials

TS-1 with an analytically determined titanium loading of 2 mol % was synthesized by the method of Taramasso *et al.* ³. Tetraethyl orthosilicate (TEOS), tetraisopropyl orthotitanate (TIPOT) and tetrapropylammonium hydroxide (TPAOH) were used as a

source

reactio

accom

hund

T

% w

as a

respe

used

were

asse

(CT

solu

stirr

hyd.

Si :

coun

orde

typic

addit

pathw

excess

acidic

source of silica, titanium and template, respectively. The molar composition of the reaction mixture was 0.022 Ti : 1.0 Si : 0.35 TPAOH : 35 H₂O. The synthesis was accomplished by placing the reaction mixture in an autoclave and heating at 443 K for 48 h under static conditions.

Ti-MCM-41 and Ti-HMS derivatives with equivalent titanium loadings (i.e., ~2 mol %) were prepared using deionized colloidal silica or TEOS as the source of silica, TIPOT as a titanium precursor, and long chain alkylammonium or alkylamine surfactants, respectively, as templates. In contrast to the hydrothermal reaction conditions normally used to prepare Ti-MCM-41 (i.e. autoclaving above 373 K), our Ti-MCM-41 catalysts were prepared by *ambient temperature synthesis* via electrostatic S⁺I⁻ and S⁺X⁻I⁺ assembly. In both of these electrostatic pathways cetyltrimethylammonium cations (CTMA⁺) served as the template. For S⁺I⁻ assembly, a deionized 34 wt % colloidal silica solution (Aldrich) and TIPOT were added to a solution of template under vigorous stirring and the pH of the reaction mixture was adjusted to 12 with tetramethylammonium hydroxide (TMAOH). The molar composition of the reaction mixture was 0.020 Ti : 1.0 Si : 0.50 CTMA⁺ : 1.0 TMAOH : 160 H₂O. The preparation of Ti-MCM-41 by the counterion-mediated pathway (S⁺ X⁻I⁺) utilized strongly acidic conditions (pH=1.5) in order to generate and assemble positively charged silicon species from TEOS. In a typical preparation the template was dissolved in acidic aqueous solution followed by the addition of a TEOS/TIPOT solution. A higher Ti : Si gel ratio of 1:10 was used for this pathway in order to prepare a product with the desired Ti:Si ratio of 2 : 98. The use of excess Ti for this preparation was necessitated by the high solubility of Ti under strongly acidic conditions. The composition of the reaction mixture was 0.10 Ti : 1.0 Si : 0.20

CTMA+ :

aged unde

product.

Ti-HN

(DDA) as

TEOS/TiH

vigorous

0.20 DD:

under vi

comparat

omitting

thorough

Com

of hexade

reference

coordinat

2.2.2 Ch.

The

Rigaku F

($\lambda=1.542$

mode with

CTMA⁺ : 1.0 HCl : 160 H₂O. For both electrostatic pathways, the reaction mixture was aged under vigorous stirring for 24 h in order to obtain the crystalline Ti-MCM-41 product.

Ti-HMS was synthesized via a neutral S⁰I⁰ templating pathway using dodecylamine (DDA) as the surfactant and ethanol (EtOH) as a co-solvent. In a typical preparation the TEOS/TIPOT solution was added to the solution of DDA in water and ethanol under vigorous stirring. The molar composition of the reaction mixture was 0.022 Ti : 1.0 Si : 0.20 DDA : 9.0 EtOH : 160 H₂O. The reaction mixture was aged at ambient temperature under vigorous stirring for 24 h in order to obtain the crystalline product. For comparative purposes we have also prepared pure silica MCM-41 and HMS samples by omitting the Ti source in the above preparations. All samples were filtered, washed thoroughly with water, dried at ambient temperature and calcined at 923 K for 4 h.

Commercially available samples of MgTiO₃, anatase, rutile, neptunite and a sample of hexadecaphenyl-octasiloxo-spiro-(9, 9)-titanate (denoted spiro-titanate ¹⁶) were used as reference materials for XANES analysis. Spiro-titanate contains Ti atoms tetrahedrally coordinated to four siloxy oxygens ¹⁷.

2.2.2 Characterization

The powder X-ray diffraction (XRD) patterns of all samples were measured on a Rigaku Rotaflex diffractometer equipped with a rotating anode and Cu-K_α radiation ($\lambda=1.542 \text{ \AA}$). In general, the diffraction data were collected by using a continuous scan mode with a scan speed of 2 degrees (2 Θ)/min.

state

the s

deter

U

UV-V

reflec

meas

transf

spectu

T

Labor

beam

reduc

detun

that in

the m

(4966

using

0.5 s a

for ab

functi

norma

^{29}Si -MAS NMR spectra were measured at 79.5 MHz on a Varian VXR-400S solid state NMR spectrometer equipped with a magic angle spin probe. For each measurement the samples were placed in zirconia rotors and spun at 4.2 kHz. The quantitative determination of Q², Q³ and Q⁴ sites was accomplished by deconvolution of the spectra.

UV-VIS spectroscopic measurements were carried out on a Shimadzu UV-3101PC UV-VIS-NIR Scanning Spectrophotometer equipped with an integrating sphere. A reflection mode with a resolution of 10 nm and BaSO₄ reference were used for the measurements. The collected relative reflection intensity ($R_{\infty}=R_{\text{sample}}/R_{\text{reference}}$) was transformed into $F(R_{\infty})$ by using Kubelka-Munk function $F(R_{\infty})=(1-R_{\infty})^2/(2R_{\infty})$ ¹⁸. All spectra were plotted in terms of $F(R_{\infty})$ versus wavelengths.

The X-ray absorption spectra were recorded at the Stanford Synchrotron Radiation Laboratory with a SPEAR storage ring operating at 3 GeV and 50-100 mA. Wiggler beam line 10-2 was used with a Si-(220) double-crystal monochromator. In order to reduce contributions from higher harmonics the second monochromator crystal was detuned to 50% of the maximum intensity. The slit before the monochromator as well as that in front of the first ion chamber was set to 1 mm height. The energy calibration of the monochromator was checked between every two spectra by measuring the Ti-K edge (4966 eV) of a Ti metal foil reference. All spectra were recorded at room temperature using a continuous-scan technique (QEXAFS)¹⁹. The counting time per data point was 0.5 s and the distance between data points was 0.1 eV²⁰. The pre-edges were normalized for absorbance by fitting the spectral region from 4900 to 4950 eV with a Victoreen function and subtracting it as background absorption. In addition, all spectra were normalized for atomic absorption by using the average absorption coefficient of the

region from

pre-edge pe

XANES spe

symmetric p

pre-edge an

the micro- a

using a Ster

were measu

filled with a

N₂ ads

Omnisorp 3

measuremen

distributions

2.2.3 Cataly

The ca

oxidation o

benzaldehy

were perfor

condenser a

10 mmol o

amount of 3

40 mmol H

region from 5050 to 5150 eV. The normalization was performed in order to compare the pre-edge peak intensities, energy positions and peak widths. The normalized Ti K-edge XANES spectra in the energy range of 4960 to 4980 eV were fitted using a series of symmetric profile functions. Lorentzian and Gaussian functions were used for fitting the pre-edge and the ascending absorption edge features, respectively. The XANES data of the micro- and mesoporous titanosilicates were collected in the fluorescence-yield mode, using a Stern-Heald type detector filled with Ar gas ²¹, whereas all reference compounds were measured in a transmission mode using two ion chambers. The first chamber was filled with a mixture of He and N₂ (ratio 2:1) and the second only with N₂.

N₂ adsorption-desorption measurements were carried out at 77K on a Coulter Omnisorp 360CX Sorptometer using a continuous flow measurement mode. Prior measurements samples were outgassed at 423K and 10⁻⁶ Torr for 12 h. The pore size distributions were calculated by the method of Horvath-Kawazoe ²².

2.2.3 Catalytic experiments

The catalytic performance of all samples was tested for the liquid phase peroxide oxidation of: (i) methyl methacrylate (MMA) to methyl pyruvate, (ii) styrene to benzaldehyde, and (iii) 2,6-di-*tert*-butyl phenol (2, 6-DTBP) to quinones. All reactions were performed under vigorous stirring in a three-neck glass flask equipped with condenser and thermometer. The oxidation of MMA and styrene was carried out using 10 mmol of substrate, 30 mg of catalyst, and 10 ml of acetonitrile as a solvent. The amount of 30 wt % H₂O₂, the reaction temperature, and reaction time were as follows: (i) 40 mmol H₂O₂, 321 K and 6 h, respectively for MMA oxidation, and (ii) 20 mmol

H₂O

how

mm

prod

a FI

meth

and

2.3

2.3.

for

elec

min

mat

the

the

27-2

S+I

gene

S+I

to pre

H₂O₂, 321 K, and 3 h, respectively for styrene oxidation. For 2,6-DTBP oxidation, however, 10 mmol of substrate, 100 mg of catalyst, 10 ml of acetone as a solvent, and 30 mmol 30 wt % H₂O₂ were used, and the reaction was carried out at 335 K for 2 h. The products were analyzed by means of a GC equipped with a SPB-20 capillary column and a FID. The reaction products were confirmed by GC-MS analysis. The internal standard method was used for quantitative analysis of the products. The conversion of substrate and selectivities to the products were calculated through carbon balance.

2.3 Results and Discussion

2.3.1 Synthesis

A major objective of this study was to elucidate the structure-reactivity relationships for mesoporous MCM-41 and HMS titanosilicates prepared at ambient temperature by electrostatic and neutral surfactant templating pathways, respectively. In order to minimize the number of compositional and structural variables for these two classes of materials and to focus on potential differences in local Ti siting by XANES spectroscopy, the *ambient temperature* synthesis was performed in such a way that the Ti loading for the two classes of materials was 2 mol % and the framework-confined mesopore size was 27-29 Å. Cetyltrimethylammonium cations were used as templating surfactant for both S⁺I⁻ and S⁺X-I⁺ electrostatic preparations.

The *ambient temperature* synthesis of Ti-HMS materials by the neutral S[°]I[°] approach generally affords materials with larger framework-confined pores than the corresponding S⁺I⁻ or S⁺X-I⁺ pathways with surfactants of the same alkyl chain lengths. Thus, in order to prepare Ti-HMS with an average pore size of 27 Å, we selected a primary amine

template with

was accompl

2.3.2 Chara

(a) XR

catalysts pre

Table 2.1

Temperatu

Ti:S

a The uni
FWT is the
K) pore si
estimated a
 V_{fr} was de
The volum
The data in

template with shorter alkyl chain, namely, dodecylamine. In all cases, template removal was accomplished by calcination in air at 923 K for 4 hr.

2.3.2 Characterization

(a) **XRD.** Table 2.1 summarizes the properties of the Ti-MCM-41 and Ti-HMS catalysts prepared by different templating pathways. Included in the Table for

Table 2.1 Properties of Ti-substituted Mesoporous Silicas Prepared by Ambient Temperature Synthesis Using Different Templating Pathways

Parameter ^a	MCM-41 (S+I)	MCM-41 (S+X-I)	HMS (S ^o P)
Surfactant	C ₁₆ H ₃₃ N(CH ₃) ₃ ⁺	C ₁₆ H ₃₃ N(CH ₃) ₃ ⁺	C ₁₂ H ₂₅ NH ₂
Ti:Si ratio (mol):			
Initial gel	2.0:98	10:90	2.2:97.8
Calcined product	2.2:97.8	2.5:97.5	2.4:97.6
d ₁₀₀ (Å)	38.1 (36.0) ^b	36.5 (33.0)	40.2 (36.0)
Unit cell (Å)	44.0 (41.5)	42.5 (38.1)	46.4 (41.5)
Δ (Å)	4.1 (8.5)	5.6 (9.6)	0 (3.0)
H-K pore size (Å)	29 (28)	27 (26)	27 (26)
FWT (Å)	15 (12)	15 (12)	19 (15)
SBET (m ² /g)	859 (923)	1354 (1345)	1075 (1108)
V _{total} (cm ³ /g)	0.70 (0.72)	0.92 (0.95)	1.40 (1.42)
V _{fr} (cm ³ /g)	0.68 (0.70)	0.90 (0.92)	0.68 (0.70)
V _{tx} (cm ³ /g)	0.02 (0.02)	0.02 (0.03)	0.72 (0.72)
V _{tx} /V _{fr}	0.03 (0.03)	0.02 (0.03)	1.06 (1.03)

^a The unit cell parameter = $2d_{100}\sqrt{3}$ and Δ is the unit cell contraction upon calcination. FWT is the framework wall thickness obtained by subtracting the Horvath-Kawazoe (H-K) pore size from the unit cell parameter. The total liquid pore volume V_{total} was estimated at a relative pressure of 0.95. The volume of framework confined mesopores, V_{fr}, was determined from the upper inflection point of the corresponding adsorption step. The volume for textural porosity, V_{tx}, was obtained from the equation $V_{tx} = V_{total} - V_{fr}$. The data in parenthesis are for the pure silica analogs.

comparison are

parentheses).

essentially comp

the S⁺X⁻I⁺ path

achieve a simil

(based on Si) fo

S⁺X⁻I⁺ pathway

All reaction

but Ti-MCM-4

parameters (cf.

samples prepar

could be attrib

framework syla

neutral templat

framework. V

mesoporous ma

electrostatic ter

surfactant-silica

interactions in

framework wal

framework. Th

strongly suggest

comparison are the structural parameters for the pristine silicates (the values in parentheses). It should be noted that both S⁺I⁻ and S^oI^o pathways, allow for the essentially complete incorporation of the Ti in the product at the 2 mol % level, whereas the S⁺X-I⁺ pathway required a 4-fold excess of Ti in the reaction mixture in order to achieve a similar Ti loading (2.5 mol%). In addition, the yields of crystalline product (based on Si) for the S⁺I⁻ and S^oI^o pathways were more than 85%, whereas that for the S⁺X-I⁺ pathway was only about 50%.

All reaction products exhibit similar d_{100} , unit cell parameters and H-K pore sizes but Ti-MCM-41 and Ti-HMS catalysts differ dramatically by their lattice contraction parameters (cf. Table 2.1). The significant lattice contraction exhibited by Ti-MCM-41 samples prepared by the electrostatic S⁺I⁻ and S⁺X-I⁺ pathways is not surprising and could be attributed to the cross-linking of the significant amount of non-fully condensed framework silanol groups upon calcination (see below). In contrast Ti-HMS prepared by neutral templating does not exhibit lattice contraction due to its more fully cross-linked framework. We have previously noted ^{7,23}, that the neutral S^oI^o pathway affords mesoporous materials with more fully cross-linked and thicker framework walls than the electrostatic templating pathways. We have attributed this phenomenon to the absence of surfactant-silica oligomer charge matching and silica-silica oligomer charge repulsive interactions in forming the framework walls. As shown by the data in Table 2.1 the framework wall thickness of all materials increases upon Ti incorporation into the framework. The changes in unit cell size and framework wall thickness (cf. Table 2.1) strongly suggest Ti incorporation in the walls of the mesoporous silicate framework. An



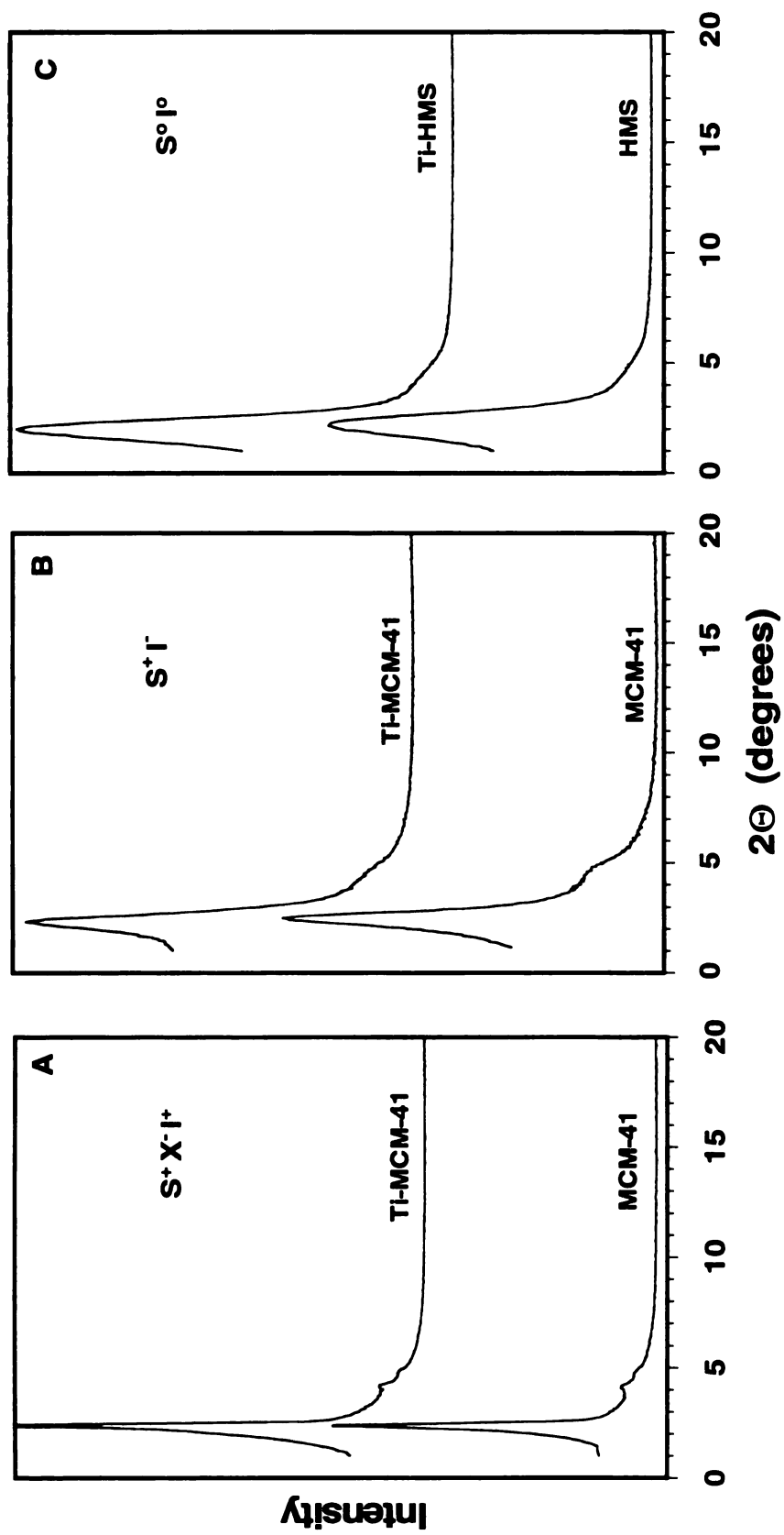


Figure 2.1 Powder XRD patterns for calcined pure and Ti-substituted (2 mol %) silica molecular sieves. (A) MCM-41 and Ti-MCM-41 prepared by S⁺X¹⁺ assembly and (B) MCM-41 and Ti-MCM-41 prepared by S⁺I⁺ assembly, and (C) HMS and Ti-HMS prepared by S⁺I⁺ assembly.

increa

incorp

It

substit

isother

produc

larger t

V_{ix} and

1.06 w

0.03. T

smaller

an imp

Fig

material

exhibit

with g

S-X-I-

narrow

MCM-

analog

HMS (

broaden

the amb

increase in the unit cell size parameter has been also noted ²⁴ to occur upon Ti incorporation into ZSM-5 frameworks.

It is noteworthy that the specific surface areas are very similar for the pure and Ti-substituted samples. On the basis of comparisons of the full N₂ adsorption-desorption isotherms (not shown), the most significant difference between the Ti-substituted products prepared by neutral and electrostatic templating pathways is in the substantially larger textural mesoporosity exhibited by the S^oP^o assembled Ti-HMS derivative (compare V_{tx} and V_{tx}/V_{fr} ratios in Table 2.1). Ti-HMS exhibits ratio of V_{tx}/V_{fr} mesoporosity of 1.06 whereas Ti-MCM-41 samples exhibit negligible small ratios in the range of 0.02-0.03. The enhanced interparticle mesoporosity of Ti-HMS, which is a consequence of the smaller particle size afforded by neutral surfactant templating, will be shown later to play an important role in liquid phase catalytic oxidation reactions of large organic molecules.

Figure 2.1 illustrates the XRD patterns of the calcined Ti-MCM-41 and Ti-HMS materials together with those for the corresponding pure silica analogs. All materials exhibit well-defined 100 reflections in their XRD patterns. Hexagonal mesostructures with greater long range order were obtained at ambient temperature conditions by the S⁺X⁻I⁺ pathway (Fig. 2.1 A). This is evidenced by the presence of additional relatively narrow 110 and 200 diffraction lines in the XRD patterns of pure and Ti-substituted MCM-41 samples. The diffraction patterns of the calcined Ti-MCM-41 and pure silica analog prepared by S⁺I⁻ pathway (Fig. 2.1 B) are very similar to these of HMS and Ti-HMS (Fig. 2.1 C). These patterns generally exhibit 100 reflections accompanied with broader unresolved higher order reflections. These results are not surprising in view of the ambient temperature conditions used for the synthesis and the lack of NaOH in our

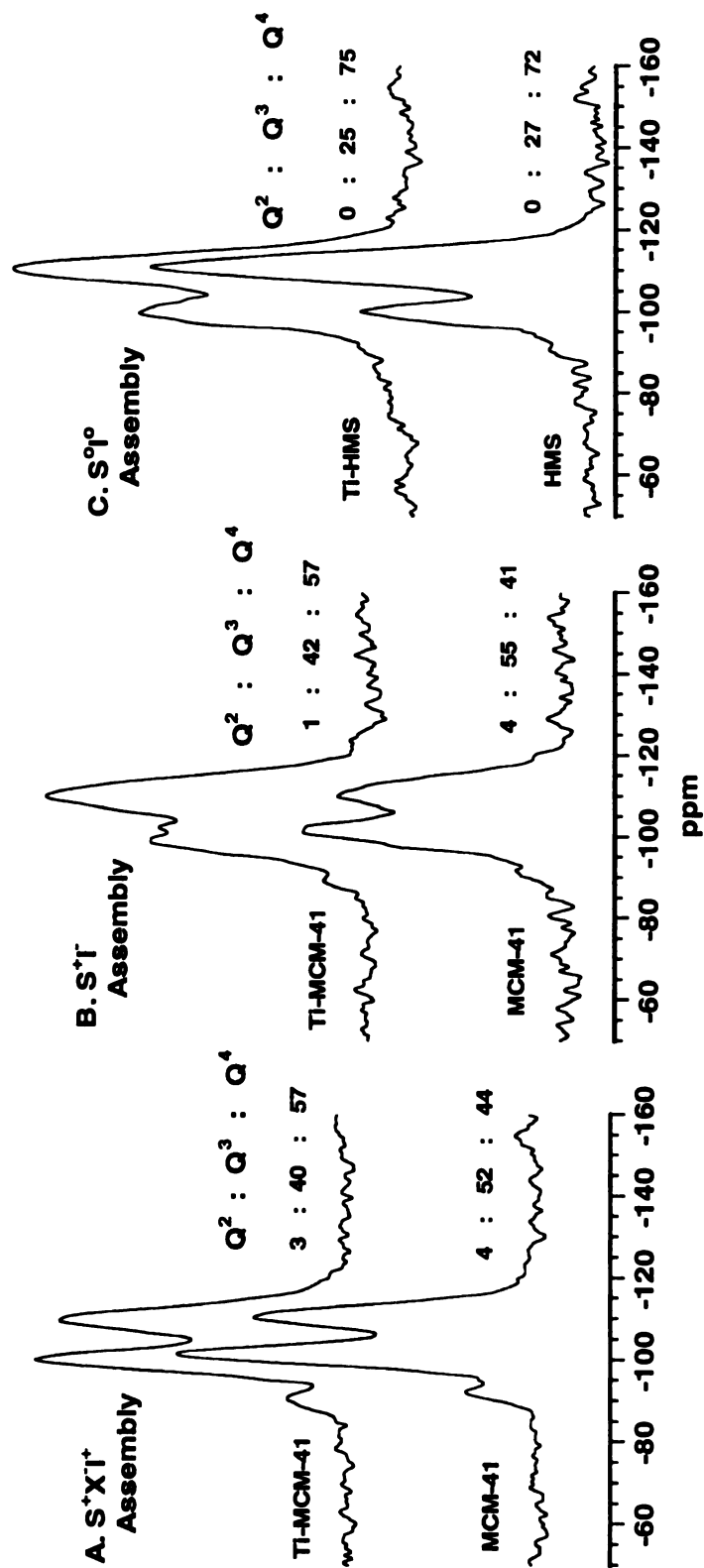


Figure 2.2 ²⁹Si-MAS NMR spectra of as-synthesized pure and Ti-substituted (2 mol %) silica molecular sieves: (A) MCM-41 and Ti-MCM-41 prepared by S⁺X⁺ assembly, (B) MCM-41 and Ti-MCM-41 prepared by S⁺T assembly, and (C) HMS and Ti-HMS prepared by S⁺O assembly.

S⁺I re

silica

assem

range

bondi

small

(b) ²

samp

temp

shifts

band

and

temp

inco

Fig

a m

Ti-s

imp

with

com

elect

incre

incre

S⁺I⁻ reaction mixtures. We observed similar lack of long range order for a series of pure silica MCM-41 materials prepared by ambient temperature synthesis by the S⁺I⁻ assembly pathway with surfactants of different alkyl chain lengths ²³. The lack of long range order exhibited by the HMS and Ti-HMS samples was attributed to the weak H bonding forces that govern the neutral S⁰I⁰ assembly process and to the corresponding small scattering domain sizes ⁷.

(b) ²⁹Si MAS NMR. Figure 2.2 shows the ²⁹Si MAS NMR spectra for *as-synthesized* samples of pure and Ti-substituted mesoporous molecular sieves prepared by ambient temperature S⁺I⁻, S⁺X-I⁺ and S⁰I⁰ assembly. In general, three bands centered at chemical shifts of -92, -100, and -110 ppm were observed for the MCM-41 derivatives. These bands can be attributed to Si(OSi)_x(OH)_{4-x} framework units where x=2 (Q²), x=3 (Q³) and x=4 (Q⁴), respectively. It is noteworthy that all *as-synthesized* electrostatically-templated pure and Ti-substituted MCM-41 samples exhibit a higher fraction of incompletely cross-linked Q² and Q³ framework units than the S⁰I⁰ HMS samples (see Figure 2.2). In addition, the *as-synthesized* pure and Ti-substituted HMS samples exhibit a much higher average ratio of Q⁴/(Q³+Q²) units (~2.8) than the *as-synthesized* pure and Ti-substituted MCM-41 samples prepared by electrostatic templating (~1.0). This implies that neutral templating allows for the preparation of mesoporous molecular sieves with more completely cross-linked frameworks. A noteworthy trend is observed by comparing the spectra of pure and Ti-substituted MCM-41 samples prepared by both electrostatic templating pathways. Significantly, Ti incorporation leads to a dramatic increase of the cross-linking of the MCM-41 framework. This is evidenced by the increase in fraction of Q⁴ sites at the expense of both Q² and Q³ framework sites. In the

case of HMS

significant d

framework.

An add

correspon

case of HMS, the increase of the fraction of Q^4 sites upon Ti incorporation is not as significant due to the much greater degree of cross-linking exhibited by the pure silica framework.

An additional consequence of Ti framework incorporation is the broadening of the corresponding Q^2 , Q^3 and Q^4 peaks in the ^{29}Si MAS NMR spectra. This broadening

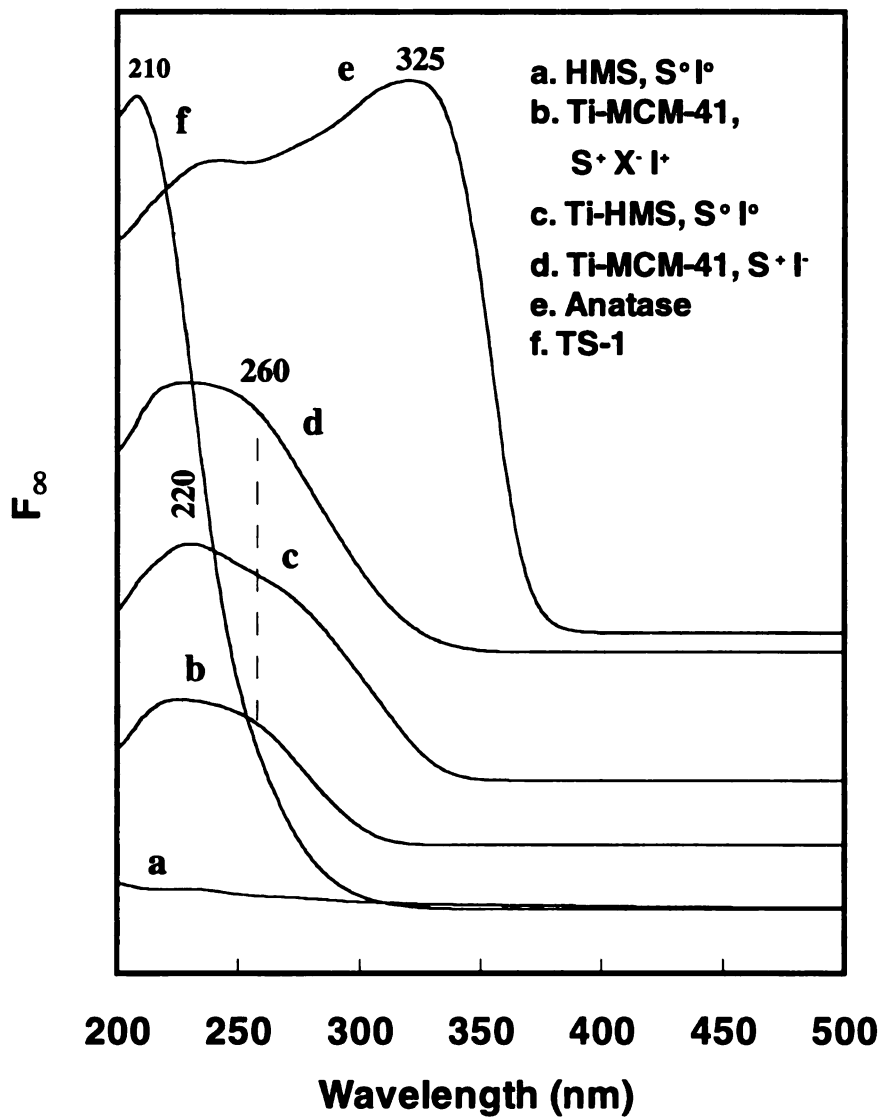


Figure 2.3 UV-VIS spectra of calcined Ti-containing materials.

could be attributed to the effect of the Ti sites on the chemical environment of the adjacent Si atoms.

(c) UV-VIS Diffuse Reflectance Spectroscopy. The incorporation of titanium into MCM-41 and HMS frameworks was further verified by UV-VIS diffuse reflectance spectroscopy. The corresponding spectra of the Ti-substituted samples are shown in Figure 2.3, along with those for TS-1, HMS and anatase. The spectrum for TS-1 shows an absorption band at 210 nm, whereas bulk titania (anatase) shows a band at 325 nm. The band at 210 nm was attributed to ligand-to-metal charge transfer associated with isolated Ti (IV) framework sites in tetrahedral coordination ²⁵. The broad absorption band centered at 325 nm is typical for ligand-to-metal charge transfer occurring in bulk titania. The spectra for the mesoporous Ti-MCM-41 and Ti-HMS derivatives lack the 330 nm band characteristic for segregated titania. This suggests that most of the Ti atoms in our Ti-MCM-41 and Ti-HMS samples occupy site-isolated positions in the silica framework.

The spectra for Ti-MCM-41 and Ti-HMS also are clearly different from the spectrum of the microporous TS-1. This is manifested by the much broader character of the absorption bands centered at 220 and 260-270 nm. The possibility of some Ti-O-Ti clustering in the framework cannot be unequivocally precluded as amorphous TiO₂/SiO₂ gels with various Ti content exhibit absorption bands in the intermediate range of 250-330 nm ⁴. However, the 220 nm band clearly signifies that much of the Ti is in site-isolated form. The slight shift and the increase in the width of the 220 nm band may be indicative of a Ti in a distorted tetrahedral environment or of the presence of Ti species in an octahedral coordination sphere.^{13,14} However, since there is very little shifting of the

band toward lower wavelengths upon thermal dehydration, we favor a distorted tetrahedral environment for most of the Ti sites in Tti-MCM-41 and Ti-HMS. The XANES data provided below verify this assignment. We believe that this distorted environment is a direct consequence of the amorphous character of the pore walls (i.e., a wide variety of Ti-O-Si bond angles).

According to several literature studies,²⁷ the absorption shoulder at 260-270 nm can be attributed to the presence of site-isolated Ti atoms in penta- or octahedral coordination. Similar UV-VIS behavior, indicative of a high fraction of higher coordinated Ti sites, also has been reported to occur upon hydration of TS-1²⁷. The presence of a significant fraction of Ti sites with coordination numbers higher than four in Ti-MCM-41 and Ti-HMS may be associated with the less crystallographic order in the pore walls, the much higher accessible surface area, and the larger mesopores. These later factors, most likely are responsible for the observed enhanced hydration of Ti sites in MCM-41 and HMS relative to silicalite-1.

It is important to note that the UV-VIS spectra of the electrostatically templated Ti-MCM-41 and Ti-HMS prepared by neutral templating are very similar and practically indistinguishable. This implies that the effect of the templating method on the Ti siting in Ti-MCM-41 and Ti-HMS samples prepared under ambient temperature conditions is negligible. Therefore, any differences in the catalytic behavior of these materials may not be attributed to intrinsic differences in Ti-siting.

(d) X-Ray absorption. In order to better elucidate the nature of the Ti-sites in mesoporous Ti-MCM-41 and Ti-HMS samples we have performed Ti K-edge XANES measurements²¹. For comparison purposes we have also obtained Ti K-edge

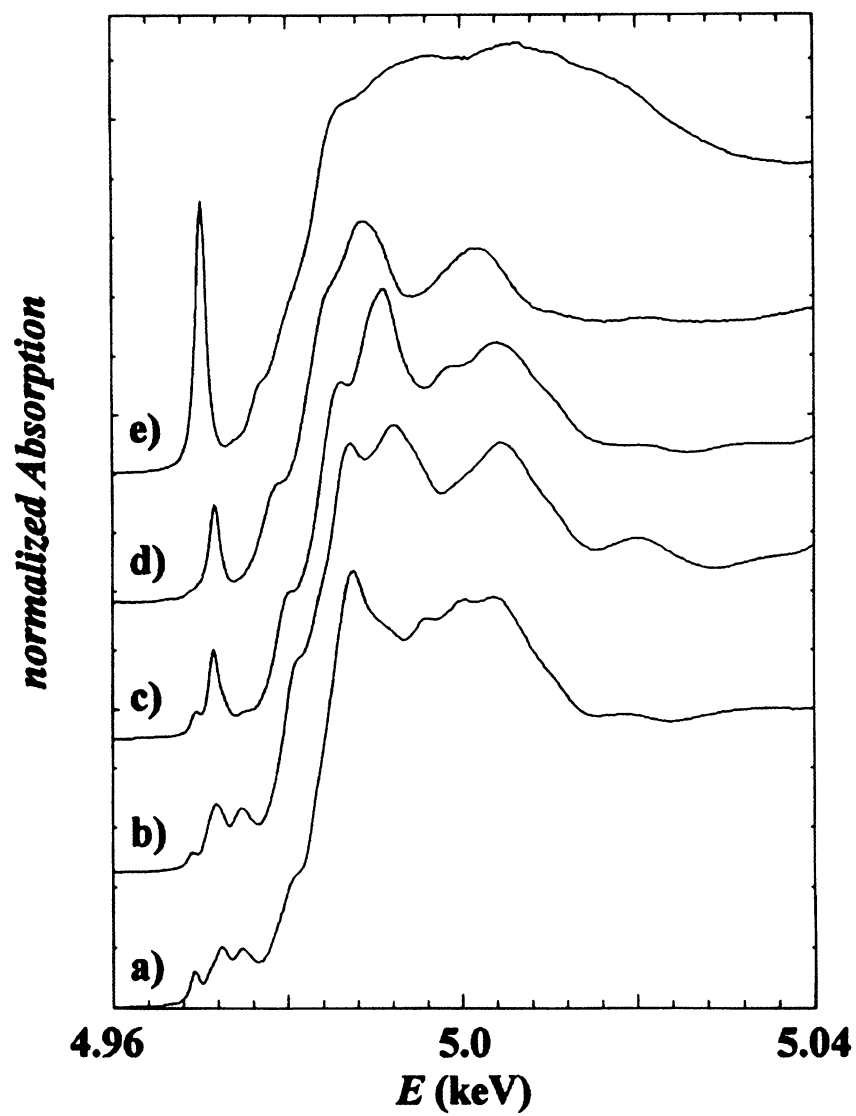


Figure 2.4 Ti K-edge XANES spectra of reference compounds containing Ti in tetrahedral and octahedral oxygen environments: (a) anatase, (b) rutile, (c) $MgTiO_3$, (d) neptunite, and (e) spirotitanate.

1
2
3
4
5
6
7
8
9
10
11
12
13
14
15
16
17
18
19
20
21
22
23
24
25
26
27
28
29
30
31
32
33
34
35
36
37
38
39
40
41
42
43
44
45
46
47
48
49
50
51
52
53
54
55
56
57
58
59
60
61
62
63
64
65
66
67
68
69
70
71
72
73
74
75
76
77
78
79
80
81
82
83
84
85
86
87
88
89
90
91
92
93
94
95
96
97
98
99
100

Table 2.2 Ti K-edge XANES Results for Ti-Containing Materials ^a

Sample	position (eV)	normalized height	FWHM ^b (eV)
Spirotitanate	4970.2	0.95	0.87
rutile	4971.7	0.20	1.5
anatase	4972.1	0.15	1.7
MgTiO ₃	4971.5	0.27	0.8 ^b
neptunite	4971.6	0.33	1.2
TS-1 (2 % Ti)	4970.5	0.52	1.0
Ti-MCM-41 (S+I, 2 % Ti)	4970.7	0.30	1.3
Ti-MCM-41 (S+X-I+, 2.5 % Ti)	4970.7	0.31	1.3
Ti-HMS (S [°] I [°] , 2.4 % Ti)	4970.8	0.31	1.3

^aThe Ti K-edge XANES parameters were obtained by fitting the central pre-edge peak to a Lorentzian Function. ^bThe full width at half maximum, FWHM, is for the central pre-edge peak.

XANES spectra of reference compounds such as octahedrally coordinated anatase, rutile, MgTiO₃, distorted octahedrally coordinated neptunite, tetrahedrally coordinated spirotitanate and TS-1. Figure 2.4 shows the Ti K-edge XANES spectra of the reference compounds. All reference compounds with nearly octahedral Ti site symmetry exhibit multiple, low intensity pre-edge peaks in the region from 4960 to 4980 eV (cf., spectra a, b). Distortion of the octahedral geometry (inversion symmetry) leads to an increase in intensity of the central peak, as shown for neptunite ²⁸ (spectra c and d). In contrast, the spirotitanate with nearly regular tetrahedral geometry exhibits a single, very high

intensity pre-edge peak (spectrum e). These results (see Figure 2.4 and Table 2.2) are in good agreement with previous studies.²⁹⁻³² We may conclude, therefore, that tetrahedral Ti sites give a single, high intensity pre-edge peak, whereas Ti-sites in regular octahedral symmetry afford multiple, low intensity pre-edge peaks. Although tetrahedral and highly distorted octahedral Ti sites exhibit similar single pre-edge peak, the two environments clearly are distinguishable by means of peak intensity and position.

The Ti K-edge XANES spectra of the mesoporous Ti-MCM-41 and Ti-HMS samples prepared by electrostatic and neutral templating methods, respectively, are shown in Figure 2.5. Included for comparison is the spectrum for microporous TS-1. The following features are evident: (i) the spectra for all three samples are very similar and contain a sharp pre-edge peak, (ii) the energy position of the pre-edge peak for Ti-substituted MCM-41 and HMS is similar to that for TS-1 and spirotitanate, but different from the reference materials containing octahedral Ti (see Table 2.2), (iii) the two Ti-MCM-41 samples and Ti-HMS exhibit weaker pre-edge peaks that are slightly shifted toward higher energies and wider FWHM than those of TS-1 and spirotitanate, suggesting in addition to tetrahedral Ti the probable presence of some Ti higher coordination sites (see below); (iv) most significantly, the spectral parameters for calcined Ti-substituted MCM-41 and HMS molecular sieves prepared via different assembly pathways at ambient temperature are very similar and practically indistinguishable. These observations are also supported by our UV-VIS results and show that the Ti siting in mesoporous MCM-41 and HMS materials is independent of the templating pathway.

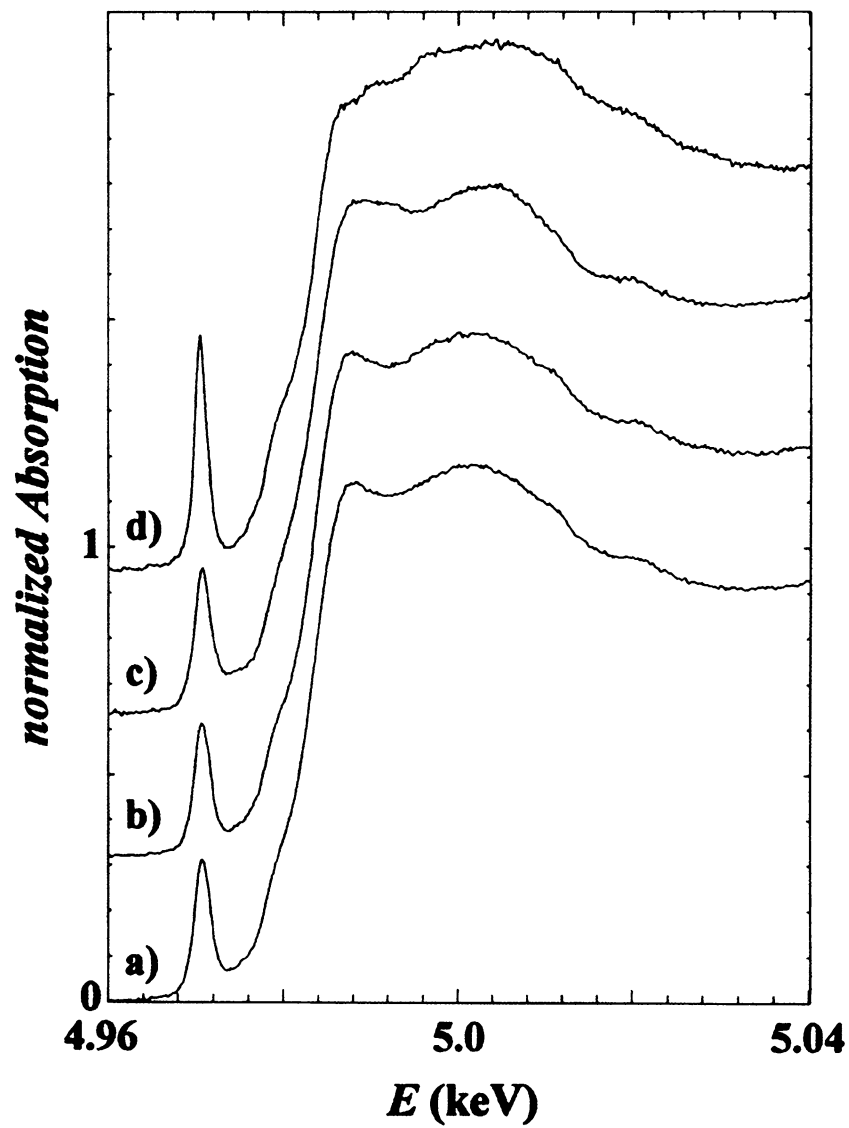


Figure 2.5 Ti K-edge XANES spectra of calcined (a) Ti-HMS prepared by $S^{\circ}T^{\circ}$ assembly, (b) Ti-MCM-41 prepared by $S^{+}XT^{+}$ assembly, (c) Ti-MCM-41 prepared by $S^{+}T$ assembly, and (d) TS-1.

Extending somewhat further our interpretation of the XANES data, we note that Farges *et al.* performed ab initio multiple-scattering calculations of the Ti K-edge XANES spectra for mixtures of reference compounds containing Ti atoms with various coordination.³³ For instance, they calculated that the normalized height of the central pre-edge peak varies from 0.6 to 1.0 for 4-fold Ti, from 0.4 to 0.7 for 5-fold Ti and from 0.05 to 0.27 for 6-fold Ti containing compounds. Besides the differences in intensity, the 4- and 6-fold Ti containing compounds were found to differ by energy position of the pre-edge peak. The energy position of the pre-edge peak for 6-fold Ti containing compounds was found to be shifted on average of 1.5 eV toward higher energies.³³ Thus, structures containing mixtures of 4-fold Ti with 5-fold or 6-fold coordinated Ti sites should exhibit pre-edge peaks with lower intensity that are slightly shifted toward higher energies. Therefore, the coordination state of Ti-sites in our Ti-MCM-41 and Ti-HMS materials may well be a mixture of 4-, 5- and 6-fold coordinations with tetrahedral coordination being in the majority. The higher coordination Ti-sites, are most likely generated through hydration of the tetrahedrally coordinated sites.

2.3.3 Catalytic results

Corma *et al.* have demonstrated⁹ that Ti-MCM-41 catalyzes the epoxidation of rather small organic molecules such as hex-1-ene and norbornene. We have reported that Ti-MCM-41 and Ti-HMS are very effective oxidation catalysts for bulky aromatic molecules that can not be converted over TS-1, such as 2, 6-DTBP¹⁰. More recently, several groups have elaborated on the preparation, characterization and catalytic activity of Ti-MCM-41¹¹⁻¹⁵ and Ti-HMS^{15,34}. All of the Ti-MCM-41 catalysts investigated to date were prepared by prolonged hydrothermal synthesis above 373 K using the

Table 2.3 Catalytic Activity of Ti-Substituted (2 Mol %) Molecular Sieves Prepared by Ambient Temperature Synthesis Using Different Templating Pathways.

Catalyst	MMA oxidation		Styrene oxidation			2,6-DTBP oxidation ^b		H ₂ O ₂ decomp.
	conv. (mol %)	select. (mol %)	PhCHO Select. (mol %)	Epoxide select. (mol %)	Diol select. (mol %)	conv. (mol %)	Quinone select. (mol %)	
TS-1	2.5	78	71	14	4.5	5	2.7	
Ti-MCM-41 (S ⁺ I ⁻)	4.0	93	82	6.2	3.8	39	3.8	
Ti-MCM-41 (S ⁺ X-I ⁺)	6.2	93	78	4.1	8.2	22	6.1	
Ti-HMS (S [°] I [°])	6.8	93	77	4.7	9.6	55	2.2	
Anatase	0	0	0	64	29	4.5	13	

^a MPV is methyl pyruvate. ^b Quinone selectivity was expressed as cumulative selectivity of monomer quinone and dimmer quinone. ^d H₂O₂ decomposition was determined by titration with 0.1 N KMnO₄ aqueous solution of a “blank” reaction mixture (without substrate) of 30 mg catalyst, 30 mmol 30 wt % H₂O₂ in 10 ml H₂O that has been subjected to heating at 321K for 2 h.

electrostatic S^+I^- pathway originally demonstrated by the pioneering work of Mobil ⁵. Here we compare the catalytic activity of Ti-MCM-41 and Ti-HMS samples prepared by *ambient temperature synthesis* using both S^+I^- and S^+X-I^- electrostatic templating pathways and the neutral S^0I^0 templating pathway, respectively. The catalytic performance of the samples was tested toward olefin and aromatic substrates of different size, such as the relatively small methyl methacrylate (MMA), styrene and the bulky 2,6-di-*tert*-butyl phenol (2,6-DTBP). The catalytic results are summarized in Table 2.3.

The mesoporous Ti-MCM-41 and Ti-HMS exhibit higher catalytic activity than microporous TS-1 for all reactions. The difference in catalytic activity between the mesoporous and microporous titanosilicates increases with increasing of the substrate size. The difference in catalytic activity is very small for the relatively small and elongated MMA molecule (2-2.5 times higher conversion for the mesoporous catalysts). However, as the substrate molecule becomes larger and more bulky (styrene and 2,6-DTBP) the difference becomes much more pronounced. Thus, the difference in catalytic activity among Ti-MCM-41, Ti-HMS and TS-1 reaches a maximum in the case of 2,6-DTBP (4 - 11 times higher conversion). This result is not surprising given the fact that the Ti-active centers are much more accessible in the larger mesopore size frameworks of Ti-MCM-41 and Ti-HMS. Due to the small micropore size of TS-1 ($\sim 6 \text{ \AA}$), the large 2,6-DTBP substrate can not penetrate into the framework pores and therefore can not be transformed (only 4.5 mol % conversion). On the other hand, anatase (bulk titania) was completely inactive for MMA and styrene oxidation. Its catalytic activity for the conversion of the large 2,6-DTBP is also negligible (only 4.5 mol %).

The oxidation of MMA proceeds with higher selectivity to methyl pyruvate (MPV) over Ti-MCM-41 and Ti-HMS, but the microporous TS-1 affords slightly higher selectivity to epoxide than Ti-MCM-41 and Ti-HMS (epoxide selectivity not included in Table 2.3). The tendency of TS-1 to oxidize olefins primarily to epoxides is well documented ³⁵. A similar trend also is observed for styrene oxidation. Generally, Ti-MCM-41 and Ti-HMS afford higher selectivity to diol, whereas more epoxide is produced over the microporous TS-1. The fact that the oxidation of MMA and styrene over Ti-MCM-41 and Ti-HMS proceeds selectively toward the alcohol derivative (through the epoxide intermediate) could be a consequence of the more hydrophilic nature of the amorphous pore walls.

Notari *et al.* have reported that bulk titania or substituted silicas containing Ti-O-Ti bonds are not suitable for catalytic peroxide oxidation reactions because they selectively decompose H₂O₂.⁴ The comparison of the results for the H₂O₂ decomposition over our samples reveals a very interesting trend (Table 2.3, last column). In accordance with Notari *et al.* our anatase sample affords 13 mol % decomposition of H₂O₂. Both TS-1 and Ti-HMS exhibit lower H₂O₂ peroxide decomposition activity, whereas Ti-MCM-41 samples prepared by electrostatic S⁺I⁻ and S⁺X⁻I⁺ templating methods exhibit a higher tendency to decompose H₂O₂. Especially noteworthy is the higher degree of H₂O₂ decomposition by Ti-MCM-41 prepared by the acidic counterion-mediated pathway S⁺X⁻I⁺. This result is probably related to the pronounced tendency of the acidic S⁺X⁻I⁺ pathway to impede incorporation of Ti atoms in the silicate framework. All of our syntheses involving the counterion-mediated pathway required at least a two to four-fold excess of Ti in the initial gel in order to achieve the desired Ti doping. It may be that the

strongly acid

mesoporous

A furth

exhibits acti

samples for

pronounced

2.1, Ti-MC

little or m

characteris

mesoporos

usually eq

These dif

molecular

XANES d

liquid pha

mesoporos

large organ

2.4 Conclu

Hexag

prepared a

approaches

neutral S²⁺

strongly acidic conditions used in the synthesis limit the incorporation of Ti atoms in the mesoporous framework.

A further comparison of the catalytic data reveals that $S^{\circ}I^{\circ}$ -assembled Ti-HMS exhibits activity superior to the electrostatically $S^{+}I^{-}$ and $S^{+}X^{-}I^{+}$ -assembled Ti-MCM-41 samples for all reaction systems. This enhanced activity for Ti-HMS is especially pronounced in the case of the large 2,6-DTBP. As shown by the data presented in Table 2.1, Ti-MCM-41 samples possess predominantly framework-confined mesoporosity and little or no significant textural mesoporosity.¹⁰ In contrast, Ti-HMS samples characteristically exhibit significant complementary textural or interparticle mesoporosity. The ratio of textural to framework-confined mesoporosity of Ti-HMS is usually equal or higher than 1, whereas that of Ti-MCM-41 is usually close to zero. These differences in catalytic behavior of Ti-HMS and Ti-MCM-41 mesoporous molecular sieves are not due to differences in Ti siting, as judged from UV-VIS and XANES data. We conclude, therefore, that the superior catalytic activity of Ti-HMS in liquid phase oxidations is most likely due to the presence of complementary textural mesoporosity that facilitates access of the framework-confined mesopores, especially by large organic substrates.

2.4 Conclusions

Hexagonal mesoporous titanosilicates containing 2 mol % Ti - substitution can be prepared at ambient temperature synthesis via three different surfactant templating approaches ($S^{+}I^{-}$, $S^{+}X^{-}I^{+}$, and $S^{\circ}I^{\circ}$). Electrostatic $S^{+}I^{-}$ assembly of Ti-MCM-41 and neutral $S^{\circ}I^{\circ}$ assembly of Ti-HMS allow for almost complete incorporation of Ti in the

mesoporous framework (at 2 mol % doping level), whereas electrostatic assembly of Ti-MCM-41 under acidic conditions via a counterion-mediated $S^+X^-I^+$ pathway impedes Ti incorporation. The incorporation of Ti in the anionic framework of MCM-41 materials and in the neutral framework of Ti-HMS mesopore frameworks is accompanied by an increase of the lattice parameter and the framework wall thickness. The framework mesopore size of the MCM-41 and HMS samples remains unaffected by the framework incorporation of Ti atoms. The degree of framework cross-linking of the electrostatic S^+I^- and $S^+X^-I^+$ -templated MCM-41 samples is significantly improved by Ti-substitution as judged from the ^{29}Si MAS NMR data. The UV-VIS and XANES results for calcined forms of Ti-MCM-41 and Ti-HMS provide evidence that: (i) Ti species are incorporated and site-isolated into the framework structure; (ii) Ti atoms are predominantly in a tetrahedral coordination, but there is the possibility of some Ti sites in five- or six-coordinated sites. (Higher coordinated Ti-sites most likely are generated by rehydration of some of the tetrahedrally coordinated sites), and (iii) the Ti siting for the S^+I^- and $S^+X^-I^+$ Ti-MCM-41 and for S^+I^- Ti-HMS are practically indistinguishable. This implies that the assembly pathway method has little or no effect on the Ti siting, at least when the Ti-MCM-41 and Ti-HMS samples are prepared at ambient temperature conditions.

A comparison of the catalytic results for the liquid phase peroxide oxidations of methyl methacrylate (MMA), styrene and 2,6-di-*tert*-butylphenol (2,6-DTBP) reveals that Ti-MCM-41 and Ti-HMS exhibit catalytic activities higher than TS-1 for all reactions. The difference in activity between the mesoporous molecular sieve catalysts and microporous TS-1 increases with increasing substrate size. The difference in activity is small for the relatively small MMA molecule, but as the substrate becomes larger, as

in styrene a

pronounced.

centers emb

Due to the

penetrate in

Ti-HMS ex

electrostatic

especially p

XANES da

be attribut

thicker fra

sites can n

structural

mesoporo

facilitates

enhancing

2.5 Refer

1. a.

E

2. C

3. T

4. N

5. a.

19

in styrene and, especially 2,6-DTBP, the difference in activity becomes much more pronounced. This result is not surprising given the much more accessible Ti-active centers embedded in the larger mesopore size frameworks of Ti-MCM-41 and Ti-HMS. Due to the small micropore size of TS-1 (~6 Å) the large 2,6-DTBP substrate can not penetrate into the framework pores and therefore can not be transformed. S^oP^o-assembled Ti-HMS exhibits greater catalytic activity than the Ti-MCM-41 materials assembled by electrostatic S⁺I⁻ and S⁺X⁻I⁺ pathways. The superior performance of Ti-HMS is especially pronounced in the case of the large 2,6-DTBP. On the basis of UV-VIS and XANES data, these differences in catalytic behavior of Ti-HMS and Ti-MCM-41 cannot be attributed to differences in Ti coordination environment. Because Ti-HMS has thicker framework walls than Ti-MCM-41, an enhancement in the fraction of surface Ti sites can not be responsible for the greater activity of Ti-HMS. The most distinguishing structural feature between Ti-HMS and Ti-MCM-41 is the greater inter-particle (textural) mesoporosity for Ti-HMS. This complementary textural mesoporosity most likely facilitates substrate transport and access of the framework-confined mesopores, thus enhancing the catalytic efficiency of Ti-HMS.

2.5 References

1. a. Huybrechts, D. R. C.; De Bruycker, L.; Jacobs, P. A. *Nature* **1990**, *345*, 240; b. Esposito, A.; Neri, C.; Buonomo, F. *US Patent* **1984**, 4,480,135.
2. Clerici, M. G.; Romano, U. *US Patent* **1990**, 4,937,216.
3. Taramasso, M.; Perego, G.; Notari, B. *US Patent* **1983**, 4,410,501.
4. Notari, B. *Stud. Surf. Sci. Catal.* **1988**, *37*, 413.
5. a. Kresge, C. T.; Leonowicz, M. E.; Roth W. J.; Vartuli, J. C.; Beck, J. S. *Nature* **1992**, *359*, 710; (b) Beck, J. S.; Vartuli, J. C.; Roth, W. J.; Leonowicz, M. E.;

- Kresg
McCu
1083-4
6. a. Hu
Petrof
Margo
Firouza
1176.
7. Tanev,
8. a. Attar
S. A.; P
9. Corma.
1994. 1-
10. a. Tane
Pinnava
Material
Eds.), 1
11. Franke.
Related
Weitkar
Elsevier
12. a. Sanka
Dent. A.
F.; Sanka
13. Blasco, T
14. Reddy. J
Synthesis
press.
15. Gontier, S
16. Zeitler, V.
17. Hursthouse

- Kresge, C.T.; Schmitt, K. D.; Chu, C. T-W.; Olson, D. H.; Sheppard, E. W.; McCullen, E. B.; Higgins, J. B.; Schlenker, J. L. *J. Am. Chem. Soc.* **1992**, *114*, 10834.
6. a. Huo, Q.; Margolese, D. I.; Ciesla, U.; Feng, P.; Gier, T. E.; Sieger, P.; Leon, R.; Petroff, P. M.; Schüth, F.; Stucky, G. D. *Nature* **1994**, *368*, 317; b. Huo, Q.; Margolese, D. I.; Ciesla, U.; Demuth, D. G.; Feng, P.; Gier, T. E.; Sieger, P.; Firouzi, A.; Chmelka, B. F.; Schüth, F.; Stucky, G. D. *Chem. Mater.* **1994**, *6*, 1176.
7. Tanev, P. T.; Pinnavaia, T. J. *Science* **1995**, *267*, 865.
8. a. Attard, G. S.; Glyde, J. C.; Göltner, C. G. *Nature* **1995**, *378*, 366; b. Bagshaw, S. A.; Prouzet, E.; Pinnavaia, T.J. *Science* **1995**, *269*, 1242.
9. Corma, A.; Navarro, M. T.; Perez-Pariente, T. *J. Chem. Soc. Chem. Commun.* **1994**, 147.
10. a. Tanev, P. T.; Chibwe, M.; Pinnavaia, T. J. *Nature* **1994**, *368*, 321; b. Pinnavaia, T. J.; Tanev, P. T.; Jialiang, W.; Zhang, W. in "Advances in Porous Materials" MRS Symp. Proc. Ser. (Sh. Komarneni, J. S. Beck and D. M. Smith, Eds.), **1995**, Vol. 371, p. 53, MRS, Pittsburgh.
11. Franke, O.; Rathousky, J.; Schulz-Ekloff, G.; Starek, J.; Zukal, A. in "Zeolite and Related Microporous Materials: State of the Art 1994, Stud. Surf. Sci. Catal." (J. Weitkamp, H. G. Karge, H. Pfeifer and W. Holderich, Eds.), **1994**, Vol. 84, p. 77, Elsevier Sci. BV, Amsterdam.
12. a. Sankar, G.; Rey, F.; Thomas, J. M.; Greaves, G. N.; Corma, A.; Dobson, B. R.; Dent, A. J. *J. Chem. Soc., Chem. Commun.* **1994**, 2279; b. Maschmeyer, T.; Rey, F.; Sankar, G.; Thomas, J. M. *Nature* **1995**, *378*, 159.
13. Blasco, T.; Corma, A.; Navarro, M. T.; Pariente, J. P. *J. Catal.* **1995**, *156*, 65.
14. Reddy, J. S.; Dicko, A.; Sayari, A. in "Third International Symposium on Synthesis of Zeolites and Expanded Layered Compounds" Anaheim, **1995**, in press.
15. Gontier, S.; Tuel, A. *J. Catal.* **1995**, *157*, 124.
16. Zeitler, V. A.; Brown, C. A. *J. Am. Chem. Soc.* **1957**, *79*, 4618.
17. Hursthouse, M. B.; Hossain, M. A. *Polyhedron* **1984**, *3*, 95.

18. Kortu

19. Frahi

20. Frahi

21. Lytl

C. L.

22. Hor

23. Tan

24. van

25. Boc

Can

26. Gor

27. a. C

109

199

Su

28. Ca

29. W

30. Be

J.

31. Y

F.

32. G

C.

33. Fa

C.

34. S.

Pe

Sn

35. Ku

199

18. Kortum, G. "Reflectance Spectroscopy", Springer-Verlag, New York, 1969.
19. Frahm, R. *Nucl. Instrum. Meth. Phys. Res.* **1988**, 270, 578.
20. Frahm, R.; Wang, J. *Jpn. J. Appl. Phys.* **1993**, 32, 188.
21. Lytle, F. W.; Gregor, R. B.; Sandstrom, D. R.; Marques, D. R.; Wong, J.; Spiro, C. L.; Huffman, G. P.; Huggins, F. E. *Nucl. Instrum. Meth.* **1984**, 226, 542.
22. Horvath, G.; Kawazoe, K. J. *J. Chem. Eng. Jpn.* **1983**, 16, 470.
23. Tanev, P. T.; Pinnavaia, T. J. *Chem. Mater.* **1996**, 8, 2068.
24. van Koningsveld, H.; Jansen, J. C.; van Bekkum, H. *Zeolite* **1990**, 10, 235.
25. Boccuti, M. R.; Rao, K. M.; Zecchina, A.; Leofanti, G.; Petrini, G. *Stud. Surf. Sci. Catal.* **1989**, 48, 133.
26. Gontier, S.; Tuel, A., *Zeolites* **1995**, 15, 601.
27. a. Geobaldo, C. F.; Bordiga, S.; Zecchina, A.; Giamello, E. *Catal. Lett.* **1992**, 16, 109; b. Bonneviot, L.; Trong On, D.; Lopez, A. *J. Chem. Soc., Chem. Commun.* **1993**, 685; c. Trong On, D.; Denis, I.; Lortie, C.; Cartier, C.; Bonneviot, L. *Stud. Surf. Sci. Catal.* **1994**, 83, 101.
28. Cannillo, E.; Mazzi, F.; Rossi, G. *Acta Cryst.* **1966**, 21, 200.
29. Waychunas, G. A. *Am. Min.* **1987**, 72, 89.
30. Behrens, P.; Felsche, J.; Vetter, S.; Schulz-Ekloff, Jaeger, N. I.; and Niemann, W. *J. Chem. Soc., Chem. Commun.* **1991**, 678.
31. Yarker, C. A.; Johnson, P. A. V.; Wright, A. C.; Wong, J.; Gregor, R. B.; Lytle, F. W.; Sinclair, R. N. *J. Non-Cryst. Solids* **1986**, 79, 117.
32. Gregor, R. B.; Lytle, F. W.; Sandstrom, D. R.; Wong, J.; Schultz, P. *J. Non-Cryst. Solids* **1983**, 55, 27.
33. Farges, F.; Brown Jr., G. E.; Navrotsky, A.; Gan, H.; Rehr, J. J. *Geochimica Cosmochimica Acta* 1995, submitted.
34. Sayari, A.; Karra, V. R.; Reddy, J. S.; Moudrakovski, I. L. in "Advances in Porous Materials" MRS Symp. Proc. Ser. (Sh. Komarneni, J. S. Beck and D. M. Smith, Eds.), **1995**, Vol. 371, p81, MRS, Pittsburgh.
35. Kumar, S. B.; Mirajkar, S. P.; Pais, G. C. G.; Kumar, P.; Kumar, R. *J. Catal.* **1995**, 156, 163.

Abstract

Wat

framework

neutral (S^{\ominus})

orthosilicate

= 90 : 10

textural por

mixture, w

textural po

with high

aggregate :

porosity w

shaped fun

differences

systems. T

the framew

observed w

modifying p

binding of

Chapter 3

Tailoring the Framework and Textural Mesopores of HMS Molecular Sieves Through an Electrically Neutral ($S^{\circ}I^{\circ}$) Assembly Pathway

Abstract

Water : ethanol solvent mixtures of differing polarity have been used to tailor the framework and textural mesopores of HMS molecular sieve silicas through an electrically neutral ($S^{\circ}I^{\circ}$) assembly pathway (S° = dodecyl or tetradecylamine; I° = tetraethyl orthosilicate). Mesostructure assembly from a water-rich solvent mixture, water : ethanol = 90 : 10 (v/v), afforded wormhole-like framework structures with a complementary textural pore volume equal in magnitude to the framework pore volume. An ethanol-rich mixture, water : ethanol = 35 : 65 (v/v), also formed wormhole-like frameworks, but the textural porosity was less than 20% of the framework pore volume. HMS derivatives with high textural porosity were comprised of mesoscale fundamental particles that aggregate into larger particles. In contrast, HMS mesostructures with low textural porosity were assembled into much larger aggregates of macroscale spheroid to disk-shaped fundamental particles. The differences in particle textures were attributed to differences in I° hydrolysis rates and $S^{\circ}I^{\circ}$ nucleation and growth rates in the two solvent systems. The presence of mesitylene in the reaction mixtures resulted in an expansion of the framework pores under water-rich conditions. Pore contraction, however, was observed with mesitylene present under ethanol-rich conditions. This versatile structure-modifying property of mesitylene in $S^{\circ}I^{\circ}$ assembly is explained by the solvent-dependent binding of the aromatic molecules to two structurally distinct and size-altering

“dissolved” and “adsorbed” states at the centers and interfacial surfaces of the surfactant micelle, respectively. Thus, both the framework and the textural pores of HMS silica can be readily tailored to the needs of a particular materials application through S^oI^o assembly by a judicious choice of an appropriate solvent and an auxiliary structure modifier.

2

g

T

m

p

co

ar

to

ch

no

hy

me

an

S+

an

sili

sili

sili

elec

41

imp

3.1 Introduction

The discovery of Mobil MCM-41 mesoporous molecular sieves¹ has stimulated great interest in the surfactant-directed assembly of mesostructures by sol-gel methods. Thus far, three general assembly pathways have emerged. First, the electrostatic charge matching pathway between cationic or anionic surfactant micelles and charged inorganic precursors. Among these, the so-called S⁺I⁻ and S⁻I⁺ pathways^{2,3} represent the most commonly encountered electrostatic assembly pathways. Counterion mediated S⁺X-I⁻ and S⁻M⁺I⁻ assembly processes, where surfactant and inorganic reagents are brought together at the micelle interface through triple ion interactions, represent extensions of the charge matching pathway³. The second pathway pairs neutral amine surfactants (S[°]) or nonionic polyoxyethylene surfactants (N[°]) with neutral inorganic precursors (I[°]) through hydrogen bonding at the S[°]I[°] or N[°]I[°] interface⁴⁻⁸. The third general assembly route to mesostructures exploits dative bond formation between donor groups on the surfactant and a metal acceptor centers in the inorganic precursor⁹.

The original synthesis of hexagonal MCM-41 silicas was accomplished through a S⁺I⁻ assembly mechanism using quaternary ammonium ions as the surfactant and silicate anions as the inorganic precursor¹. Related mesoporous structures, designated HMS silicas, have been obtained through S[°]I[°] assembly, wherein S[°] is an alkylamine and I[°] is a silicon alkoxide⁵. In general, surfactant removal from the neutral frameworks HMS silicas can be achieved by simple solvent extraction, whereas the displacement of the electrostatically bound surfactants from the anionic framework of as-synthesized MCM-41 requires proton exchange or destruction of the surfactant by combustion¹⁰. More importantly, there are significant structural differences between MCM-41 and HMS

silicas. MCM-41 derivatives typically exhibit three or more X-ray diffraction lines indicative of long range hexagonal channel packing. In contrast, HMS silicas show one or, at most, two broad X-ray peaks as a consequence of a small crystallite domain size and/or a much lower degree of channel packing order.

Although they are distinguishable with regard to structural ordering, MCM-41 and HMS molecular sieves both exhibit a sharp step in their nitrogen adsorption isotherms, corresponding to the presence of a regular mesoporous framework. Owing to the very small elementary particle size of many HMS derivatives, they can exhibit complementary textural mesopores, in addition to framework pores. The textural pore volumes for HMS can be up to 1.5 or more times as large as the framework pore volumes, whereas MCM-41 exhibits very little textural mesoporosity¹¹. The textural mesopores are important because they greatly facilitate mass transport to the framework mesopores. For this reason the catalytic reactivity of HMS is usually superior to MCM-41, especially for conversions involving large substrates in a liquid reaction medium where reaction rates are diffusion limited¹².

Another potential benefit of $S^{\circ}I^{\circ}$ assembly is the possibility of conducting mesostructure synthesis in media of diverse polarity. Unlike their ionic counterparts, S° and I° reagents are generally soluble in a wide range of solvents. Thus, solvation effects on the rates of hydrolysis and assembly might be an effective means of controlling structure. One of the objectives of the present study was to examine the possibility of tailoring both the framework and textural mesopores of HMS silicas by controlling the polarity of the reaction medium in which the assembly process is carried out. Our

approach m

nich and the

We

directing a

equilibrium

micelles¹³

structure

be of gr

materials

3.2 Expe

F

ethanol

tetraethy

and te

surfacta

under v

surfacta

tempera

ventilat

reaction

added t

All of t

approach makes use of two water : ethanol compositions to control polarity, one water-rich and the other ethanol-rich.

We also have investigated the role of mesitylene as an auxiliary structure-directing agent in both solvent systems. By using solvation effects to shift the equilibrium between structurally distinct binding states of mesitylene in the surfactant micelles¹³⁻¹⁵, we are able to effect an expansion or contraction of the framework pore structure of HMS. The ability to control both framework and textural mesoporosity can be of great value in designing HMS materials as catalysts, adsorbents and sensor materials.

3.2 Experiment

HMS molecular sieves were prepared by S^oI^o assembly pathways in water : ethanol solvent mixtures of differing composition and polarity. In both reaction media tetraethyl orthosilicate (TEOS) served as the neutral silica precursor and dodecylamine and tetradecylamine were the neutral structure director. In a typical synthesis the surfactant was dissolved in ethanol, and then the desired amount of water was added under vigorous stirring to obtain a homogeneous solution. TEOS was added to the surfactant solution and the mixture was allowed to react under stirring at ambient temperature for about 20 h. The reactions were carried out in an open beaker in a well ventilated hood to allow for some evaporation of solvent and concentration of the solid reaction products. When mesitylene was used as an auxiliary structure director, it was added to the surfactant solution and stirred for 15 minutes before the addition of TEOS. All of the HMS reaction products were filtered and dried in air. Although the surfactant

o
l
o
l
A
k
re
O
di
m

can be readily removed from HMS mesostructures by solvent extraction, there was no need to recover the surfactant from the small quantities of products formed in the present work. Consequently, the as synthesized products were directly calcined at 650 °C in air for 4 h to simultaneously remove the surfactant and dehydroxylate the framework.

For the purposes of probing the effect of solvent polarity on textural porosity, it was desirable to form HMS silicas from water-rich and ethanol-rich solutions with equivalent framework porosities. To achieve equivalent framework pore structures, we used reagent concentrations in the ethanol-rich system that were twice the concentrations for the water-rich medium. For HMS assembly in the relatively low polarity, ethanol - rich reaction medium, where water : ethanol volume ratio was 35 : 65 , the molar composition of the reaction mixture was 1.0 TEOS : 0.25 Surfactant : 18 EtOH : 34H₂O. For assembly in a relatively high polarity, water - rich solvent mixture, namely, 90 : 10 (v/v) water : ethanol, the molar composition was 1.0 TEOS : 0.25 Surfactant : 10 EtOH : 130 H₂O.

Powder X-ray diffraction patterns were measured using Cu-K α radiation ($\lambda=1.542$ Å) and a Rigaku Rotaflex diffractometer equipped with a rotating anode operated at 45 kV and 100 mA. The scattering and receiving slits were 1/6 degree and 0.3 degree, respectively.

N₂ adsorption and desorption isotherms at -196 °C were obtained on a Coulter Omnisorp 360CX Sorptometer operated under continuous adsorption mode. Pore size distributions were calculated from the N₂ adsorption branch using the Horvath-Kawazoe model.¹⁶

T

100CX

accelerat

estimate

high ma

about 30

suspensi

minutes.

sectionin

3.3 Resu

T

temperat

mesostru

The othe

: ethanol

structure

and the e

as an aux

Fi

silicas o

respective

surfactant

Transmission electron microscopy (TEM) studies were carried out on a JEOL 100CX instrument using an electron beam generated by a CeB₆ filament and an acceleration voltage of 120 kV. The resolution of the instrument was about 6 Å, as estimated by indirect measurement of the spherical aberration constant¹⁷ under medium-high magnification (i.e., 100,000X). Therefore, it was possible to resolve pores above about 30 Å. The specimens were prepared by dipping a carbon coated copper grid into a suspension (0.1 wt %) of mesoporous material in ethanol that was pre-sonicated for 10 minutes. Attempts to use thin-sectioned specimens were abandoned, because thin sectioning caused damage and loss of texture-pore information.

3.3 Results

Two versions of HMS silicas were prepared through S[°]I[°] assembly at ambient temperature in reaction media that differed in solvent polarity. In one reaction system the mesostructures were formed from a “water-rich” solution of 90 : 10 (v/v) water : ethanol. The other reaction medium was a less polar “ethanol-rich” solution of 35 : 65 (v/v) water : ethanol. Two S[°] surfactants, namely, dodecylamine and tetradecylamine, were used as structure directors. The reaction stoichiometries were the same for both the water-rich and the ethanol-rich reaction systems (S[°]/I[°] = 0.25). When mesitylene (Mes) was present as an auxiliary structure director, the Mes/S[°] molar ratio was 1.0 or 4.5.

Figures 3.1 and 3.2 provide N₂ adsorption-desorption isotherms for the HMS silicas obtained from dodecylamine and tetradecylamine as structure directors, respectively. The adsorption properties of the mesostructures assembled from the two surfactants under the same reaction conditions are qualitatively equivalent. As can be

Figure 3.1

t
d
et
fo
so
va

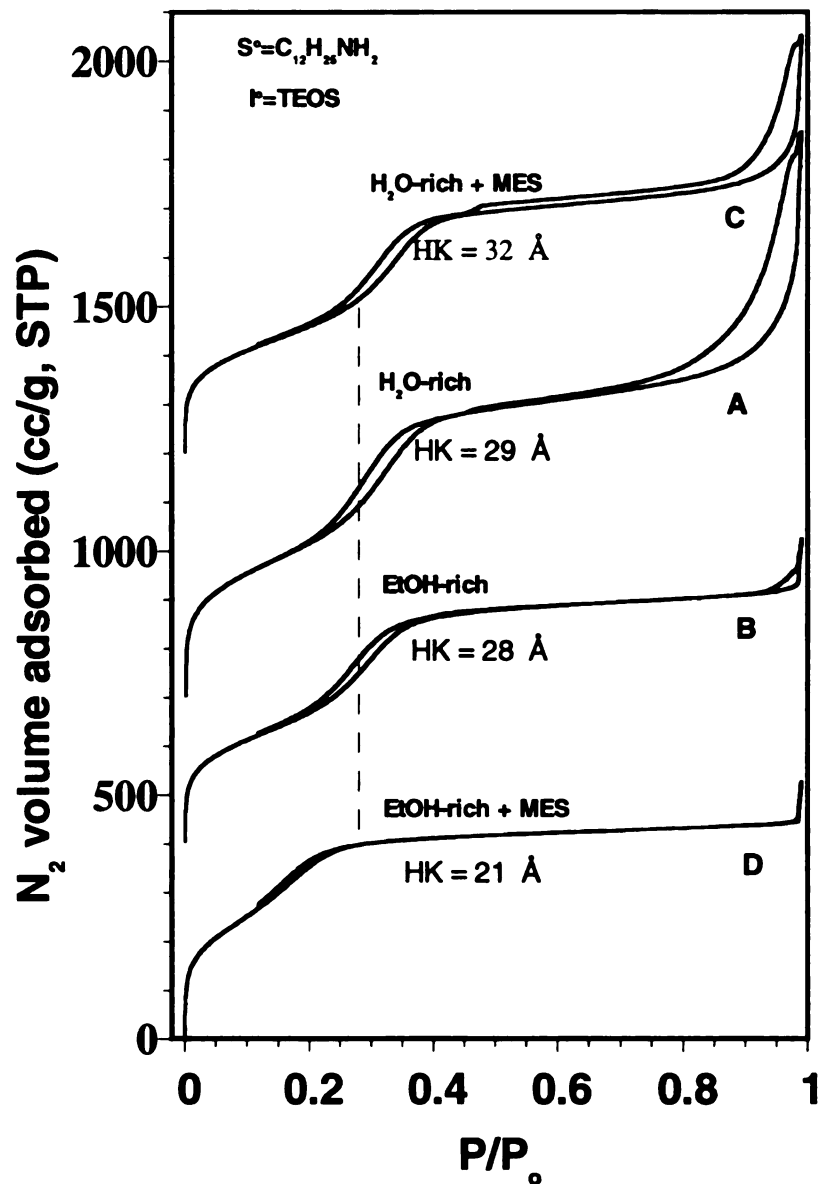


Figure 3.1 N_2 adsorption-desorption isotherms for HMS silicas assembled at ambient temperatures from dodecylamine and TEOS: Curves A and B are for derivatives obtained from a water-rich (water : ethanol = 90 : 20 (v/v)) and ethanol-rich solution (water : ethanol = 35 : 65 (v/v)); curves C and D are for derivatives prepared from the same water-rich and ethanol-rich solutions, but in the presence of mesitylene ($Mes/S^\circ =$ of 1.0). The HK values are the Horvath-Kawazoe pore diameters.

N₂ volume adsorbed (cc/g STP)

Figure 3.2

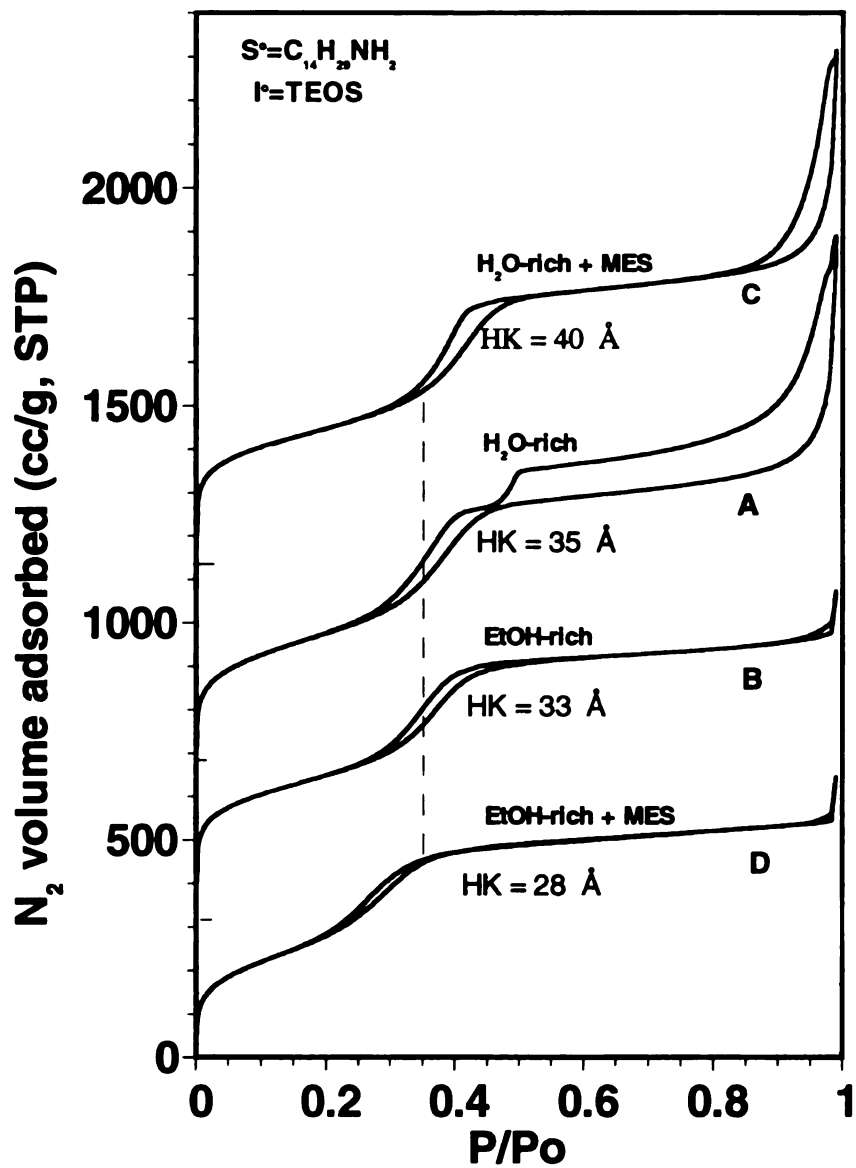


Figure 3.2 N₂ adsorption-desorption isotherms for HMS silicas prepared from tetradecylamine and TEOS in water-rich and ethanol-rich solution. The labeling of the isotherms is the same as in Figure 3.1.

seen fr

water-r

positio

(S°=C

have

adsorp

the m

pore

mediu

TEM

assoc

textur

soluti

adsor

mesit

signif

to a 3

of m

corres

seen from the isotherms labeled A and B in both Figures, the structures obtained from the water-rich and ethanol-rich solutions give stepped-shaped isotherms at $P/P_0 < 0.4$. The positions of the steps correspond to Horvath-Kawazoe pore sizes of 28-29 Å ($S^\circ = C_{12}H_{25}NH_2$) and 33-35 Å ($S^\circ = C_{14}H_{29}NH_2$).

Although the mesostructures obtained from the water-rich and ethanol-rich media have equivalent frameworks, the textural mesoporosity, as evidenced by the N_2 adsorption/desorption in the region $P/P_0 > 0.4$, depends dramatically on the polarity of the medium used for assembly. A textural pore volume even larger than the framework pore volume can be obtained from the water-rich system, whereas the ethanol-rich medium generates a mesostructure with little or no textural pores. As will be seen from TEM images presented below, the high textural mesoporosity for the water-rich system is associated with the presence of extremely small fundamental particles.

We consider next the effect of mesitylene on the framework pore structure and textural mesoporosity of HMS silicas assembled from water-rich and ethanol-rich solutions. The structure mediating properties of mesitylene is manifested in the adsorption-desorption curves labeled C and D in Figures 3.1 and 3.2. The presence of mesitylene at $Mes/S^\circ = 1$ in the water-rich systems causes the adsorption step to be significantly shifted to higher relative pressure. The shift in the step position corresponds to a 3-5 Å *increase* in HK pore size. In the ethanol-rich medium, however, the presence of mesitylene results in a shift of the step position to lower relative pressures, corresponding to a 5-7 Å *decrease* in HK pore diameter.

N volume adsorbed (cc/g, STP)

Figure
dodecy
after ca
after ca
textural
°C.

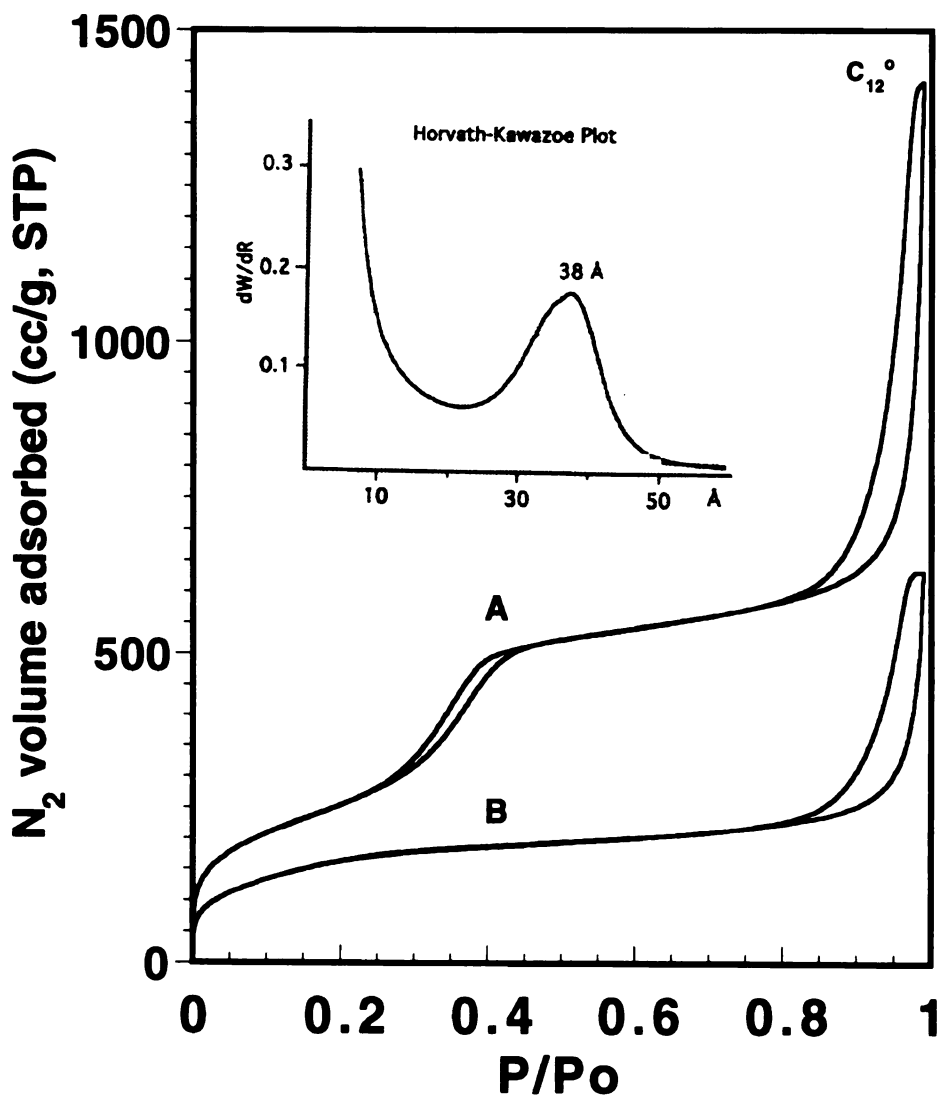


Figure 3.3 N₂ adsorption-desorption isotherms for a HMS silica prepared from dodecylamine in water-rich solution in the presence of mesitylene (Mes/S = 4.5): (A) after calcination at 650 °C with retention of framework and textural mesopores and (B) after calcination at 1000 °C with collapse of framework pores but with retention of textural pores. Insert: Horvath-Kawazoe pore size distribution after calcination at 650 °C.

depend

solvent

increas

a mino

under e

from a

ethanol

3.3, the

pressur

obtaine

the HK

the hys

substan

-850 m

and not

$S^{\circ} = C_1$

to collap

curve B

by the lo

Although mesitylene can substantially expand or contract the framework pores depending on the polarity of the reaction medium, it does not alter the key role of the solvent in regulating the textural porosity. As will be shown below, mesitylene actually increases the textural mesoporosity under water - rich assembly conditions, but it has only a minor influence on the extremely low textural pore volume of HMS when assembled under ethanol - rich conditions.

To further probe the influence of mesitylene on the framework pores assembled from a water-rich environment, we repeated HMS assembly in 90 : 10 (v/v) water : ethanol at a much higher Mes/S^o ratio of 4.5. As shown by the N₂ isotherms in Figures 3.3, the adsorption step due to framework pore filling is further shifted to higher relative pressure as a consequence of a HK pore size (38Å) that is 9Å larger than the value obtained in the absence of mesitylene. The insert to Figure 3.3 shows the half width of the HK pore distribution to be ~10 Å, a value typical of HMS materials. On the basis of the hysteresis loop at higher relative pressure, it appears that the textural pore volume is substantially increased by ~ 50 % from ~550 ml STP/g in the absence of mesitylene to ~850 ml STP/g by the presence of mesitylene.

In order to verify that the textural pores do indeed arise from interparticle voids and not from a large pore component of the framework, the HMS silica assembled from S^o = C₁₂H₂₅NH₂ at 90:10 (v/v) H₂O : ethanol and Mes/S^o = 4.5 was calcined at 1000 °C to collapse the framework pores. The N₂ adsorption/desorption isotherms are given by curve B of Figure 3.3. Note that the framework pores indeed have collapsed, as signified by the loss of the pore filling step, but a substantial fraction (>50%) of the textural

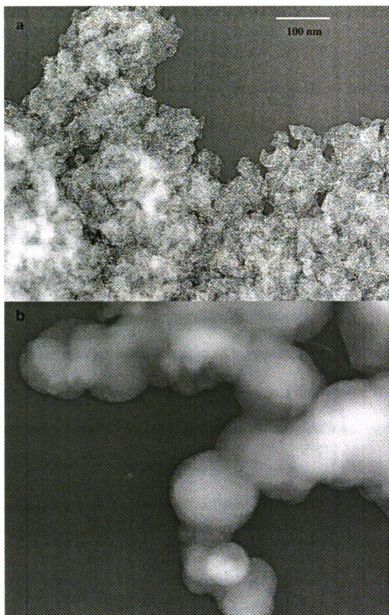


Figure 3.4 TEM images of calcined (650 °C) HMS molecular sieve silicas assembled from dodecylamine : a. mesoscale fundamental particles obtained from water-rich solution; b. the spheroid fundamental particles and macroscale beads-on-a-string texture obtained from ethanol-rich solution.

porosity is

structure.

Th

structure

- and etha

solvent sy

the space

is no app

more wor

T

reaction

reaction

fundamen

aggregate

are sugg

mesoscal

forms sp

size (see

aggregate

typically

Fi

solution in

porosity is retained. Thus, the textural porosity cannot be a consequence of framework structure.

The TEM images shown in Figure 3.4 provide insights into the framework structure and textural mesoporosity associated with HMS materials assembled from water - and ethanol - rich media. Regular framework pores are readily observed, regardless of solvent system used to prepare the products. It is quite clear that the pores originate from the space initially occupied by uniform supramolecular assemblies of surfactant, but there is no apparent long range order to the pore arrangement. Instead the pore packing motif is more wormhole - like , perhaps, even sponge-like, in character.

The most important distinguishing feature between the water - and ethanol - rich reaction products is the particle texture. As shown in Figure 3.4a, the water - rich reaction mixture yields irregularly-shaped mesoscale fundamental particles. These fundamental particles aggregate into larger particles. The coastline - like silhouette of the aggregates, which persists over length scales differing by at least an order of magnitude, are suggestive of a fractal texture. Textural mesopores comparable in size to the mesoscale fundamental particles are clearly evident. In contrast, the ethanol-rich medium forms spheroid to disk-like fundamental particles that are typically 100 nm or larger in size (see Figure 3.4b). These macroscale fundamental particles are linked into larger aggregates with a beads-on-a-string texture. The interparticle voids are much larger, typically in the macropore range (>50 nm).

Figure 3.5 provides TEM images for a HMS derivative assembled from water-rich solution in the presence of a relatively high concentration of mesitylene ($Mes/S^{\circ} = 4.5$)

Figure 3

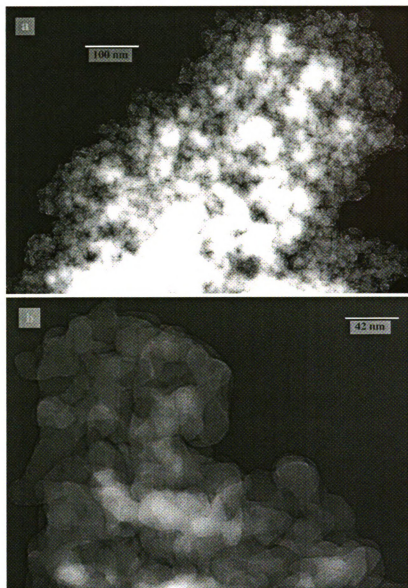


Figure 3.5 TEM images of HMS silica prepared from dodecylamine in water-rich solution in the presence of mesitylene ($Mes/S = 4.5$) and calcined at 1000 °C to collapse the framework pore structure.; (a) Low magnification image showing the retention of the textural mesopores and, (b) High magnification image showing the absence of framework pores.

Figure 3

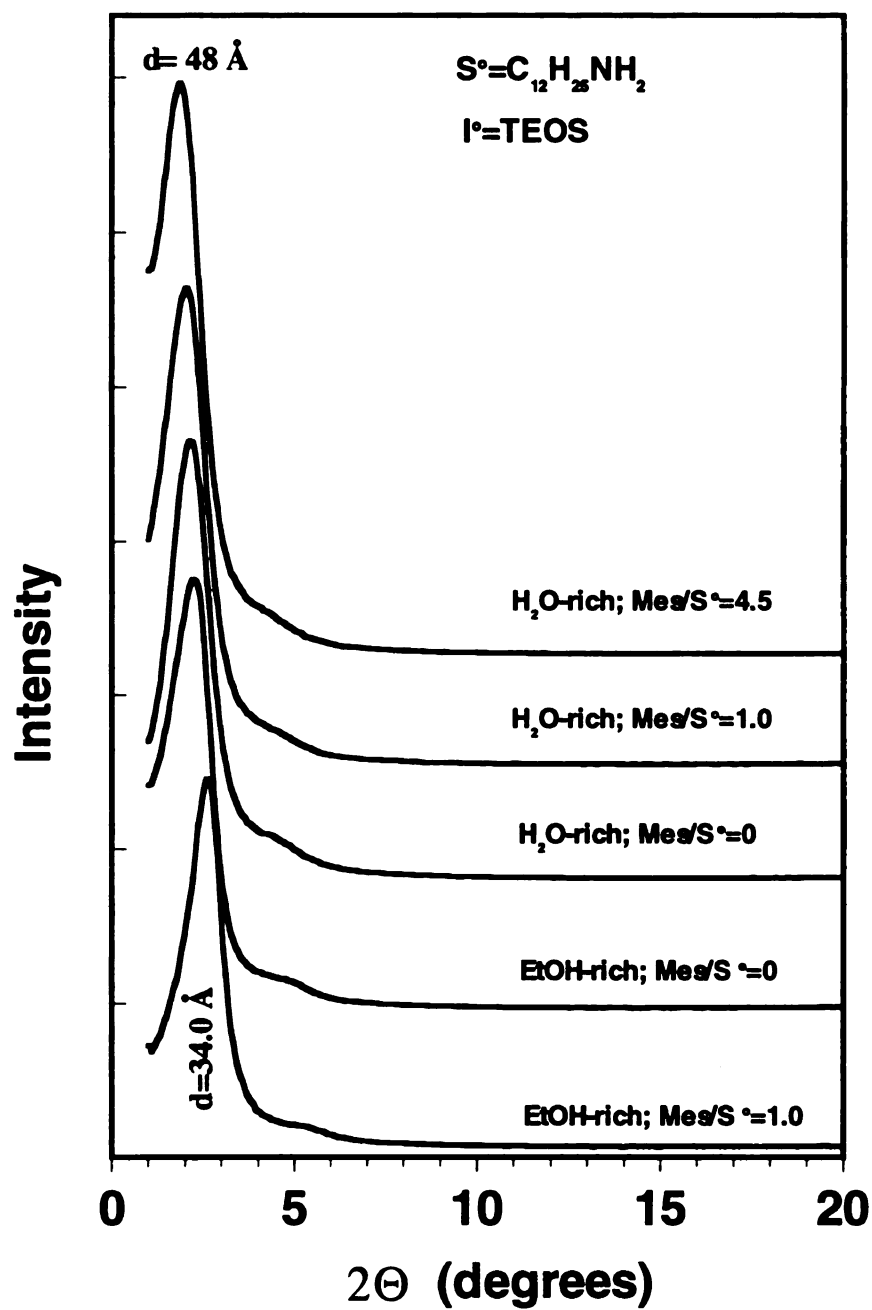


Figure 3.6 X-ray powder diffraction pattern of calcined (650 °C) HMS silicas assembled from dodecylamine amine in water-rich and ethanol-rich solution with or without mesitylene as an auxiliary structure director.

but calcina
obtained at
obtained at
destroyed b
results desc

the origin o

Fig

assembled

showed qu

relatively t

near 5.0°

rich polar

positions

polarity o

Ta

(S_{BET}), to

textural t

materials.

with the B

BET surf

the synthe

decreases

pore sizes

but calcined at 1000 °C to collapse the framework mesopore structure. Image (a), obtained at low magnification, shows the retention of the textural pores. Image (b), obtained at higher magnification, shows that the framework mesopores indeed have been destroyed by thermal treatment. This result, which is consistent with the N₂ adsorption results described earlier (*cf.*, Figure 3.3), further identifies the interparticle voids as being the origin of the textural mesopores.

Figure 3.6 provides the X-ray powder diffraction patterns for HMS derivatives assembled from C₁₂H₂₅NH₂ as the structure director. Structures formed from C₁₄H₂₉NH₂ showed qualitatively equivalent diffraction features. The patterns all contain a strong, relatively broad reflection at 2.0 - 3.0° 2θ and a very weak broad shoulder in the region near 5.0° 2θ. The qualitative form of the patterns is not affected by the water- or ethanol-rich polarity of the assembly medium or by the presence of mesitylene. However, the positions of the intense reflection and the weak broad shoulder are dependent by the polarity of the reaction medium and by the presence of mesitylene.

Table 3.1 summarizes the basal spacings, HK pore sizes, N₂ BET surface areas (S_{BET}), total liquid pore volumes (V_t), liquid framework pore volumes (V_{fr}), the ratio of textural to framework pore volumes (V_{tx}/V_{fr}), and the bulk densities for our HMS materials. The basal spacings represented by the strong diffraction line are correlated with the HK pore sizes, even though the framework lacks regular long-range order. The BET surface areas are in the range 900-1464 m²/g. The incorporation of mesitylene into the synthesis of HMS from a water - rich medium increases the HK pores size and decreases the surface area of the mesostructure. Conversely, mesitylene *decreases* the pore sizes and increases the surface areas of HMS assembled from ethanol-rich solution.

It is
are much l
ethanol -ric
the approxi
pore volum
water-rich m
framework v
In contrast,
equivalent t
differences
substantiall
ethanol-ric

3.4 Discus

Th
assembly
HMS silic
, which g
judicious
10 (v/v) w
TEM ima
are on a
Conversely

It is especially noteworthy from the results in Table 3.1 that the total pore volumes are much larger for HMS derived from a water - rich medium (~1.3 - 1.7 cc/g) than an ethanol -rich medium (~0.5 - 0.7 cc/g). Yet, the framework pore volumes are confined to the approximate range 0.5 - 0.7 cc/g. The difference between the total and framework pore volumes is expressed as the textural pore volume, V_{tx} . For HMS assembled from a water-rich medium, the textural pore volume which can be up to 1.6 times as large as the framework volume, depending on the amount of mesitylene used as a structure modifier. In contrast, the textural pore volume for HMS obtained from an ethanol-rich medium is equivalent to only a small fraction (6 - 18 %) of the framework volume. Finally, the differences in total pore volumes is manifested in the bulk densities, which are substantially lower for HMS derived from a water-rich medium (0.16 - 0.35 g/cc) than an ethanol-rich medium (0.53 - 0.67 g/cc).

3.4 Discussion

The results of the present work demonstrate several important advantages of $S^{\circ}I^{\circ}$ assembly for the preparation of mesoporous metal oxide molecular sieves. In the case of HMS silicas we have shown through N_2 adsorption studies that the textural mesoporosity, which greatly facilitates access to the framework mesopores, can be controlled by a judicious choice of solvent (cf., Figures 3.1 and 3.2). A water-rich solvent, such as 90 : 10 (v/v) water : ethanol, promotes the formation of mesopore fundamental particles sizes. TEM images show that the interparticle voids responsible for the textural mesoporosity are on a length scale comparable to the fundamental particles (cf., Figure 3.4a). Conversely, a solvent of lower polarity, namely, 35 : 65 (v/v) water : ethanol, minimizes

Table 1.

Physical parameters for calcined (650 °C) HMS molecular sieve silicas prepared by SiO_2 assembly in H_2O -rich and EtOH -rich

Table 1. Physical parameters for calcined (650 °C) HMS molecular sieve silicas prepared by S^o assembly in H₂O-rich and EtOH-rich medium

S ^o	Reaction Medium ^a	d (Å)	H-K pore (Å)	SBET m ² /g	V _t cc/g	V _{fr} cc/g	V _{tx} /V _{fr}	d _{bulk} g/cc
C ₁₂ H ₂₅ NH ₂	H ₂ O-rich; Mes/S ^o =0	41.7	29	1035	1.30	0.62	1.10	0.33
	H ₂ O-rich; Mes/S ^o =1.0	43.3	32	993	1.37	0.65	1.11	0.21
	H ₂ O-rich; Mes/S ^o =4.5	48.0	38	957	1.63	0.63	1.59	0.16
	EtOH-rich; Mes/S ^o =0	39.4	28	1070	0.66	0.56	0.18	0.53
C ₁₄ H ₂₉ NH ₂	EtOH-rich; Mes/S ^o =1.0	34.0	21	1464	0.51	0.48	0.06	0.67
	H ₂ O-rich; Mes/S ^o =0	44.2	34	1035	1.28	0.65	0.97	0.35
	H ₂ O-rich; Mes/S ^o =1.0	50.2	40	927	1.30	0.67	0.94	0.20
	H ₂ O-rich; Mes/S ^o =4.5	55.2	45	900	1.67	0.67	1.49	0.16
	EtOH-rich; Mes/S ^o =0	49.1	33	936	0.69	0.61	0.13	0.57
	EtOH-rich; Mes/S ^o =1.0	38.7	28	1117	0.62	0.57	0.09	0.65

The compositions of H₂O-rich and EtOH-rich solutions were 90 : 10 and 35 : 65 (v/v) for H₂O:EtOH, respectively

the texture

There is no

water : et

hysteresis

pores even

Figure 3.3

application

The

likely is dete

the reaction

mesostructur

virtually with

rapid nuclea

fundamental

3.4a). Howe

and mesostr

temperature

mesostructur

in size. The

interparticle

The r

polarity of th

results in Tab

the textural porosity by forming much larger fundamental particles (cf., Figure 3.4b). There is no doubt that the textural mesoporosity for HMS assembled in 90 : 10 (v/v) water : ethanol arises from interparticle pores. The retention of a well expressed hysteresis loop in the N₂ adsorption/desorption isotherm show the retention of textural pores even after the framework pores have been collapsed by calcination at 1000°C (cf., Figure 3.3). Thus, the textural porosity can be tailored to a particular materials application by simply controlling the polarity of the solvent for supramolecular assembly.

The relationship between fundamental particle size and solvent polarity most likely is determined by the relative rates of I^o hydrolysis and supramolecular assembly in the reaction medium. A water - rich medium leads to rapid nucleation of the mesostructure. For assembly in 90 : 10 (v/v) water : ethanol, a solid product is formed virtually within minutes of mixing the reagents at ambient temperature. This leads to rapid nucleation and the formation of irregularly shaped fundamental particles. The fundamental particles further aggregate into a self-similar agglomerates (cf., Figures 3.4a). However, in the lower polarity 35 : 65 (v/v) water : ethanol solvent, I^o hydrolysis and mesostructure assembly is relatively slow, requiring several hours at ambient temperature for the onset of product formation. The slower nucleation and growth of the mesostructure results in spheroid to disk-shaped fundamental particles 100 nm or larger in size. These fundamental particles interpenetrate to form even larger aggregates with interparticle voids beyond the mesopore range (cf., Figure 3.4b).

The role of mesitylene as an auxiliary structure director is highly dependent on the polarity of the medium in which mesostructure assembly is carried out. As shown by the results in Table 3.1 for HMS assembly in the water-rich medium, mesitylene enlarges the



Figure 3.7
HMS assembly
central core of
mesitylene pre
head group size

Micellar Binding States of Mesitylene in S⁹⁵ assembly

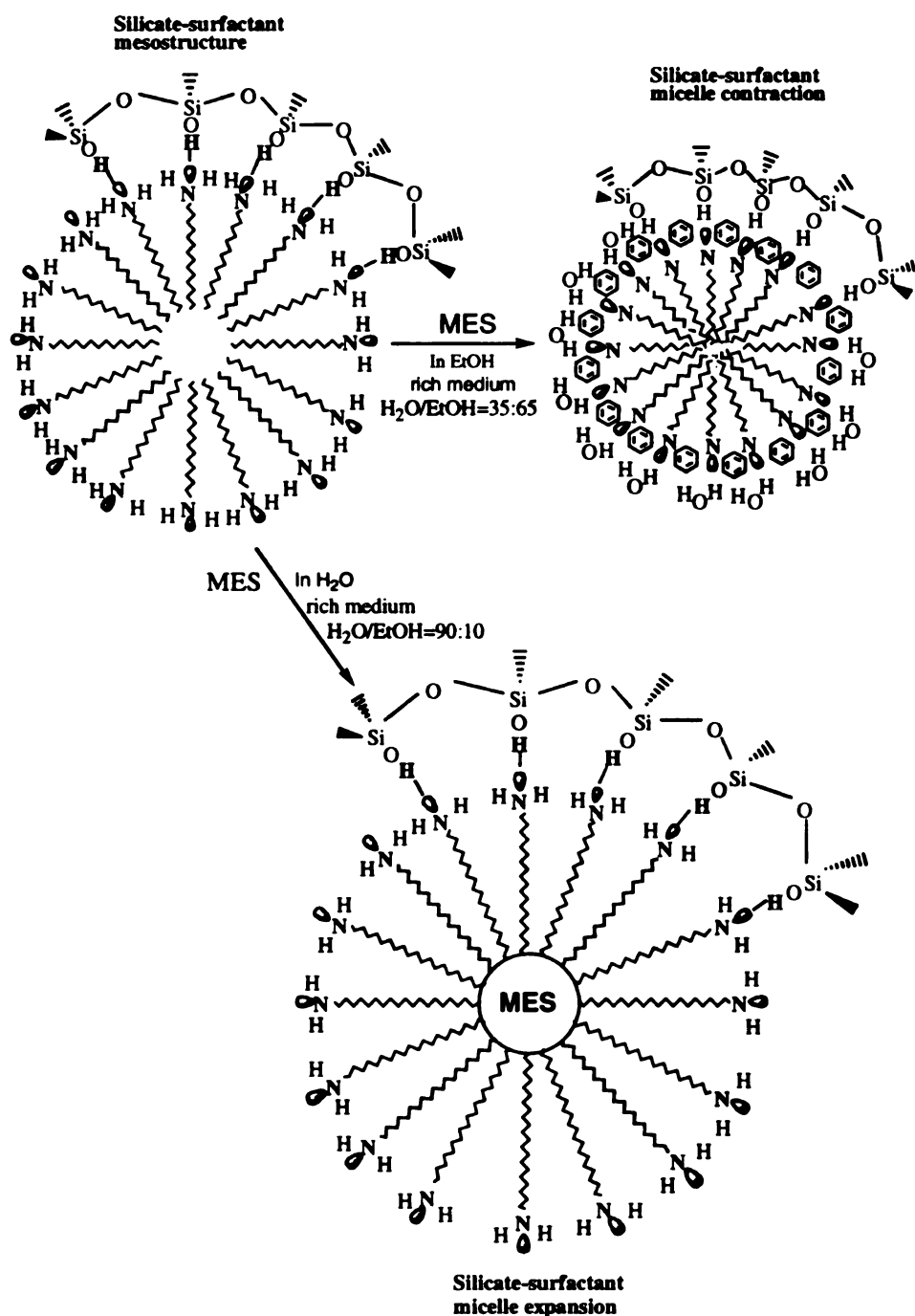


Figure 3.7 Schematic representation of the structure-directing effects of mesitylene on HMS assembly. In the water-rich media, the mesitylene “dissolves” in the hydrophobic central core of the micelle leading to pore expansion. In the ethanol-rich environment, mesitylene preferentially “adsorbs” to interfacial head groups, thus increasing effective head group size and subsequently decreasing the pore size.

framework

with the e

On the oth

framework

The

is known t

"dissolved"

the hydroph

between the

the surfactan

states of me

Figure 3.7 fo

HMS assem

"dissolved" t

of the micell

mesostructur

in the mediu

Hydrogen bo

with the pola

adsorbed stat

the size of th

decrease in th

hydrophobic

framework pores and increases the textural mesoporosity. This latter result is consistent with the effect of mesitylene on the pore size of MCM-41 prepared by S+I assembly ¹. On the other hand, for assembly in the ethanol-rich medium, mesitylene *reduces* the framework pore size and decreases still further the already low textural pore volume.

The role of mesitylene on the framework pore structure is intriguing. Mesitylene is known to bind to surfactant micelles in at least two binding states, namely, in a “dissolved” state at the hydrophobic center of the molecule, and in an “adsorbed” state at the hydrophilic micelle / solvent interface ¹³⁻¹⁵. It is reasonable to expect the equilibrium between these structurally distinct states to depend on the polarity of the solvent in which the surfactant micelles are formed. In accordance with the structurally distinct binding states of mesitylene in surfactant micelles, we propose the mechanism illustrated in Figure 3.7 for the expansion or contraction of the framework pores by mesitylene during HMS assembly. In water-rich solvent, in which the solubility of mesitylene is low, the “dissolved” binding state should be favored over the adsorbed state. In this case the size of the micelle will be increased and this will be manifested as an enlarged pore in the mesostructure. But in the lower polarity ethanol-rich solvent, the solubility of mesitylene in the medium will be increased and this will favor binding at the “adsorption” site. Hydrogen bonding between the p-electrons of the aromatic and water dipoles associated with the polar head groups at the micelle-solvent interface is believed to stabilize the adsorbed state of mesitylene ¹³. Binding of mesitylene at the micelle surface increases the size of the effective polar head group. The increase in head group size leads to a decrease in the radius of curvature and to a reduction in micelle size in order to retain hydrophobic interactions between the surfactant chains at the micelle center.

Consequent

mesostruct

In c

that certain

textural me

tetradecylar

sensitive to

the present

mesoporosit

Figures 3.1

We

framework

channels w

diffraction p

the results o

HMS mater

obtained for

the much

Consequentl

important re

obtained in t

long range cl

has been pre

Consequently, a framework with a smaller pore size is formed in the assembled mesostructure.

In our earlier studies of HMS assembly in 50:50 (v/v) water : ethanol we noted that certain alkylamine surfactants (e.g., dodecylamine) gave derivatives with high textural mesoporosity, whereas others afforded relatively low textural pore volumes (e.g., tetradecylamine) ¹⁸. It is now apparent that the degree of textural mesoporosity is quite sensitive to both the solvent polarity and the nature of the S^o surfactant. The results of the present work show that dodecylamine and tetradecylamine afford high textural mesoporosity when the solvent is highly polar, as in 90 : 10 (v/v) water : ethanol (cf., Figures 3.1 and 3.2).

We have previously described as-synthesized HMS materials as neutral framework analogs of hexagonal MCM-41 ⁵. Evidence for the hexagonal ordering of channels was obtained from selected area electron diffraction ⁴. The X-ray powder diffraction patterns were attributed to a very small scattering domain size. It is clear from the results of the present study, however, that the broad diffraction lines characteristic of HMS materials are not due exclusively to a small scattering domain size. The patterns obtained for the fine grained HMS particles are indistinguishable from those obtained for the much larger spheroid to disk-like fundamental particles (cf., Figure 3.6). Consequently, framework disorder, in addition to small scattering domain sizes, plays an important role in broadening the diffraction lines. On the basis of the TEM images obtained in the present work (cf., Figures 3.4 and 3.5), we find no evidence for hexagonal long range channel packing order. Even "disordered" hexagonal channel packing, which has been previously documented for MCM-41 prepared by S⁺I⁻ assembly, ¹⁹ appears to

be difficu

the reactio

-like HMS

Wo

obtained by

like frame

electrostatic

ethylenedi

structures is

nearly unifor

On the basis

work and the

HMS materi

quantitative d

these and othe

be difficult to achieve by S⁺I⁻ assembly. Additional work is progress to better describe the reaction conditions that determine the assembly of hexagonal vs. wormhole or sponge-like HMS framework structures.

Wormhole motifs have been observed for silica and alumina mesostructures obtained by N^oI^o assembly, where N^o is a polyoxyethylene surfactant ⁶⁻⁸. Also, sponge-like framework structures have been described for mesoporous silicas obtained by electrostatic S⁺I⁻ assembly in the presence of a structure disrupter (e.g., ethylenediaminetetraacetate) ²⁰. Distinguishing between wormhole and sponge-like pore structures is not a straight forward matter. “Wormholes” imply channel structures with nearly uniform diameters, whereas “sponges” imply substantially reticulated structures. On the basis of the relatively narrow HK pore size distributions observed in the present work and the presence of channel-like voids in the TEM images, we prefer describing HMS materials as wormhole frameworks. Future work will require more incisive quantitative descriptions based in part on the X-ray and neutron scattering properties of these and other highly disordered framework structures.

3

1

2

3.

4.

5.

6.

7.

8.

9.

10

11

12

13

14.

15.

16.

17.

18.

19.

20.

3.5 References

1. Beck, J. S.; Vartuli, J. C.; Roth, W. J.; Leonowicz, M. E.; Kresge, C. T.; Schmitt, K. D.; Chu, C. T-W.; Olson, D. H.; Sheppard, E. W.; McCullen, B.; Higgins, J. B.; Schlenker, J. L. *J. Am. Chem. Soc.* **1992**, *114*, 10834.
2. Huo, Q.; Margolese, D. I.; Ciesla, U.; Demuth, D. G.; Feng, P.; Gier, T. E.; Sieger, P.; Firouzi, A.; Chmelka, B. F.; Schüth, F.; Stucky, G. D. *Chem. Mater.* **1994**, *6*, 1176.
3. Huo, Q.; Margolese, D. I.; Ciesla, U.; Feng, P.; Gier, T. E.; Sieger, P.; Leon, R.; Petroff, P. M.; Schüth, F.; Stucky, G. D., *Nature* **1994**, *368*, 317.
4. Tanev, P. T.; Chibwe, M.; Pinnavaia, T. J. *Nature* **1994**, *368*, 321.
5. Tanev, P. T.; Pinnavaia, T. J. *Science* **1995**, *267*, 865.
6. Bagshaw, S. A.; Prouzet, E.; Pinnavaia, T. J. *Science* **1995**, *269*, 1242.
7. Bagshaw, S. A.; Pinnavaia, T. J. *Angew. Chem. Int. Ed. Engl.* **1996**, *35*, 1102.
8. Prouzet, E.; Pinnavaia, T. J. *Angew. Chem. Int. Ed. Engl.* **1997**, *36*, 516.
9. Antonelli, D. M.; Ying, J. Y. *Angew. Chem. Int. Ed. Engl.*, **1996**, *35*, 426.
10. Whitehurst, D. M. *U.S. Patent*, **1992**, 5,143,879.
11. Schmidt, R. E.; Hansen, W.; Stocker, M.; Akporiaye, D.; Ellestad, O. H. *J. Am. Chem. Soc.* **1995**, *117*, 4049.
12. Zhang, W.; Froba, M.; Wang, J.; Tanev, P.; Wong, J.; Pinnavaia, T. J. *J. Am. Chem. Soc.* **1996**, *118*, 9164.
13. Mukerjee, P.; Cardinal, J. R. *J. Phys. Chem.* **1978**, *82*, 1620.
14. Eriksson, J.E.; Gillberg, G. *Acta Chem. Scand.*, **1966**, *20*, 2019.
15. Gordon, J. E.; Robertson, J. C.; Thorne, R. L. *J. Phys. Chem.*, **1970**, *74*, 957.
16. Horvath, G.; Kawazoe, K. J. *J. Chem. Eng. Jpn.* **1983**, *16*, 470.
17. Spence, J.C.H., "*Experimental High-Resolution Electron Microscopy*", **1988**, P264, Oxford University Press, New York.
18. Tanev, P.T.; Pinnavaia, T.J. *Chem. Mater.* **1996**, *8*, 2068.
19. Chen, C. Y.; Xiao, S. Q.; Davis, M. E. *Microporus Mater.* **1995**, *4*, 1.
20. Ryoo, R.; Kim, J. M.; Ko, C. H.; Shin, C. H. *J. Phy. Chem.* **1996**, *100*, 17718.

Chapter 4

In-situ Alumination of Mesoporous HMS Molecular Sieves Silica for Use as Alkylation Catalysts

Abstract

The in-situ alumination of mesoporous HMS molecular sieves assembled via an electrically neutral assembly mechanism using primary amine surfactant as the structure director, tetraethylorthosilicate (TEOS) as the silicon source and NaAlO_2 or $\text{Al}(\text{sec-OBu})_3$ as the alumination agent was conducted at ambient temperature. The majority of Al-sites (i.e. >90%) were found in a tetrahedral environment by ^{27}Al -NMR. The textural porosity was not alternated by alumination of structurally well formed HMS for Al-loadings up to 8 mol%. Al-HMS with 4 different amounts of textural porosity (0-tex, 0.5-tex, 1-tex, 1.5-tex) relative to framework mesoporosity were purposely prepared through control of solvent polarity and the time of introducing the aluminum precursor following the addition of TEOS. The results indicate that the alumination of HMS at ambient temperature, using either NaAlO_2 or $\text{Al}(\text{sec-OBu})_3$, are as effective as the hydrothermal post synthesis alumination of other mesoporous molecular sieves.¹ It is not necessary to remove the surfactant prior to effectively incorporate aluminum into framework of mesostructural HMS at ambient temperature. It is also not necessary to use surfactant-free materials to convert sodium-forms of Al-HMS and Al-MCM-41 into their proton forms by ammonium-exchange. The total acidity of Al-HMS catalysts measured by TGA analysis of cyclohexylamine desorption were reasonably equivalent to each other when the Al-loading was ~2 mol%. Al-HMS with higher textural porosity, regardless of the aluminum precursor used, showed significantly higher conversion (up to 65%) of the

bulky 2,4-di-*tert*-butylphenol (2,4-DTBP) reacting with cinnamyl alcohol to a bulky flavan (selectivity up to 87%) under very mild reaction conditions (i.e. 60 °C, 6 h).

4.1 Introduction

Mesoporous HMS, as a product of electrically neutral assembly, is distinguished from other mesoporous molecular sieves such as MCM-41 by exhibiting significant textural mesoporosity. The complementary textural porosity of HMS, in addition to framework mesoporosity, was observed in the first HMS sample.² Improving and tailoring textural porosity was reported more recently.³ The textural porosity of HMS facilitates diffusion limited catalytic reactions.⁴ For example, HMS catalysts have better performance than MCM-41 analogous for both 2,6-di-*tert*-butylphenol (2,6-DTBP) peroxidation⁵ and NO reduction by NH₃.⁶ No significant physical and chemical property differences except textural porosity have been found between these two analogs. The better performance for HMS derivatives can not be attributed to different active sites for those mesoporous molecular sieves. For cumene cracking, substantially higher activity of Al-HMS than MCM-41 analogous have been reported.^{7,8} Higher acidity and smaller domain size of HMS with apparently shorter diffusion channels might account for the better performance of Al-HMS in cumene cracking.

Another very important feature of Al-HMS is that the negative charges generated by substitution of Al into the silica framework can be automatically balanced by the hydrolysis of the primary amine to its protonated form. Thus, the H-form Al-HMS could be easily obtained by calcination without tedious ion exchange required for transformation of sodium-form Al-MCM-41 to H-form. And also, the majority of

surfactant in Al-HMS (>90%) can be easily removed by simple ethanol extraction. Dealumination upon removal of surfactant by calcination can be purposely avoided through facile ethanol extraction for Al-HMS, but this is more difficult to accomplish for Al-MCM-41.⁹⁻¹¹

Aluminum substituted mesoporous molecular sieves with mild acidity¹⁰ and large pores have been recognized as good catalysts for fine chemical syntheses where large molecular substrates are usually used.¹² Al-HMS with high meso-textural pores is apparently better than other Al-substituted mesoporous molecular sieves in terms of accessibility to framework active sites. Therefore, it is very important for catalysis to have HMS derivatives that are rich in textural porosity and have meso-scaled fundamental particles that limit the pore channel lengths to being comparable to the fundamental particle size itself. One of the objectives of this report is to prepare Al-HMS derivatives with large textural porosity, as well as a small (<150 Å) fundamental particle size. The importance of these physical properties to catalysis were verified in the alkylation of 2,4-di-tert-butylphenol (2,4-DTBP) with cinnamyl alcohol to a flavan. This particular liquid phase reaction was first reported by Corma and his coworkers.¹³ It was reported that this reaction was not possible to take place inside the microporous channels of H-Y because the molecular size of the substrates prevented them from accessing acidic centers in the smaller channels. Even though the conversion of 2,4-DTBP catalyzed by Al-MCM-41 was high, a very significant amount of it was dealkylated to 4-tert-butylphenol (4-TBP, ~25% yield) rather than to flavan.¹³ In our study, Al-HMS with meso-scaled fundamental particles and high textural porosity has shown remarkable selectivity (i.e. 86%) to flavan

at a significantly higher conversion of 2,4-DTBP (i.e. 65%) without detectable amounts of 4-TBP in the reaction products.

Another objective is to prepare Al-HMS with cost-effective aluminum sources such as NaAlO_2 , because all of the Al-HMS derivatives reported so far were synthesized using aluminum alkoxide, which is expensive and sensitive to moisture.

4.2 Experimental

Our approach to the synthesis of Al-HMS with high textural porosity and a small fundamental particle size using either aluminum alkoxide or NaAlO_2 was based on assembly of HMS framework in a relatively high polarity medium³ and a follow-up alumination step. A water medium with 10 vol% ethanol as co-solvent in the presence of mesitylene (MES) as a textural porosity promoter was used. The synthesis was carried out using dodecylamine as the neutral surfactant and tetraethyl orthosilicate (TEOS) as the neutral inorganic precursor. The aluminum precursor was introduced into the synthesis mixture in a follow-up manner. Three different Al-HMS derivatives were prepared by control the time of introducing the aluminum precursor. First, add aluminum precursor solution ($\text{Al}(\text{sec-OBu})_3$ in sec-butanol or NaAlO_2 in water) immediately after addition of TEOS to surfactant solution; Second, add aluminum precursor solution 20 minutes after addition of TEOS; Third, add aluminum precursor solution 20 h after addition of TEOS. The reaction mixture was aged under stirring at ambient temperature for 20 h after addition of aluminum precursor. The molar composition of our synthesis mixture was:

0.02~0.08 Al : 1.0 Si : 0.25 Surf. : 1.12 MES : 5.0 EtOH : 130 H_2O .

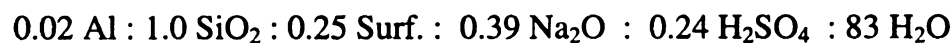
For comparison, a zero-textural porosity Al-HMS was synthesized using aluminum alkoxide as the alumination agent in a more non-polar medium comprised of EtOH/H₂O with a volume ration of 50/50. The molar composition of this synthesis was



The product for each synthesis was filtered and dried in air.

The samples prepared using aluminum alkoxide as the aluminum source were calcined at 650 °C for 4 h without prior NH₄⁺-ion-exchange. The as-made samples prepared using NaAlO₂ as the aluminum source were ion-exchanged at ambient temperature for 4 h using 0.1 M NH₄NO₃ solution with a solution to solid ratio of 50 ml/g. The obtained product was dried in air and calcined at 650 °C for 4 h.

The Al-MCM-41 was prepared using 27wt% sodium silicate solution as the silicon source, and cetyltrimethyl ammonium bromide as the structure director. The pH was initially adjusted to 10.5 using sulfuric acid and adjusted again to 10 after the reaction mixture was heated at 100 °C for 1 day. Subsequently, the reaction mixture was heated at 100 °C for another day. Then, Al₂(NO₃)₃ aqueous solution was added at ambient temperature under stirring to the reaction mixture, which was statically aged at 100 °C for another 2 days. Aluminum nitrate was chosen as the aluminum precursor over other aluminum sources such as aluminum sulfate and sodium aluminate. The purpose for this choice is to avoid the undesired acidic sites generated by residual anions (i.e. SO₄²⁻) in the case of aluminum sulfate and the structural alternation caused by pH increase in the case of sodium aluminate. The molar composition of the reactant in this synthesis was:



The product was filtered and washed thoroughly with water. The filter cake was dispersed in 0.1 M NH_4NO_3 solution for 4 h at ambient temperature to have it ion-exchanged. Then it was filtered and dried in air before calcination at 540 °C for 6 h.

The powder X-ray diffraction pattern of the samples was recorded on a Rigaku Rotaflex Diffractometer using $\text{Cu K}\alpha$ radiation ($\lambda = 1.542 \text{ \AA}$). N_2 adsorption and desorption isotherms were measured on an ASAP 2000 sorptometer at $-196 \text{ }^\circ\text{C}$. The sample was evacuated under 10^{-5} torr at 150 °C over night before the measurement. ^{27}Al NMR spectra were recorded on a Varian VXR-400S spectrometer with a 7-mm zirconia rotor, and a spinning frequency of 4 kHz. TEM images were taken on a JEOL 100CX with a CeB_6 gun that was operated at an acceleration voltage of 120 kV. The specimen was loaded onto a holey carbon film that was supported on a copper grid by dipping the grid into a solid sample suspension in ethanol. The total acidity of a catalyst was measured by means of TGA analysis of cyclohexylamine desorption in the temperature region 240 to 420 °C. Cyclohexylamine was pre-adsorbed on the catalyst and the sample was then purged with N_2 at 200 °C for 1 h before temperature programmed desorption was started.

Alkylation of 2,4-di-tert-butylphenol (2,4-DTBP) with cinnamyl alcohol was carried out in a 100 ml round bottom flask. A 1.0mmol quantity of 2,4-DTBP, 1.0mmol cinnamyl alcohol and 50 ml of isooctane as the solvent were used. A 500mg quantity of catalyst was added when the reaction mixture was heated to 60 °C. The reaction was kept at 60 °C under magnetic stirring for 6 h. After reaction, the catalyst was filtered and washed with dichloromethane. The dichloromethane was separated from the filtrate by distillation at $\sim 30 \text{ }^\circ\text{C}$ under reduced pressure so that heat-induced side reactions could be

prevented. The reaction products were qualitatively confirmed using a GC-MS. They were quantitatively analyzed by an internal standard method using a GC with a FID detector and a 15 m long SPB-1 type capillary column. In order to obtain the response factor of the flavan relative to internal standard that was 2,4-di-tert-butylbenzene, pure flavan (i.e. ~95%) was purified from a large batch reaction using a TLC approach. The conversion was calculated by dividing the amount of 2,4-DTBP consumed by the amount initially present. The selectivity toward flavan was calculated by dividing the amount of flavan formed by the amount of 2,4-DTBP consumed. The yield of flavan was obtained by dividing the amount of flavan formed by the amount of 2,4-DTBP added. The conversion of cinnamyl alcohol was virtually complete in most reactions because cinnamyl alcohol alone could transform into many undesirable products¹⁴ such as cinnamyl aldehyde, 1,5-di-phenyl pentadiene, and polymeric aldehyde. The latter products formed a tar on the catalyst, which required calcination in air to regenerate the catalyst.

4.3 Results and Discussion

4.3.1 Catalyst Synthesis

In order to obtain acidic sites for catalysis, aluminum is usually incorporated into the framework of microporous zeolite or mesoporous silica molecular sieves under hydrothermal conditions *in situ*.^{15,16} Alumination of mesoporous silica MCM-41 by sodium aluminate in a previous report showed that the aluminum species were predominantly incorporated into the framework near the pore openings, if the alumination was carried out in the presence of surfactant molecules inside the mesoporous channels.¹⁷

This is a particularly significant problem for well-ordered large particle sized MCM-41. The interpretation for this result might be as following. First, the surfactant molecules in the uni-dimensional channels of MCM-41 limit the diffusional migration of aluminum species to deep inside the channels. Second, the interfacial electrostatic charge matching¹⁸ between framework and surfactant micelles generated a large electrostatic repulsion to negatively charged aluminum species, therefore, the aluminum was predominantly incorporated at the opening of the pores. In contrast, the framework of HMS assembled through an electrically neutral mechanism was easily aluminated at ambient temperature even in the presence of surfactant micelles in the pores. A reasonable interpretation for this might be that the diffusion resistance was minimized for aluminum species to migrate into the meso-scaled pores with relatively short lengths in meso-scaled fundamental particles to become incorporated into the neutral framework.

For sodium forms of mesoporous molecular sieves, previous reports very much rely on ammonium exchange of the (calcined) surfactant free materials and further calcination to generate the H-form.^{19,20} However, we found that it is not necessary to remove the surfactant before ammonium exchange to obtain effective catalysts. Sodium form of Al-HMS and Al-MCM-41 were transformed into their ammonium forms easily through NH_4^+ -exchange at ambient temperature in the presence of surfactant molecules without noticeable NH_4^+ diffusion limitations.

4.3.2 Catalyst Characterization

Figure 4.1 and 4.2 show N_2 adsorption-desorption isotherms of Al-HMS prepared using $\text{Al}(\text{sec-OBu})_3$ and NaAlO_2 , respectively. The textural porosity increases with the

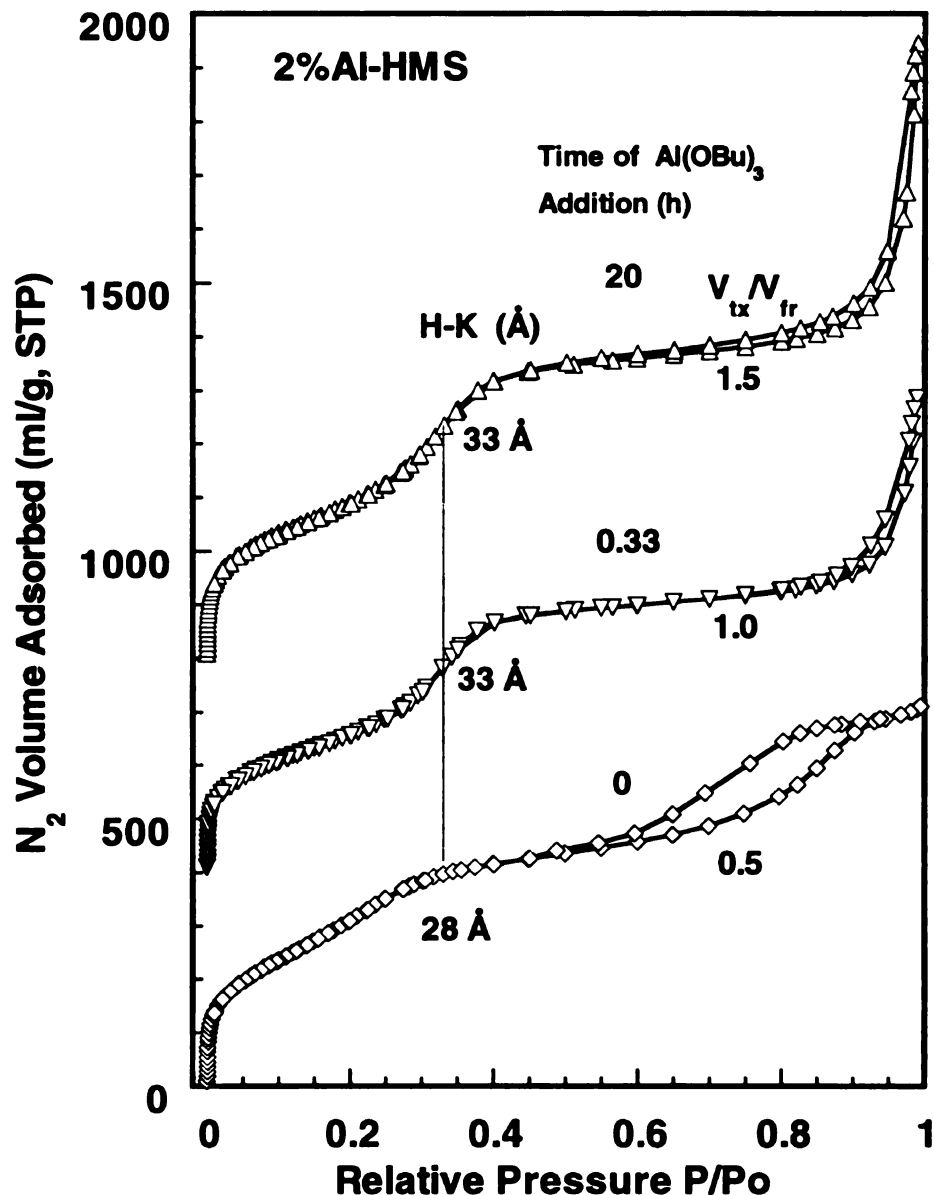


Figure 4.1. N_2 adsorption and desorption isotherms for calcined ($650\text{ }^\circ\text{C}$) Al-HMS molecular sieves with different textural porosity. Each sample was prepared at ambient temperature using dodecylamine as the structure director, TEOS as the silicon source, and using $\text{Al}(\text{sec-OBu})_3$ as the alumination agent, but the alumination agent was added to the reaction mixture 0, 0.33, and 20 hrs after mixing the TEOS and the surfactant. The aluminum content in each case is 2.0 mole%. The Horvath-Kawazoe (H-K) framework pore size, and the ratio of textural to framework mesoporosity ($V_{\text{tx}}/V_{\text{fr}}$) is provided for each sample.

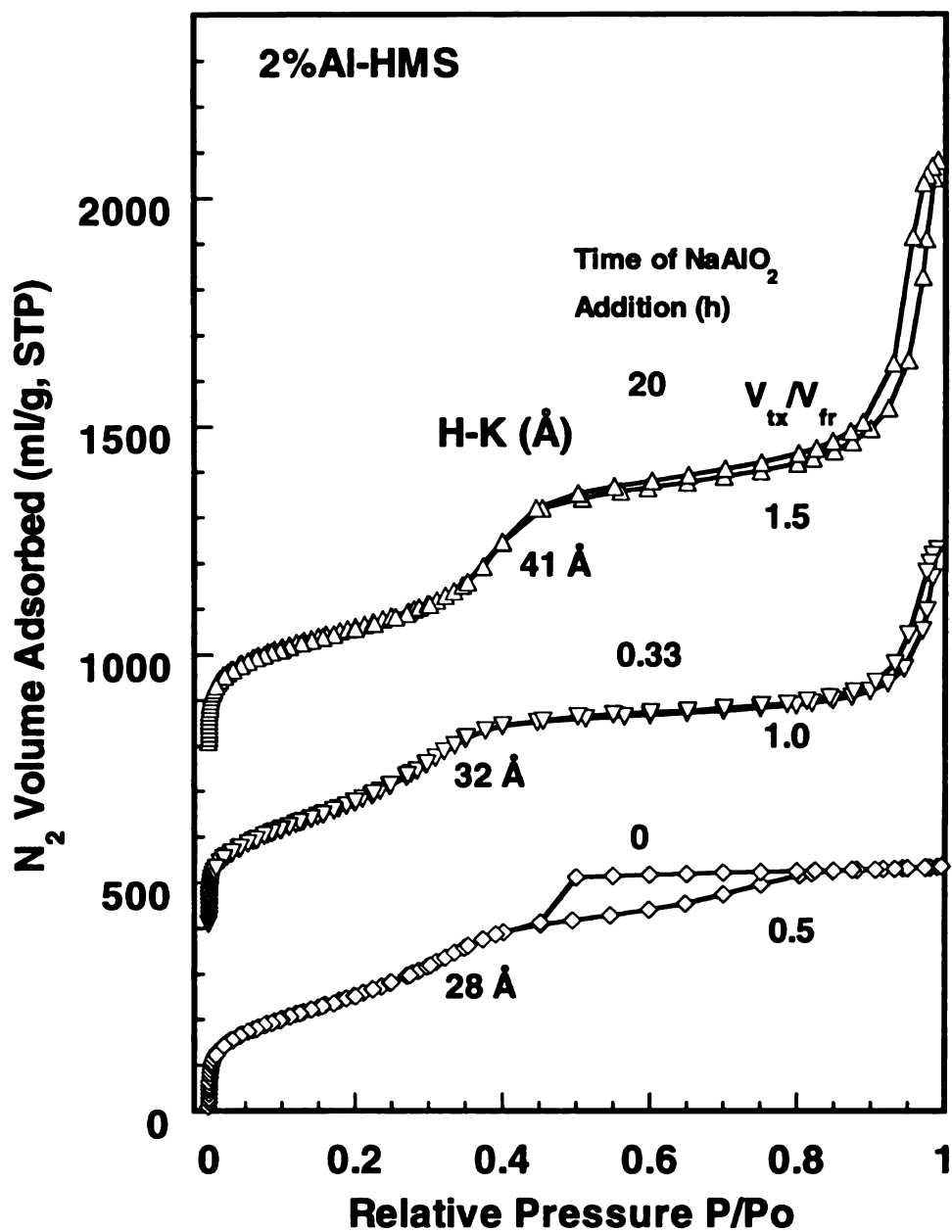


Figure 4.2. N_2 adsorption-desorption isotherms for calcined ($650\text{ }^\circ\text{C}$) Al-HMS molecular sieves prepared as described in the caption to Figure 4.1, except that the alumination agent was sodium aluminate.

delay-time for introduction of the aluminum precursor after addition of TEOS. It is obvious to conclude from Figure 4.1 and 4.2 that the textural pore volume depends very closely on the time of the aluminum precursor addition to the synthesis medium. The highest textural pore volume relative to framework pore volume, was achieved from an in-situ alumination of siliceous HMS with the surfactant micelle still in the mesopore channels. Al-HMS with high textural porosity as high as ~1.5 times of framework mesoporosity (denoted 1.5-tex-Al-HMS) was obtained when the alumination agent was added 20 h after the hydrolysis of the TEOS in the presence of the surfactant at ambient temperature. Due to the fact that most of the framework skeleton of HMS is formed within first 20 minutes after addition of TEOS to the surfactant solution, structural alternation would be minimized if aluminum precursor was added 20 minutes after addition of TEOS. Actually, a Al-HMS with the textural porosity equivalent to the framework mesoporosity, (denoted 1.0-tex-Al-HMS) was obtained at this alumination time. Interestingly, when the aluminum precursor was added immediately after TEOS in an aluminum-silicon co-incorporation manner, the Al-HMS exhibits much lower textural porosity with smaller meso-scaled textural pores indicated by the uptake of N₂ at relatively smaller P/P₀ (i.e. 0.7). The ratio of textural to framework pore volume (V_{tx}/V_{fr}) was ~0.5, hence, denoted 0.5-tex-Al-HMS. In addition, the step in the isotherm indicative of N₂ filling of framework mesopores at P/P₀ ~0.3 was smeared, and the framework pore volume and pore size was decreased. This suggests that aluminum incorporation at the initial stage of the assembly deteriorate the formation of framework, especially for neutral S^oT^o assembly. This result is in agreement with Al-MCM-41 which exhibits a much broader (100) reflection, and weakened higher order reflections, in comparison with

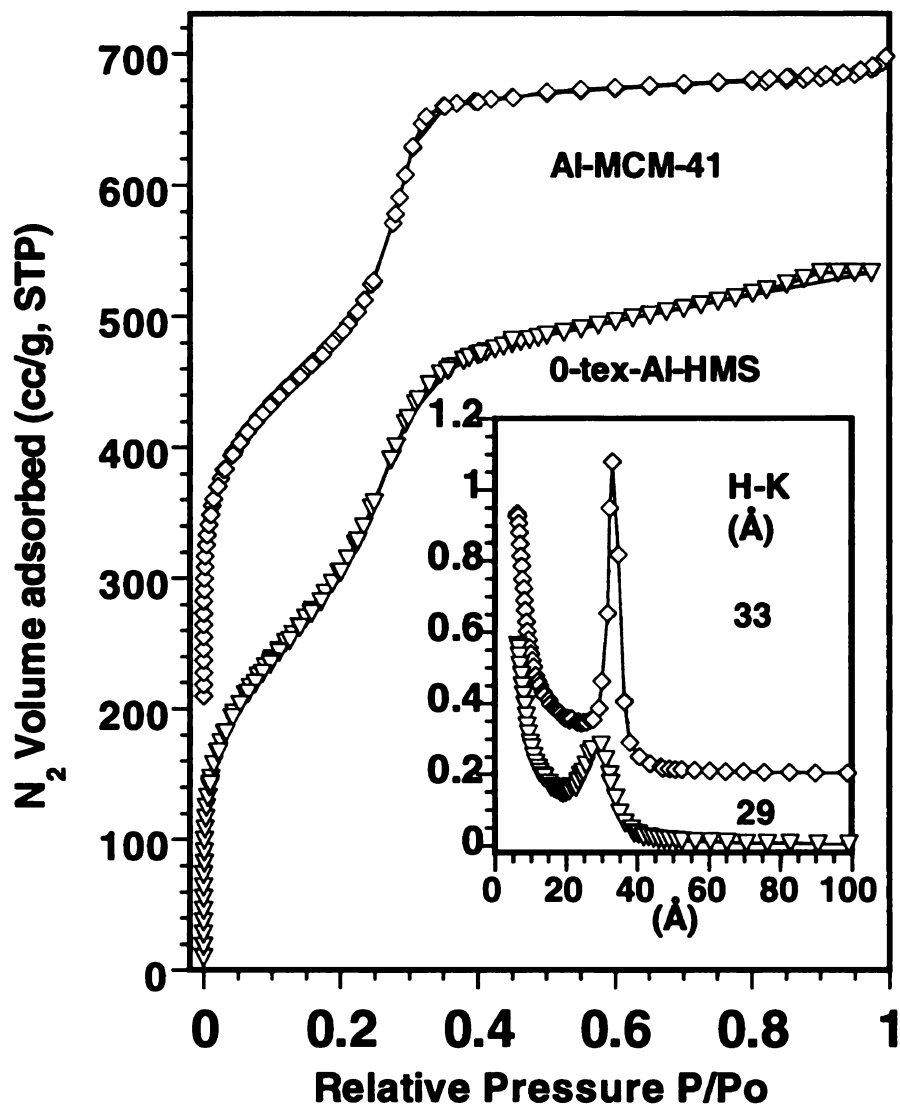


Figure 4.3. N_2 adsorption-desorption isotherms for calcined (650 °C) 2% Al-HMS and calcined (540 °C) Al-MCM-41 with zero-textural porosity. The inset shows Harvath-Kawazoe pore size distributions for these two samples. This Al-HMS was prepared using aluminum sec-butoxide as the alumination agent, which was added to the reaction mixture 20 minutes after mixing the TEOS and the surfactant solution.

siliceous MCM-41.²¹ Our observations on the effect of co-assembly of aluminum with silicon in HMS is in agreement with the results of Al-HMS prepared by Jones and his co-worker.⁷ They mixed aluminum alkoxide and TEOS before adding the mixture to the surfactant solution. The total pore volume of their mesostructure was significantly reduced from 1.68 ml/g for the pure silica analogous to 0.65 ml/g by incorporation of just ~2.5 mol% Al into the framework. Interestingly, the Al-HMS prepared by Jones et al did exhibit higher acidity than Al-MCM-41 analogous although textural porosity was not observed. We verified their result by preparing a Al-HMS in a relatively less polar solvent medium with a EtOH/H₂O ratio of 50/50 (see below for discussion about acidity). As showed in Figure 4.3, this Al-HMS exhibits no hysteresis loop for textural pores in the isotherm and so does the Al-MCM-41. Actually, the N₂ isotherm for Al-MCM-41 exhibits very sharp framework mesopore filling step at relative pressure of 0.3. Consequently, the pore size distribution is relatively sharp and narrow also. In contrast, 0-tex-HMS exhibits a somewhat wider pore size distribution. The differences in framework structure, hexagonal vs. wormhole, are reflected in the widths of the pore size distribution.

Figure 4.4 and 4.5 show the powder X-ray diffraction patterns of Al-HMS prepared by addition of Al(*sec*-Obu)₃ and NaAlO₂ respectively to the TEOS-dodecylamine hydrolysis mixture after various reaction times. Three Al-HMS samples with different textural porosity prepared using aluminum alkoxide as the aluminum precursor show nearly identical d-spacing at 4.2 nm (Fig. 4.4). Relatively higher d-spacing (52 Å) along with larger pore size (41 Å) was obtained for Al-HMS prepared using NaAlO₂ (Fig. 4.5). This may indicate that sodium cations facilitates the pore size

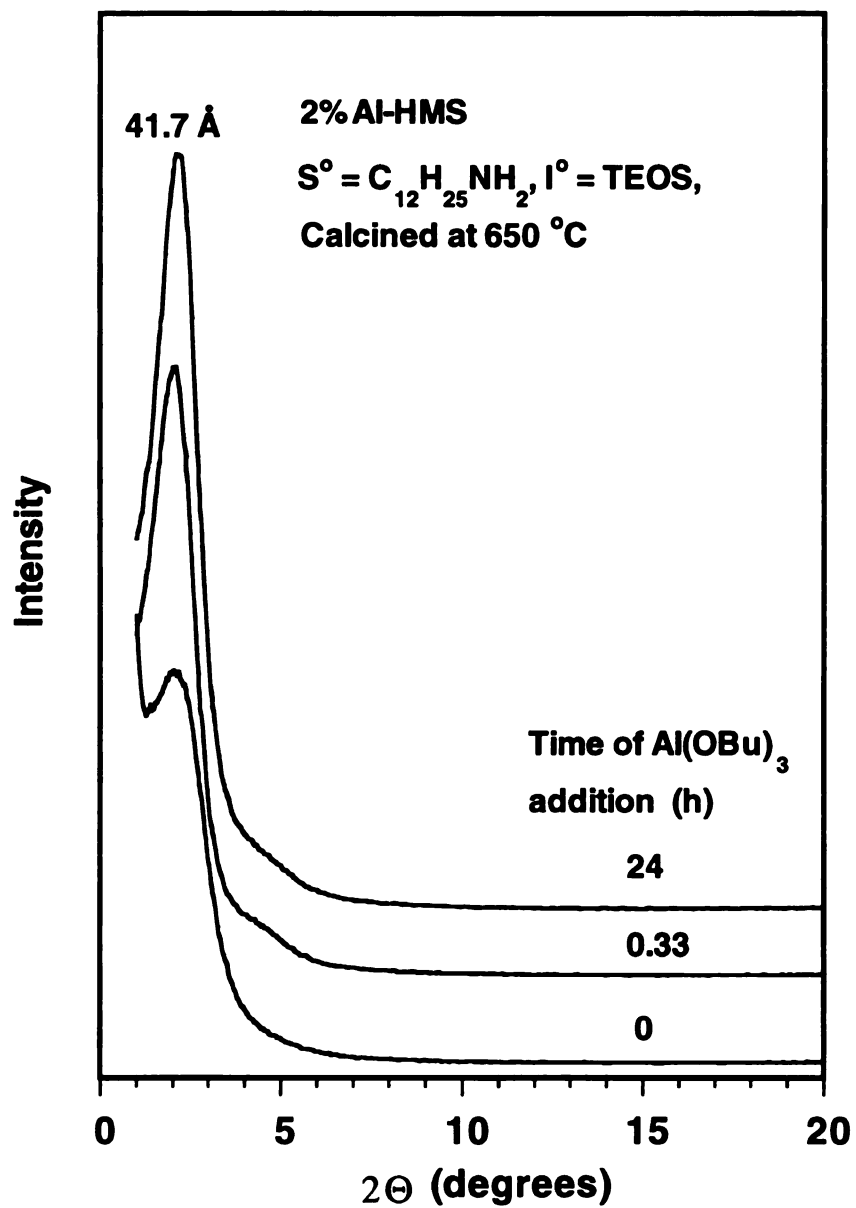


Figure 4.4. XRD patterns of calcined 2%Al-HMS molecular sieves prepared as described in the caption to Figure 4.1.

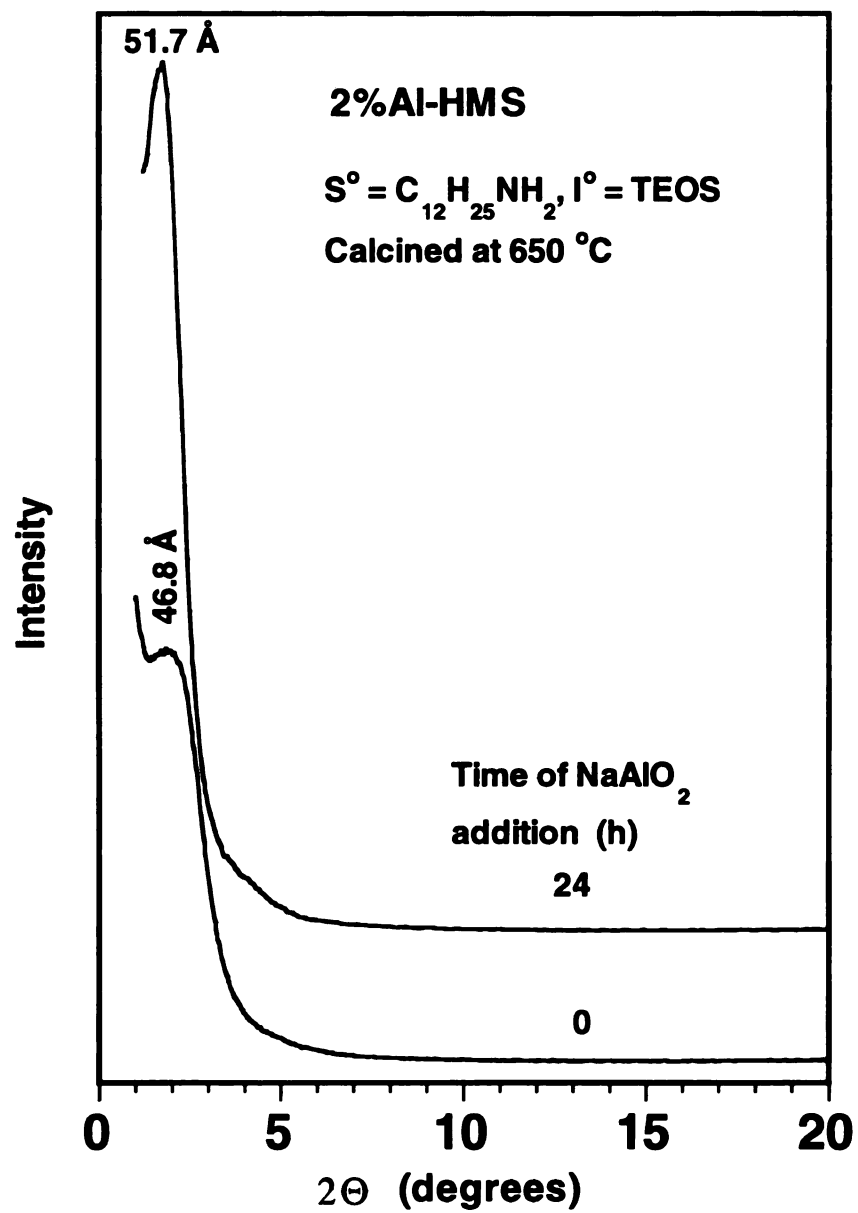


Figure 4.5. XRD patterns of 2%Al-HMS prepared as described in the caption to Figure 4.1, except that NaAlO₂ was the Al-source.

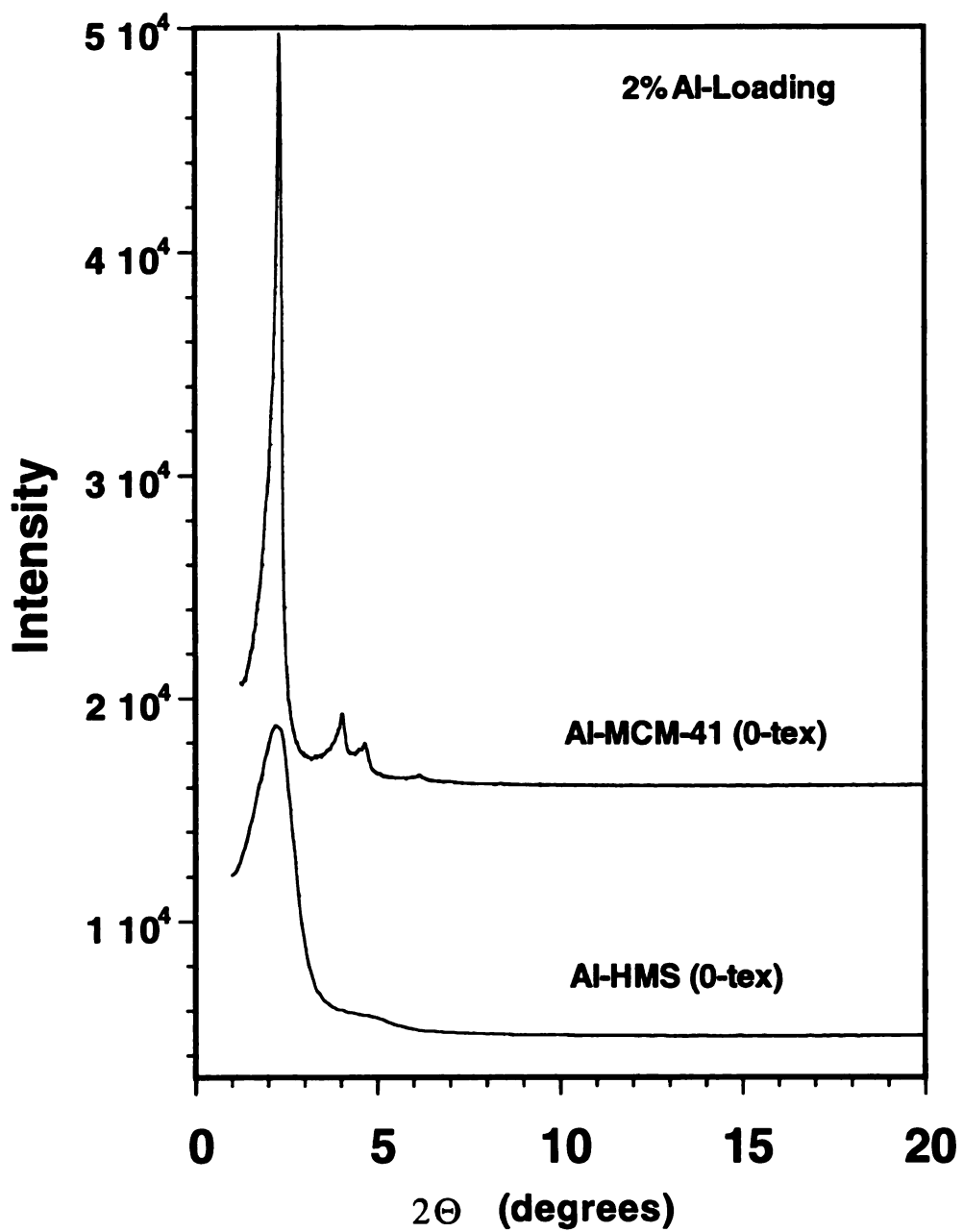


Figure 4.6. XRD patterns of calcined 2% Al-HMS and Al-MCM-41 with zero-textural porosity as described in the caption to Figure 4.3.

enlargement by exchange into the interface of surfactant and framework wall as proposed for larger pore MCM-41 synthesis.²² It worth pointing out that this kind of pore enlargement process takes place at elevated temperature for MCM-41, but it occurs for HMS at ambient temperature. Regardless of the type of aluminum precursors, the sample prepared by the addition of an aluminum precursor immediately after addition of TEOS caused the intense reflection to be broadened. This loss of wormhole framework structure is in agreement with the N₂ adsorption-desorption isotherms (cf. Fig. 4.1 and 4.2).

The XRD patterns for 0-tex-Al-HMS and Al-MCM-41 are showed in Figure 4.6. 0-tex-Al-HMS exhibits equivalent reflection to that of pristine HMS.³ Al-MCM-41 exhibits well resolved hexagonal X-ray reflections. Apparently, the structural order of both HMS and MCM-41 were fully retained since both samples were prepared through a follow-up in-situ alumination. Even though they were assembled from a different mechanism, the total pore volumes for both of them are virtually the same (c.f. Fig. 4.3).

As stated earlier, it is very important to have mesoporous molecular sieves with small fundamental particle size so that the porous channels can be shortened and diffusion resistance minimized. It was found that meso-scaled fundamental particles are always associated with high textural porosity in pristine HMS. To confirm this for Al-HMS, we examined three derivatives prepared using either Al-alkoxide or NaAlO₂ by TEM. As exemplified in Figure 4.7A, fractal-like particles with a worm-hole-like structural motif prevail for both 1.0-tex-Al-HMS and 1.5-tex-Al-HMS. Irregularly shaped inter-particle voids (~150 to ~500 Å) are present between aggregates of the fundamental meso-scaled particles ~100 to ~500 nm in size. These voids are the textural pores responsible for the hysteresis loop observed in the high textural pore materials at partial

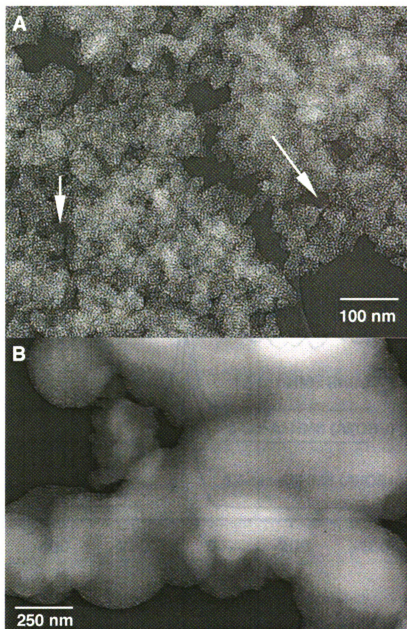


Figure 4.7. TEM images showing meso-scaled textural pores as well as worm-hole like framework mesopores for calcined 1.5-tex-Al-HMS and 0-tex-Al-HMS.

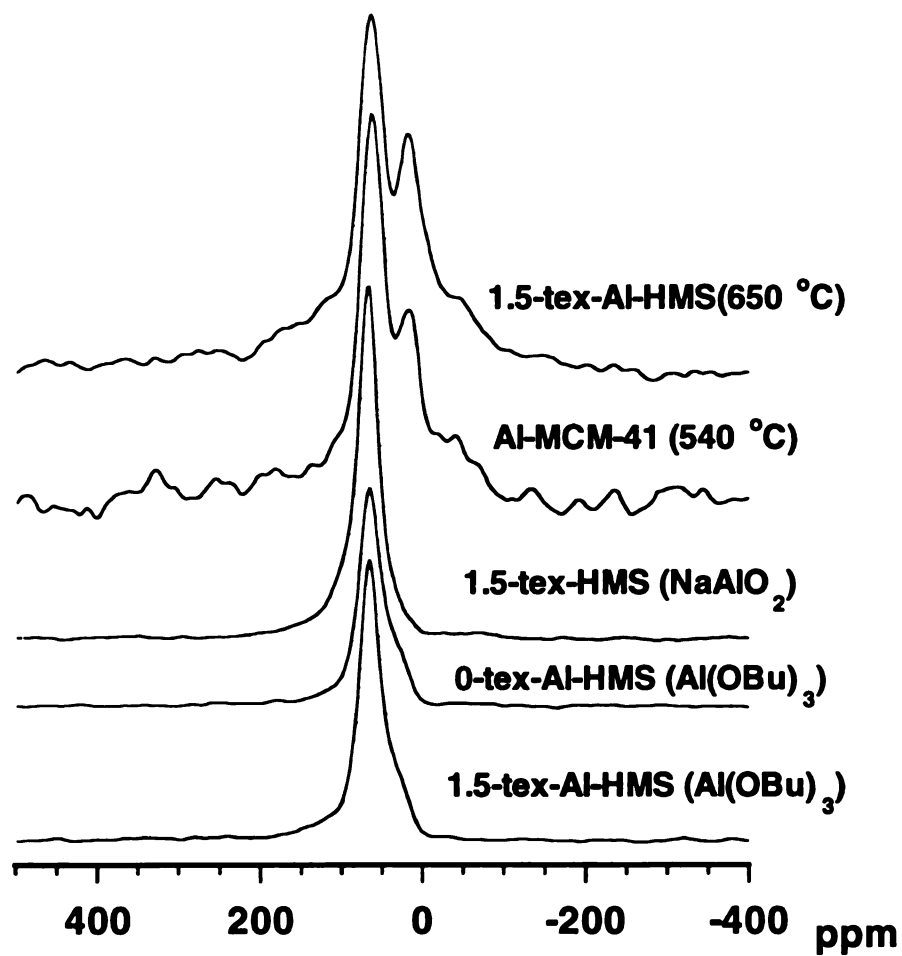


Figure 4.8. ^{27}Al -NMR spectra showing predominantly tetrahedral Al-sites (63 ppm) and a small amount (~10%) of octahedral Al-sites (18 ppm) in as-made Al-HMS prepared using $\text{Al}(\text{sec-OBu})_3$ as the alumination agent. Calcined forms of Al-HMS, as well as calcined Al-MCM-41, show 70% tetrahedral and 30% octahedral Al-sites.

pressures above 0.9. Unlike the textural porosity-rich sample, Al-HMS with zero-textural porosity shows sub-micro-sized beads on string type of spheroidal particles (Fig. 4.7B). Although the particle size for a 0.5-tex-Al-HMS is about 2 times larger (not shown) than 1.0-tex-Al-HMS, but they are still about 5 times smaller than that of 0-tex-Al-HMS.

²⁷Al-NMR spectra are shown in Figure 4.8. Obviously, the vast majority of aluminum species in as-made Al-HMS are in a tetrahedral coordination environment. These aluminum sites possess a chemical shift at ~63 ppm. The NMR spectra differences between high and low textural porosity samples are practically indistinguishable. Al-HMS prepared using Al-alkoxide shows a slightly higher content of octahedral aluminum species (c.f. the shoulders at around 16 ppm) than the one prepared using NaAlO₂, possibly because of aluminum oxide clusters generated by fast hydrolysis of aluminum alkoxide. Calcined Al-MCM-41 and calcined Al-HMS exhibited about 30% octahedral (indicated by 18 ppm shoulders) and 70% tetrahedral aluminum sites that possesses a chemical shift position at 63 ppm also. Nevertheless, the completion of the alumination of HMS at ambient temperature suggests that the surfactant molecules inside the framework pores be disregarded by aluminum precursors. As a consequence of a neutral interfacial interaction (H-bonding) between the surfactant and the framework, anionic aluminum precursor species is allowed to migrate easily through the neutral interfacial gaps in the absence of charge repulsion, and to become incorporated into the framework.

The amount of acid of each catalyst was measured through TGA analysis of the amount of cyclohexamine (CHA) desorbed in the temperature range 240 to 420 °C. As shown in Table 4.1, among all five Al-HMS samples regardless of textural porosity and

aluminum precursor, the average amount of acidity was 0.34 mmol CHA/g. This accounts up to 100% of the loading of Al, if it is assumed that each Al generates one acid site. This indicates that both tetrahedral and octahedral Al-sites in Al-HMS contribute to the total acidity, which suggest that octahedral Al-sites in Al-HMS be isolated, possibly grafted Al-sites rather than aluminum oxide clusters. In agreement with the results reported by Jones et al, the acidity observed for our 2 mol% Al-HMS is about 3 times higher than that of 2 mol% Al-MCM-41 (i.e. 0.10 CHA mmol/g). The difference in the acidity strongly

Table 4.1. Physical and chemical properties for Al-substituted mesoporous molecular sieves

Catalyst	Aluminum Source	S_{BET} (m^2/g)	Pore Volumes ^a (cc/g)			H-K Pore Size (nm)	Acidity ^b (mmol /g)
			V_t	V_{fr}	V_{tex}		
0-tex-Al-HMS	Al(OBu) ₃	1234	0.86	0	0	2.9	0.37
0.5-tex-Al-HMS	Al(OBu) ₃	968	1.08	0.67	0.41	2.8	0.36
1.0-tex-Al-HMS	Al(OBu) ₃	976	1.38	0.73	0.65	3.3	0.38
1.5-tex-Al-HMS	Al(OBu) ₃	1020	1.77	0.80	0.97	3.3	0.30
1.5-tex-Al-HMS	NaAlO ₂	978	1.95	0.80	1.15	4.1	0.30
Al-MCM-41	Al(NO ₃) ₃	1070	0.87	0	0	3.1	0.10

^a. The total pore volume (V_t), including the textural pore volume (V_{tex}), was measured on the isotherm at $P/P_0 = 0.99$. The framework pore volume (V_{fr}) was measured at $P/P_0 = 0.5$. ^b. The total acidity for these catalysts were obtained by means of TGA through measurement of cyclohexylamine desorption between 230 to 420 °C.

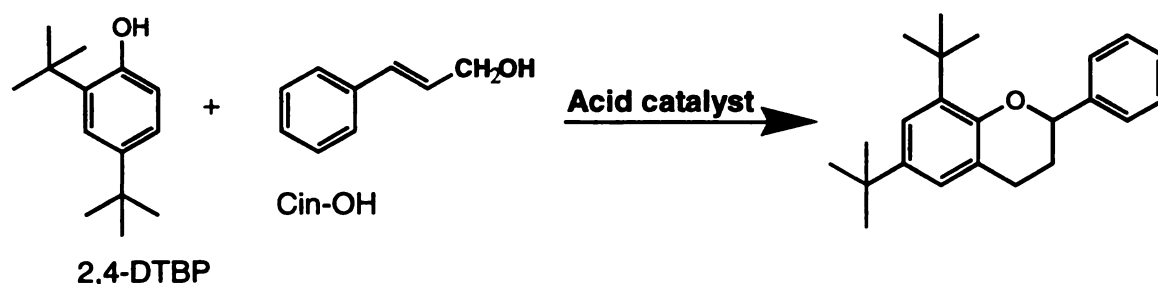
suggest that about 2/3 of Al-sites for Al-MCM-41 be inaccessible by cyclohexylamine. As long as a ^{27}Al -NMR spectrum of Al-MCM-41 does not exhibit a significantly higher number of octahedral Al-sites, the difference in acidity between Al-MCM-41 and Al-HMS with the same Al-loading can not be attributed to large amount of extra-framework aluminum sites. It appears more likely that the lower total acidity in the case of Al-MCM-41 is due to lower accessibility of Al-sites buried in the ~ 12 Å thick walls. The possibility of Na^+ blocking the acid sites was excluded by the fact that a low Na/Al ratio of 0.1 was observed by ICP elementary analysis of this Al-MCM-41. The acidity for all Al-HMS samples are not considerably different from each other. Therefore, the performance differences in acid catalyzed reaction for Al-HMS molecular sieves can not be attributed to the intrinsic difference of acid sites (see below).

In summary, Al-HMS with high textural porosity, small fundamental particle size, and wormhole framework porous structure was prepared by carefully controlling the addition of aluminum precursor during the syntheses. In order to minimize the framework deterioration caused by Al incorporation and to maintain the high textural porosity, the aluminum precursor was introduced into the reaction mixture after the formation of the silica framework (i.e., after 20 h of TEOS hydrolysis in the presence of the primary amine structure directors). It worth to pointing out that both aluminate anion and $\text{Al}(\text{OH})_x(\text{OBu})_{3-x}$ type of hydrolysis molecules (i.e., possible aluminum species involved in the alumination process) can diffuse into the surfactant-filled framework mesopores and became incorporated into the silica framework at ambient temperature.

4.3.3 Catalytic Results

As discussed before, four type of Al-HMS molecular sieves with different amount of textural porosity were prepared through control of the reaction conditions. In order to compare the catalytic activity for the Al-substituted mesoporous molecular sieves, the acid catalyzed alkylation of 2,4-di-tert-butylphenol was chosen because bulky reagents are completely inaccessible to the acid centers inside the micropores of H-Y zeolite ¹³.

The



importance of diffusion might be manifested in this large molecule reaction. In the first report of this reaction using mesoporous MCM-41 as the catalyst, the reaction was carried out at 90 °C for 24 h.¹³ We found that it is not necessary to carry out this reaction for that long, because one of the two reactants, cinnamyl alcohol, is nearly 100% consumed after 6 h at even 60 °C. Most of the by-products from this reaction were transformed from cinnamyl alcohol alone in the presence of catalyst. Three products were identified from the conversion of 2,4-di-tert-butylphenol by GC-MS analysis. These three products account for up to ~90% of consumed 2,4-di-tert-butylphenol. The major product is flavan. Two by-products were 4-tert-butylphenol and 4,6-di-tert-butyl benzofuran. Since these

two by-products only account for less than 5% of consumed 2,4-di-tert-butylphenol, they are not listed in Table 4.1. Interestingly, 4-tert-butylphenol, the product of dealkylation

Table 4.2. Alkylation of 2,4-di-tert-butylphenol with cinnamyl alcohol catalyzed by Al-substituted mesoporous molecular sieves^a

Catalyst	Aluminum Source	Conv. (%) 2,4-DTBP	Selectivity for Flavan (%)	Yield of Flavan (%)
0-tex-Al-HMS	Al(OBu) ₃	50.8	71.3	36.2
0.5-tex-Al-HMS	Al(OBu) ₃	59.6	77.9	46.4
1.0-tex-Al-HMS	Al(OBu) ₃	60.9	77.1	46.9
1.5-tex-Al-HMS	Al(OBu) ₃	61.9	83.2	51.5
1.5-tex-Al-HMS ^b	NaAlO ₂	65.3	86.8	56.6
Al-MCM-41 ^b	Al(NO ₃) ₃	47.2	71.8	33.9

^a. Each catalyst contains 2 mol% Al; the reaction was carried out using 10.0 mmol of each reactant, 500 mg of catalyst, in 50 ml of isooctane at 60 °C for 6 h.

^b. These catalysts were ion-exchanged with 0.1 M NH₄NO₃ before calcination.

of 2,4-DTBP was barely detectable for most Al-HMS catalysts. However, this was a much more apparent by-product for conventional Al-MCM-41 as the catalyst. As shown in Table 4.2, the conversion of 2,4-DTBP and the selectivity as well as the yield of the desired product flavan all increase with the textural porosity of Al-HMS. The selectivity to flavan was un-precedently high (i.e. ~87%).

It is particularly noteworthy that 0-tex-Al-HMS and Al-MCM-41 exhibit very similar catalytic activity, but the activity is much lower than their HMS analogs with high

textural porosity. These results signify the importance of textural porosity in facilitating the access of substrate molecules to acid sites. Our MCM-41 sample exhibited almost the same flavan yield as reported by Corma et al for Al-MCM-41 with approximately the same Al-loading. Corma's Al-MCM-41 catalyst was NH^{4+} -exchanged after removal of the surfactant by calcination whereas our Al-MCM-41 was NH^{4+} -exchanged prior to removal of the surfactant. An important conclusion from the similarity in catalytic activity would be that our approach for ammonium exchange prior to removal surfactant is as efficient as normal ammonium exchange for surfactant-free MCM-41 molecular sieves.

The physical and chemical properties for all the catalysts, as shown in Table 4.1, are approximately similar to each other except for the BET surface area and pore volume. Even though both of the BET surface area and the framework mesopore volume for 0.5-tex-Al-HMS are smaller than that of 0-tex-Al-HMS, the catalytic conversion and the yield of flavan for the former catalyst are higher. Therefore, the activities of these Al-HMS catalysts are not directly related to BET surface area and mesopore volume. Indistinguishable differences in Al-siting indicated in ^{27}Al -NMR (Fig. 4.8) agrees very well with the amount of total acidity for all Al-HMS catalysts measurement by thermal gravity analysis (TGA) of cyclohexamine desorption. As shown in Table 4.1, the average total acidity for all Al-HMS with 2% Al-loading was about 0.34 mmol/g, which was very close to the theoretical acidity of 0.33 mmol/g. Therefore, it is impossible to attribute the differences in catalytic activity to intrinsic differences in Al-siting among Al-HMS catalysts. However, Al-HMS generally exhibit three times higher total acidity than analogous MCM-41, which is in agreement with the results reported.⁷ The acidity

difference between Al-MCM-41 and Al-HMS with the same Al-loading might be indicative of the fundamental differences in their assembly mechanisms rather than the residual Na^+ , because the amount of Na^+ left in this Al-MCM-41 was only 10 mol% of the total Al.

The results in Table 4.2 unambiguously suggest that textural porosity indeed improve the catalytic conversion of bulky substrates in liquid reactions. In addition to textural pores, the Al-HMS samples with high textural porosity also exhibit very thin (i.e. < 100 nm, this is the maximum specimen thickness for electron beam accelerated at 120 kV to go through easily to obtain good quality TEM pictures) and small fundamental particles (~ 150 nm). Consequently, this feature of Al-HMS would provide limited pore channel lengths that should be comparable to the fundamental particle size. Thus the diffusion resistance of bulky molecules would be minimized and this enhances the accessibility of catalytic active centers in the framework channels and favors the maximum conversions.

4.4 Conclusions

Al-substituted HMS molecular sieves with different amounts of textural porosity relative to the framework mesoporosity were prepared through control of solvent polarity and the time of introduction of the aluminum precursor to the developing wormhole frameworks. Alumination of HMS molecular sieves assembled in the presence of neutral amine surfactant at ambient temperature using NaAlO_2 or $\text{Al}(\text{sec-Obu})_3$ was as effective as literature-reported hydrothermal aluminum incorporation processes for MCM-41 molecular sieves. The purpose for in-situ follow-up alumination is to avoid alternation of

structural features (i.e. high textural porosity etc.) desirable for condensed phase catalysis. Ammonium exchange of sodium-form Al-HMS and Al-MCM-41 at ambient temperature in the presence of surfactant in porous channels was also effective enough to achieve sufficient active H-form mesoporous catalysts. The complementary meso-scaled textural pores as well as meso-scaled fundamental particles of mesoporous molecular sieves were very important to improve the catalytic alkylation of bulky 2,4-DTBP with cinnamyl alcohol to flavan under very mild conditions (60 °C, 6h). The conversion of 2,4-DTBP and the yield of flavan both were dramatically improved in comparison with Al-HMS and Al-MCM-41 catalysts without textural pores.

4.5 References:

1. Ryoo, R.; Jun, S.; Kim, J.M.; Kim, M.J. *J. Chem. Soc., Chem. Commun.* **1997**, 2225.
2. Tanev, P.T.; Chibwe, M.; Pinnavaia, T.J. *Nature* **1994**, 368, 321.
3. Zhang, W.; Pauly, T.R.; Pinnavaia, T.J. *Chem. Mater.* **1997**, 9, 2491.
4. Pinnavaia, T.J.; Zhang, W. *Stud. Surf. Sci. Catal.* **1998**, 117, 23 (Elsevier Science B.V.).
5. Zhang, W.; Froba, M.; Wang, J.; Tanev, P.T.; Wong, J.; Pinnavaia, T.J. *J. Am. Chem. Soc.* **1996**, 118, 9164.
6. Yang, R.; Pinnavaia, T.J.; Li, W.; Zhang, W. *J. Catal.* **1997**, 172, 488.
7. Mokaya, R.; Jones, W. *J. Chem. Soc., Chem. Commun.* **1996**, 983 and *J. Catal.* **1997**, 172, 211.
8. Kloetstra, K.R.; van Bekkum, H.; Jansen, J.C. *J. Chem. Soc., Chem. Commun.* **1997**, 2281.
9. Tuel, A.; Gontier, S. *Chem. Mater.* **1996**, 8, 114.
10. Corma, A.; Fornes, V.; Navarro, M.T.; Perez-Pariente *J. Catal.* **1994**, 148, 569.
11. Hitz, S.; Prins, R. *J. Catal.* **1997**, 168, 194.
12. Corma, A. *Chem. Rev.* **1997**, 97, 2373; and Sayari, A. *Chem. Mater.* **1996**, 8, 1840.
13. Armengol, E.; Cano, M.L.; Corma, A.; Garcia, H.; Navarro, M. *J. Chem. Soc., Chem. Commun.* **1995**, 519.
14. Armengol, E.; Corma, A.; Garcia, H.; Primo, J. *Appl. Catal. A: General* **1995**, 126, 391.
15. Szostak, R.; *Molecular Sieves Principles of Synthesis and Identification*; Van Nostrand Reinhold: New York, **1989**.
16. Beck, J.S.; Vartuli, J.C.; Roth, W.J.; Leonowicz, M.E.; Kresge, C.T.; Schmitt, K.D.; Chu, C.T.-W.; Olson, D.H.; Sheppard, E.W.; McCullen, S.B.; Higgins, J.B.; Schlenker, J.L. *J. Am. Chem. Soc.* **1992**, 114, 10834.
17. Ryoo, R.; Ko, C.H.; Howe, R.F. *Chem. Mater.* **1997**, 9, 1607.

18. Janicke, M.T.; Landry, C.C.; Christiansen, S.C.; Kumar, K.; Stucky, G.D.; Chmelka, B.F. *J. Am. Chem. Soc.* **1998**, 120, 6940.
19. Luan, Z.H.; Cheng, C.F.; He, H-Y.; Klinowski, J. *J. Phys. Chem.* **1995**, 99, 10590.
20. Gunnewegh, E.A.; Gopie, S.S.; van Bekkum, H. *J. Mol. Catal. A: Chemicals* **1996**, 106, 151.
21. Luan, Z.H.; Cheng, C.F.; Zhou, W.Z.; Klinowski, J. *J. Phys. Chem.* **1995**, 99, 1018.
22. Corma, A.; Kan, Q.; Navarro, M.T.; Perez-Pariente, J.; Rey, F. *Chem. Mater.* **1997**, 9, 2123.

Chapter 5

Toward MCM-41 with Meso-scaled Channel Lengths and Textural Pores for Catalysis

Abstract

The concept of altering structures of mesoporous silica molecular sieves through introducing organic promoters to bind to the head group of charged surfactants in the electrostatic S⁺T assembly has been successfully illustrated. Mesoporous silica molecular sieves with well ordered 3-dimensional hexagonal, cubic, and uni-dimensional hexagonal phases were selectively assembled using cetyltrimethyl ammonium bromide as the structure director and sodium silicate as the silicon source under a relatively low surfactant to silicon ratio (i.e. 0.11) at 150 °C. Intrinsically, the structural variation was strategically realized through surfactant-organic promoter association that leads to the variation of surfactant micelle packing parameters ($g = V/a_0l$) and, ultimately, the inorganic meso-structures. Organic promoters such as salicylic, tartaric, oxalic, and citric acid were found effective to alter meso-structures from hexagonal to either 3-dimensionally hexagonal or cubic. These promoters were also effective at mild hydrothermal condition (i.e. 100 °C) for synthesis of particular MCM-41 with a flaky morphology. These flakes exhibit mesopore channels running orthogonal to the flaky sheets with meso-scaled lengths. Considerably well ordered MCM-41 molecular sieves with meso-scaled fundamental particles and high textural porosity were also prepared by careful control of the addition of organic acids.

Consequently, a follow-up in situ alumination of the flaky and textural porosity MCM-41 in the presence of surfactant micelles inside the pores affords well incorporated

Al-sites with over 95% are in tetrahedral coordination even for Al-loading up to 8.8mol%. However, up to a third of these Al-sites are transformed into octahedral sites upon the surfactant removal by calcination. Al-sites judged from ^{27}Al -NMR and the total acidity measured from TPD of cyclohexylamine are indistinguishable from each other for similarly loaded Al-MCM-41 catalysts regardless of particle morphology. Consequently, any differences in catalysis for these Al-MCM-41 catalysts can not be attributed to any differences in the intrinsic acid siting. The number of Al-sites with stronger acidity indicated by the desorption of pyridine at 350 °C was proportionally increased with Al-loading, but the number of Al-sites with weaker acidity indicated by the desorption of pyridine at 217 °C remained the same.

The results of the studies of 2,4-DTBP alkylation with cinnamyl alcohol proves that the accessibility of the active Al-sites in flaky and textural porous Al-MCM-41 with short channel lengths is significantly facilitated. At least 30% higher conversion of 2,4-DTBP and 50% higher yield of flavan are obtained relative to Al-MCM-41 catalyst without a flaky or textural porous morphology. This alkylation reaction is likely catalyzed by the mild acid sites since increasing the number of stronger acid sites by increasing the Al-loading does not improve the activity considerably.

5.1 Introduction

M41S materials are ordered, mesoporous silicas and aluminosilicate molecular sieves with pore size in the range of 20 – 100 Å.¹ Among M41S family members, hexagonal MCM-41 and cubic MCM-48 are very promising catalysts and catalyst supports for chemical reactions involving large molecular substrates.² The pore channels for MCM-48 are bi-continuous, branched and tortuous.³ The pore channels for MCM-41, however, are uni-dimensional. Uni-dimensional channels may invoke counter-stream diffusion resistance, because the reactants need to diffuse in and the products need to diffuse out of the tubular channels.⁴ The significance of this particular drawback for MCM-41 has not yet attracted attention.

Even though MCM-48 exhibits attractive 3-d pore connectivity, the difficulty to synthesize hetero-atom incorporated cubic meso-structures severely limited the study of this particular meso-structure and far fewer reports have been published.⁵⁻⁸ Actually, the synthesis of Al-MCM-48 is even more problematic, most of the time the obtained materials lack catalytic properties that are distinctive from MCM-41. Other than the 3-d pore connectivity, MCM-48 has not been found to be fundamentally different from MCM-41.⁷ Therefore, for the purpose of catalysis it is desirable to simplify MCM-48 synthesis or to improve the accessibility to the uni-dimensional channels of MCM-41.

MCM-41 silica molecular sieves have been synthesized under various conditions. Two distinguishable electrostatic assembly pathways have been reported using positively charged quaternary ammonium surfactants (S^+) as the structure director. One is the surfactant-inorganic precursor charge matching mechanism (S^+T) working under basic conditions using silicate species (I^-) and the other is the counterion mediated assembly

mechanism (S^+XT^+) working under acidic conditions using protonated silicon alkoxide species (I^+).⁹ The later one encounters significant difficulties for the synthesis of metal-substituted derivatives since the catalytically active metal-centers are barely incorporated into the silica framework under the severe acidic conditions (i.e. $pH < 2$).¹⁰ Although it is possible to synthesize MCM-41 under ambient conditions via the S^+T assembly pathway, the structure obtained, however, is lacking in thermal and hydrothermal stability.¹¹ Therefore, most MCM-41 samples for catalysis, especially Al-substituted analogs, were synthesized under hydrothermal conditions through the S^+T pathway.^{1,12}

To prepare MCM-41 with well ordered hexagonal structure via S^+T pathway, relatively high concentrations of surfactant and high temperatures ($> 100\text{ }^\circ\text{C}$) were adopted by Mobil scientists.¹ Unlike most zeolitic structures that normally crystallize under very basic conditions (for example, NaY forms at pH above 12), mesoporous MCM-41 structures with amorphous silica framework walls usually form under less basic condition (i.e. $pH < 11$) to minimize the dissolution of amorphous silica walls. Therefore, MCM-41 synthesis under basic conditions using sodium silicate as the silicon source has to use some kind of acid to lower the pH. Ryoo and his co-worker reported a step-by-step acid titration approach to obtain well ordered MCM-41 using acetic acid over 4 days at $100\text{ }^\circ\text{C}$.¹³ White and his co-worker later reported that sulfuric acid was the best acid for adjusting pH during MCM-41 synthesis by following this titration approach.¹⁴ Similarly, Mou and his co-workers¹⁵ prepared a hierarchical tubular MCM-41 structure through a day by day addition of sulfuric acid at $100\text{ }^\circ\text{C}$. The function of acid, other than adjusting pH in these preparations, is not clear yet.

In general, meso-structures form through surfactant micelle assembly involving inorganic reagents cross-linking and condensing around the micelles to build a framework. As reviewed by Behrens¹⁶ the interfacial interactions between surfactant micelle and inorganic precursors are very crucial for assembly of meso-structures. The interactions primarily determine the final phase of the meso-structures.¹⁷ Actually, in the classical surfactant micelle chemistry,¹⁸⁻²⁰ the interaction energy is the key factor for the surfactant packing parameter g ($g = V/(a_0l)$). If g is around $1/2$, surfactant micelles tend to form a hexagonal phase. A cubic phase forms for g values between $1/2$ and $2/3$. If the g value approaches $1/3$, a 3-dimensional (3-d) hexagonal or a spherical cubic phase is favored. Therefore, to tailor the structure and pore conductivity of MCM-41, the easiest way would be to control interfacial interactions.

The first objective of the present study was to alter the interfacial interaction to obtain versatile mesostructures using organic acid as the structure promoter. The second objective of our study is to slightly alter the interfacial interaction using organic acid as structure modifier so that meso-scaled fundamental particles and channel lengths could be obtained for MCM-41. Organic acid was chosen, because salicylic acid was known to associate with the head group of cetyltrimethyl ammonium bromide to form helical fibers.²¹ By using carboxylic acid, our strategy is to minimize the association energy to such a point that it is not strong enough to cause a phase transition but towards a phase transition, allowing the channel lengths and the orientation of particle growth to be tailored.

The third objective was to prepare a well-ordered MCM-41 aluminosilicate with textural porosity. Davis and his coworkers reported²² that the textural porosity for MCM-

41 was closely related to the disorder caused by surfactant-rod-micelle-entangling because a significant amount of N₂ uptake in the isotherm for textural pores was accomplished without seeing higher order X-ray reflections in the powder patterns. Our results indicate that the textural porosity is not necessarily associated with the structural disorder. However, it is closely associated with meso-scaled fundamental particles. Fundamental particles aggregate to form meso-scaled inter-particle voids as the textural pores.

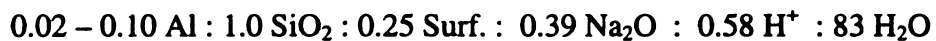
Textural porosity along with meso-scaled fundamental particles indeed facilitates the access to catalytic centers inside mesopore channels.²³ In order to show the importance of textural porosity for catalysis, alkylation of 2,4-di-tert-butylphenol with cinnamyl alcohol in the presence of MCM-41 aluminosilicate molecular sieves as the catalyst was conducted under very mild conditions (i.e. 60 °C, 6 h). Significantly higher conversion (i.e. >60%) of 2,4-DTBP and higher yield of the desired product flavan (~50%) was obtained for Al-MCM-41 with high textural porosity and meso-scaled fundamental particles relative to the analogs without textural porosity.

5.2 Experimental

MCM-48 and 3-dimensional hexagonal mesoporous silicas were synthesized at 150 °C through surfactant directed assembly in the presence of organic promoters such as salicylic, citric, tartaric and oxalic acids. A typical synthesis was started by mixing a sodium silicate aqueous solution as the silicon source and cetyltrimethyl ammonium bromide as the structure director at ambient temperature. The structure promoters were added to the mixture at ambient temperature under vigorous stirring for 15 minutes

before the mixture was transferred to a Teflon lined autoclave to age at 150 °C for 15 h. The composition for the synthesis was following: 1.0Si : 0.11CTAB : 0.39Na₂O : 0.28H⁺ : 130H₂O. In the case of salicylic acid, the promoter to surfactant ratio was controlled to 1, which also contributed part of 0.28 mole H⁺ per mole of silicon and the rest part of H⁺ was compensated by sulfuric acid. In the case of citric, tartaric and oxalic acid, all of the H⁺ were came from these promoters.

MCM-41 sample was prepared using 27wt% sodium silicate solution as the silicon source and cetyltrimethyl ammonium bromide as the structure director. An organic acid such as tartaric, oxalic, citric, gluconic, and salicylic acid was used as the pH adjuster, as well as the structure modifier. Sulfuric acid was included for comparison. Three types of MCM-41 with different textural porosity were prepared by controlling the amount and the time for acid modifier addition. The molar composition for the synthesis of MCM-41 with textural porosity was:



To control the pH as well as the association energy between the organic acid and the surfactant head group, part of the acid was added to the sodium silicate aqueous solution before the surfactant was added. The remaining part was added later. In a typical experiment, 83% of the total amount of acid shown in the aforementioned composition formula was added to the sodium silicate solution at the beginning, and the remaining 17% was added after 1 day heating at 100 °C. The MCM-41 obtained exhibits textural pores similar to the textural pores formed by aggregates of layered clay particles. A high textural porosity MCM-41 was synthesized by the addition of 100% of the required

amount of acid in one-lot after mixing the surfactant and sodium silicate solution, and then heating at 100 °C for 2 days.

A typical Mobil MCM-41 without textural porosity was prepared using sulfuric acid at 100 °C for 2 days. The amount of sulfuric acid was 17% less than organic acid used in the aforementioned compositions. The acid was added at the very beginning and the pH of this synthesis was ~10.5.

For siliceous MCM-41, the product was filtered after 2 days aging at 100 °C. For Al-MCM-41, $\text{Al}_2(\text{NO}_3)_3$ aqueous solution was added at ambient temperature under stirring to the as-made siliceous MCM-41 in its mother liquor, and then it was statically aged at 100 °C for another 2 days. Actually, this was still an in situ alumination process in a follow-up manner. Aluminum nitrate was chosen as the aluminum precursor over other aluminum sources such as aluminum sulfate and sodium aluminate. The purpose for this choice is to avoid the undesired acidic sites generated by residual anions (i.e. SO_4^{2-}) in the case of aluminum sulfate and structural alternation due to pH increase in the case of sodium aluminate.

The product was filtered and washed thoroughly with water. The filter cake was ion-exchanged in 0.1 M NH_4NO_3 solution at ambient temperature for 4 h if needed. Otherwise, the filter cake was dried in air and directly transformed into the final catalyst without prior NH_4^+ -exchangment by calcination at 540 °C for 6 h. It is possible that the Na^+ for neutralization of the negative framework charges generated by Al-incorporation might be replaced by charged surfactant molecules inside the mesopores. In this case, Al-MCM-41 prepared using sodium silicate may not require ammonium exchange to transform it into a catalytically efficient H-form.

The powder X-ray diffraction patterns of the samples were recorded on a Rigaku Rotaflex Diffractometer using Cu K α radiation ($\lambda = 1.542 \text{ \AA}$). N₂ adsorption and desorption isotherms were measured on an ASAP 2000 sorptometer at $-196 \text{ }^\circ\text{C}$. The sample was evacuated under 10^{-5} torr at $150 \text{ }^\circ\text{C}$ over night before the measurement. ²⁷Al NMR spectra were recorded on a Varian VXR-400S spectrometer with a 7-mm zirconia rotor and a spin frequency of 4 kHz. TEM images were taken on a JEOL 100CX with a CeB₆ gun that was operating at acceleration voltage of 120 kV. The specimens were loaded onto a holey carbon film that was supported on a copper grid by dipping the grid into a solid sample suspension in ethanol.

Alkylation of 2,4-di-tert-butylphenol (2,4-DTBP) with cinnamyl alcohol was carried out in a 100 ml round bottom flask. A 1.0 mmol quantity of 2,4-DTBP, 1.0 mmol cinnamyl alcohol and 50 ml isooctane as the solvent were used. A 500 mg quantity of catalyst was added when the reaction mixture was heated to $60 \text{ }^\circ\text{C}$. The reaction was kept at $60 \text{ }^\circ\text{C}$ under magnetic stirring for 6 h. The catalyst was filtered and washed with dichloromethane after the reaction. The dichloromethane was separated from the filtrate by distillation under reduced pressure at $\sim 30 \text{ }^\circ\text{C}$, so that heat-induced side reactions could be prevented. The reaction products were qualitatively confirmed using a GC-MS. They were quantitatively analyzed by an internal standard method by using a GC with a FID detector and a 15m long SPB-1 type capillary column. The conversion was calculated by dividing the amount of 2,4-DTBP consumed by the amount initially present. The selectivity toward flavan was calculated by dividing the amount of flavan formed by the amount of 2,4-DTBP consumed. The yield of flavan was obtained by dividing the amount of flavan formed by the amount of 2,4-DTBP added. The conversion

of cinnamyl alcohol was virtually complete in most reactions because cinnamyl alcohol alone could transform into many undesirable products²⁴ such as cinnamyl aldehyde, 1,5-di-phenyl pentadiene, and polymeric aldehyde. The latter product formed a tar on the catalyst, which required calcination in air to regenerate the catalyst.

5.3 Results and Discussion

5.3.1 Effect of Organic Acid Addition on Silica Mesostructure Formation

It has been known for a decade that salicylic acid can associate with head group of cetyltrimethyl ammonium surfactant to form remarkable helical micelle fibers.²¹ Some other α - and β -hydroxyl carboxylic acids interact with charged surfactants in basic medium to form similar micelle fibers too. It has also been known that the surfactant packing parameter g can be varied upon variation of the surfactant head group size and the alkyl chain length. Actually, variation of g parameter to achieve new meso-structures has been shown quite successful in the preparation of SBA-2.²⁵ Landry and his co-worker recently reported²⁶ that the g parameter of cetyltrimethyl ammonium bromide could be varied to allow formation of cubic MCM-48 instead of hexagonal MCM-41 by using 3 mole of EtOH per mole of silicon. Presumably, association of carboxylic acid to the head group of surfactant would affect the g parameter also. We report here that carboxylic acids indeed promote cetyltrimethyl ammonium bromide surfactant to form 3-d hexagonal as well as cubic silica meso-structures under the reaction conditions normally give rise to uni-dimensional MCM-41.

As shown in Figure 5.1, a MCM-48 like cubic silica meso-structure was formed in stead of MCM-41 upon addition of 1 mole of salicylic acid per mole of surfactant. The

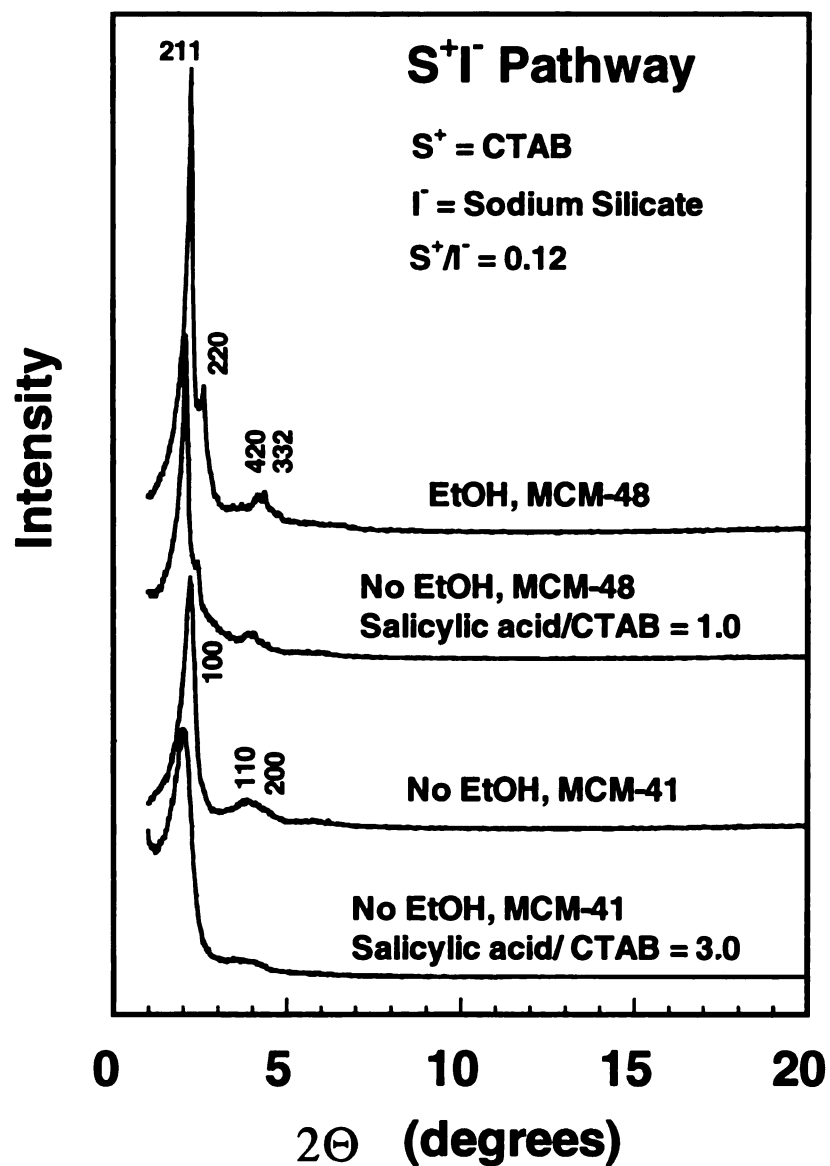


Figure 5.1. X-ray diffraction patterns for calcined (540 °C) cubic silica mesostructures formed at 150°C with a reaction composition of 1.0Si : 0.11CTAB : 0.39Na₂O : 0.28H⁺ : 130H₂O. The diffraction patterns for MCM-48 prepared by following Landry's method as well as the diffraction patterns for a sample prepared in the absence of both EtOH and salicylic acid are included.

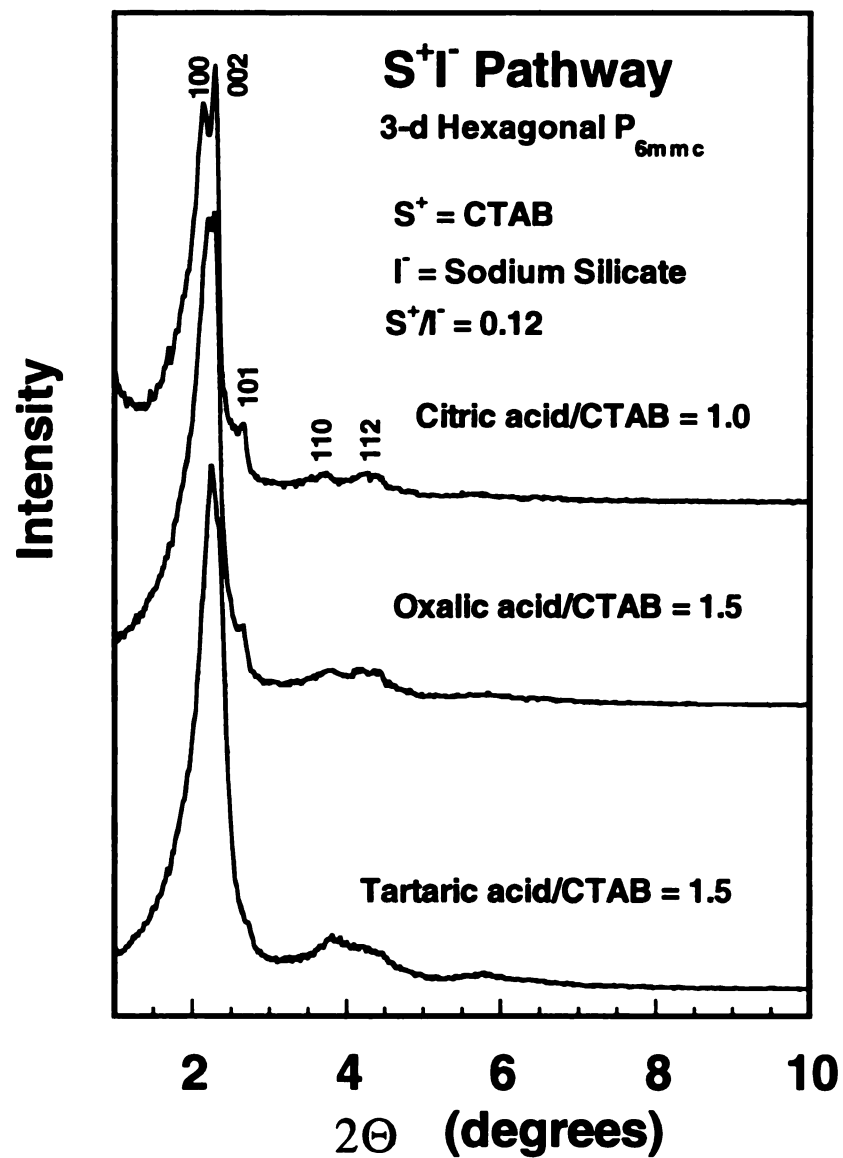


Figure 5.2. X-ray diffraction patterns for calcined (540 °C) 3-d hexagonal silica mesostructures formed under the same conditions as noted in Figure 5.1 with the promotion of citric, oxalic and tartaric acids.

diffraction patterns of MCM-48 prepared through Landry's procedure and a comparison MCM-41 sample prepared in absence of salicylic acid and ethanol are included in Figure 5.1 too. Interestingly, too much salicylic acid deteriorates the meso-structure while 3 mole of salicylic acid per mole of surfactant was used. This indicated that the association²¹ of carboxylic acid with the charged surfactant head group results in diminished long range S⁺T electrostatic interaction. Consequently, the structure was less ordered judged by X-ray diffractions. Figure 5.2 shows the well resolved XRD patterns for 3-d hexagonal silica formed upon the addition of 1 mole of citric acid per mole of surfactant. Oxalic acid and tartaric acid shown similar promotion effects. These results strongly suggest that carboxylic acids can function as promoters to change the surfactant packing parameter and ultimately cause the silica meso-structure to change from uni-dimensional hexagonal to 3-d hexagonal and even cubic phases under certain reaction conditions. In comparison to the formation of conventional MCM-41, 3-d hexagonal and cubic meso-structures were formed under relatively lower surfactant to silicon ratio (i.e. 0.11 vs. 0.25) and H⁺ to NaOH ratio (i.e. 0.5 vs. 0.75) at 150 °C under the promotion of organic acids.

5.3.2 Siliceous MCM-41 Type Meso-structure Formation

Mou and his co-workers proposed¹⁵ that a hierarchical tubular MCM-41 formed through a sheet-like intermediate. The tubular MCM-41 formed at 100 °C by ultimately reaching an over all H⁺ to Si ratio of 0.57 when sulfuric acid was added day-by-day one time a day over 4 days. Our original goal was to synthesize MCM-41 with thin sheet morphology so that the accessibility of framework channels would be greatly enhanced.

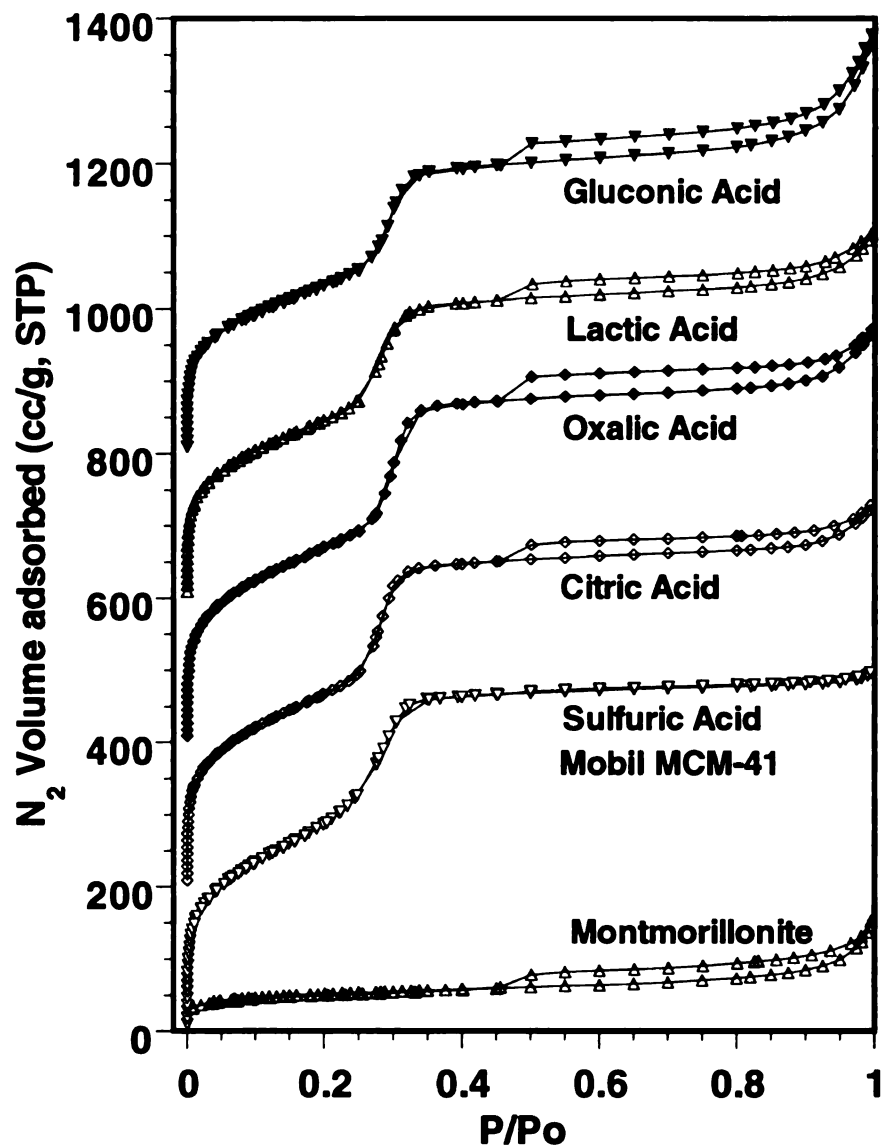


Figure 5.3. N_2 adsorption and desorption isotherms for calcined ($540\text{ }^\circ\text{C}$) siliceous MCM-41 prepared under the promotion of gluconic, lactic, oxalic, and citric acids with a $H^+/NaOH$ ratio of 0.75 showing framework mesoporosity as well as clay-like textural porosity similar to that of montmorillonite. The Mobil MCM-41 sample was prepared using sulfuric acid to adjust the pH (i.e. ~ 10.5) at the very beginning of the synthesis by control the over-all $H^+/NaOH$ ratio to 0.625.

In order to form and isolate the "sheet intermediate" organic acid was purposely added one time a day, and the mixture was aged only for two days instead of 4 days at 100 °C. The over all H⁺ to NaOH ratio was controlled to 0.75. MCM-41 with characteristic N₂ adsorption-desorption hysteresis loop similar to that for textural pores of layered montmorillonite was obtained (c.f. Figure 5.3). The isotherm for a typical MCM-41 prepared using sulfuric acid does not show any textural pores in contrast. TEM and SEM images of this sample showed tubular MCM-41 particles as the dominant form (Figure 5.4A and 5.4B) along with minor portion of flake-like particles (<20%). The flaky morphology in the MCM-41 samples prepared using organic acids, however, was the major morphology (c.f. Figure 5.4C and 5.4D), no tubular particles were observed. The pores of flaky particles were running orthogonal to the flaky-surface. Obviously, the pore channel lengths were limited to the thickness of the flakes. That is estimated to be less than 100 nm, because the penetration depth for an electron beam accelerated at 120 kV is about 100 nm.²⁷ These uni-dimensional pores with short channel lengths should be beneficial for diffusion limited catalytic reactions.

Actually, MCM-41 molecular sieves with clay-like flaky features indicated by the presence of textural porous hysteresis loop in the isotherms (Figure 5.3) were prepared using many organic acids while keeping the over-all H⁺/NaOH ratio at 0.75. All of them exhibited a ~3 Å width at half of maximum for the Harvorth-Kawazoe pore size distribution. They all exhibit very well resolved hexagonal X-ray patterns with (100), (110), (200), (220) and (300) reflections clearly seen (Figure 5.5). Although White and his co-workers claimed¹⁴ that a well ordered MCM-41 was obtained through tedious sulfuric acid titration during 4 days heating at 100 °C, the sample prepared by following

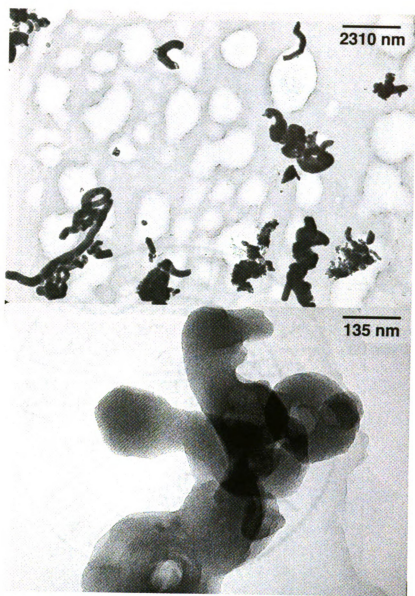


Figure 5.4A and 5.4B

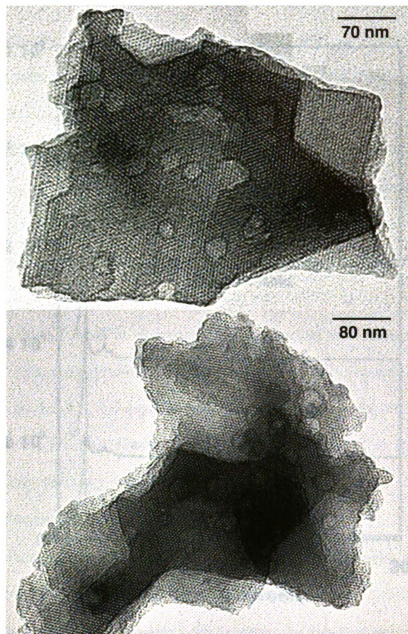


Figure 5.4 TEM images showing (A and B) interwoven tubular MCM-41 formed upon use of sulfuric acid; (C and D) thin sheet MCM-41 (formed upon use of citric acid) with pore channels running orthogonal to sheet surface (the thickness of the sheet estimated to be ~100nm according to the penetration depth of electron beam accelerated at 120 kV); Both samples were prepared with an over all $H^+/NaOH$ ratio of 0.75.

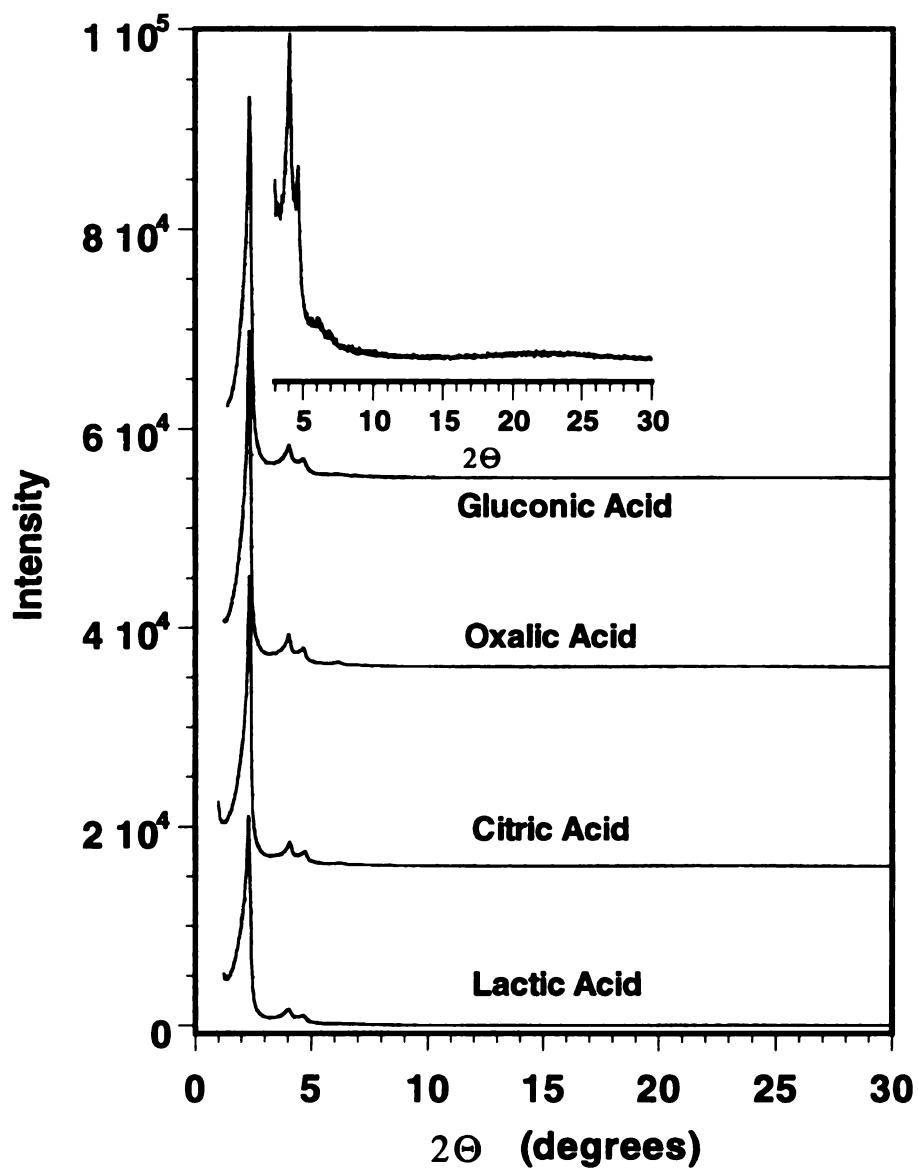


Figure 5.5. X-ray diffraction patterns for MCM-41 molecular sieves as noted in Figure 5.3.

their procedures using sulfuric acid does not exhibit significantly superior order over the sample prepared using organic acid. TEM images (c.f. Figure 5.4) for flaky MCM-41 show primarily sub-micrometer sized thin ($< 100\text{nm}$) sheets with pore channels running orthogonal to the sheet surface. However the particle size of MCM-41 reported by White and Ryoo et al are in micrometers.²⁸

Textural porosity HMS molecular sieves with inter particle voids of aggregated meso-scaled fundamental particles normally form upon fast hydrolysis and nucleation of hydroxylated neutral silicon species in the presence of alkylamine surfactant.²⁹ In order to facilitate the nucleation of silicate species in MCM-41 synthesis, we purposely added an amount of organic acid equivalent to a H^+/NaOH ratio of 0.75 in one lot instead of two to allow the pH drop down to ~ 9 immediately, and then let the reaction mixture to age at $100\text{ }^\circ\text{C}$ for 2 days. As illustrated in Figure 5.6, MCM-41 with a significant textural pore volume was produced in this way. The same type of synthesis performed at ambient temperature, however, afforded MCM-41 with lower framework as well as textural pore volume. Accordingly, the X-ray reflection patterns for this particular sample only showed a broad (100) reflection with a hump at higher 2θ angles (c.f. Figure 5.7). This signifies the importance of temperature in nucleation and assembly of meso-structures.

In agreement with HMS materials,²⁸ the high textural porosity of MCM-41 was correlated with the low bulky density ($\sim 0.2\text{ g/cc}$), which is only half of the value of the MCM-41 without textural pores. This suggests that the high textural porosity MCM-41 samples contain large amount of fluffy tiny particles. In addition, Figure 5.7 shows that MCM-41 with textural porosity still exhibits X-ray patterns with well resolved (100), (110) and (210) reflections. This is in contrast to the report by Davis and his co-

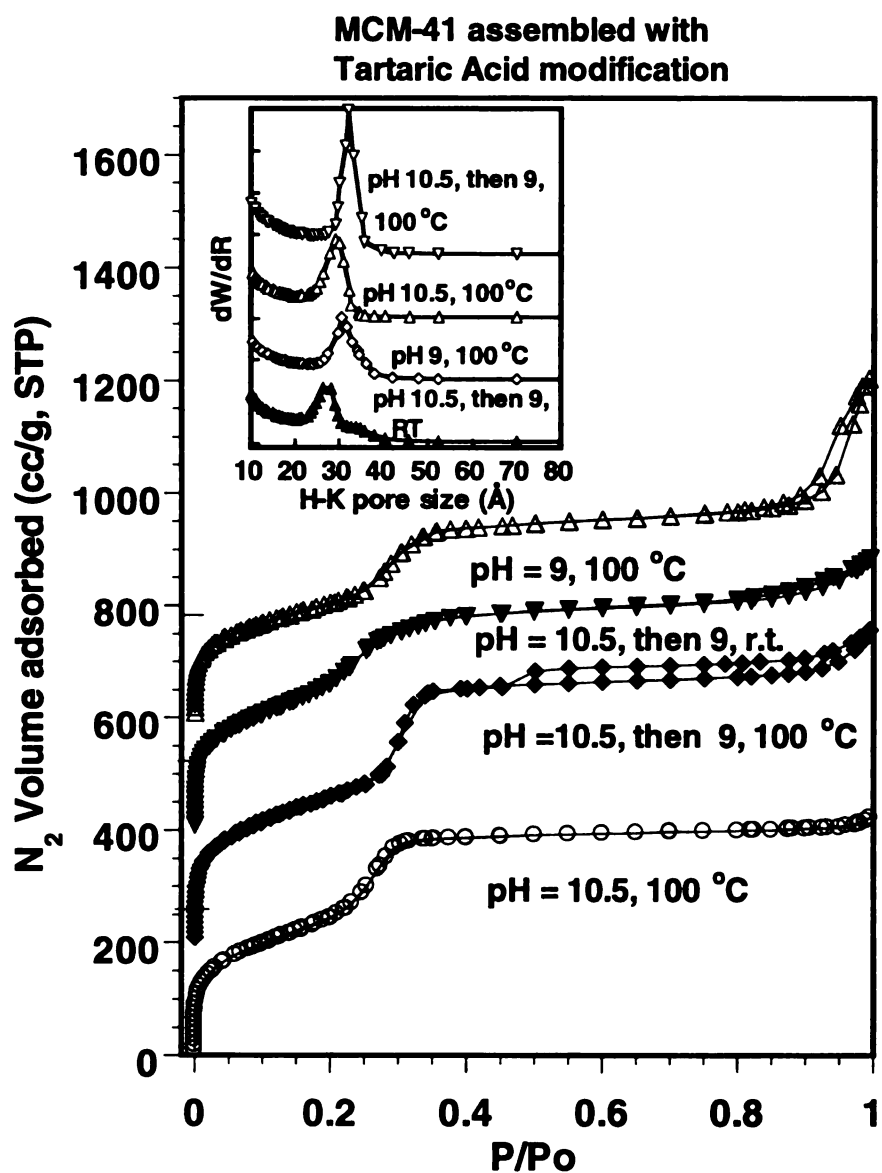


Figure 5.6. N_2 adsorption and desorption isotherms for MCM-41 molecular sieves prepared using tartaric acid as the structure promoter under various conditions showing the controlled formation of significant amount of HMS-like textural pores as well as clay-like textural pores. Horvath-Kawazoe pore size distribution plots are included in the inset.

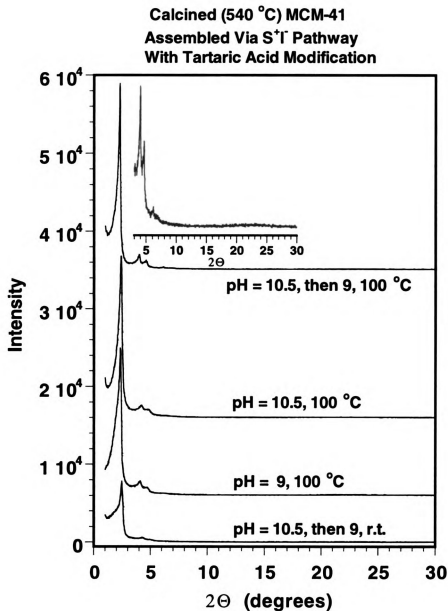


Figure 5.7. X-ray powder diffraction patterns for MCM-41 molecular sieves as noted in Figure 5.6. Notably, the MCM-41 with high textural porosity exhibits well resolved (100), (110) and (200) reflections.

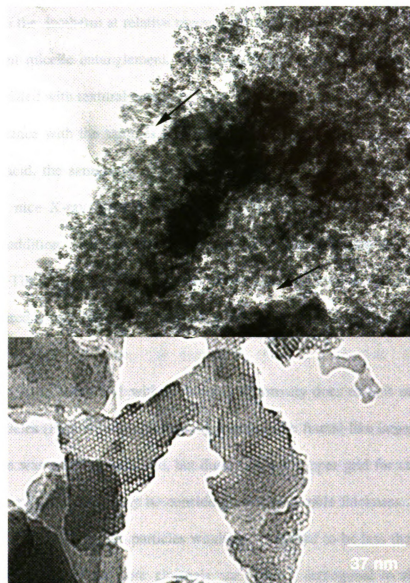


Figure 5.8. TEM image of MCM-41 showing meso-scaled fundamental particles with inter particle voids as textural pores and regular hexagonal framework mesopores running orthogonal to thin sheet surfaces exemplified by a sample prepared using tartaric acid as the structure promoter.

workers,²² which stated that disordered MCM-41 with single X-ray reflection and a N₂ hysteresis loop in the isotherm at relative pressure larger than 0.7 was a consequence of rod-like surfactant micelle entanglement. Therefore, X-ray disorder of MCM-41 is not necessarily associated with textural porosity.

In accordance with the samples prepared using citric acid, oxalic acid, gluconic acid and acetic acid, the sample synthesized through two step addition of tartaric acid also exhibited a nice X-ray diffraction pattern containing 5 well resolved reflections (Figure 5.7). In addition, they all exhibited a nice flaky-type hysteresis in the isotherm (c.f. Figure 5.6). These results suggest that the “intermediate sheets” to tubular MCM-41 were likely captured to form flaky MCM-41 under the promotion of those carboxylic acid promoters.

Similar to HMS, MCM-41 with high textural porosity does exhibit meso-scaled fundamental particles (Figure 5.8), which are aggregated into fractal-like larger particles. Since this sample was not thin-sectioned, but dusted on the copper grid for taking TEM images, the specimen thickness may be considered as the particle thickness. Therefore, the thickness of these fundamental particles would be estimated to be less than 100 nm, also. Moreover, as long as the pore channels are running orthogonal to the particle surface, the channel length of this particular MCM-41 would be estimated as ~100 nm, comparable to the particle thickness.

5.3.3 Catalyst Preparation

Normally, Al-MCM-41 is synthesized through an aluminum-silicon co-assembly process. However, Al-MCM-41 prepared in this way loses higher 2 Θ angle X-ray

reflections most of the time. The higher the Al-loading, the broader the (100) reflection. In order to obtain well ordered Al-MCM-41, a follow-up in-situ alumination in the presence of surfactant micelles in the pores was reported by Ryoo and his co-workers.²⁸ However, this particular sample indicated inhomogeneous alumination of the framework with more aluminum incorporated near the pore openings than deep inside the channels. Actually, Ryoo's MCM-41 was synthesized through an acid titration approach which gave rise to a well ordered MCM-41 with a relatively large particle size (even larger than $2 \mu\text{m}^{28}$). Therefore, the migration of aluminum species to deep inside of the channel is very likely hindered in the presence of surfactant molecules. Moreover, the electrostatic interfacial interaction would generate an electric field to prevent negatively charged aluminum species from accessing the negatively charged framework. Hence, the alumination would not be fully completed. To overcome this difficulty and make the alumination of the pore walls more homogeneous in the pores, using aluminum nitrate as the alumination agent for our MCM-41 with meso-scaled fundamental particles and meso-scaled channel lengths should have advantages over other MCM-41 samples.

The follow-up in-situ alumination of MCM-41 with flaky particles was only successful for Al-loading up to 9%. The flaky particle morphology was lost in attempts to introduce 20% aluminum. At these higher Al loading, the characteristic hysteresis loop responsible for inter particle voids in the isotherms was diminished. Seemingly, the flaky particles were stacked into larger particles. This suggests that flaky sheets are more likely an intermediate of tubular MCM-41.

In contrast to intermediate flaky sheets, MCM-41 with textural porosity showing meso-scaled fundamental particles is stable to the follow-up in situ alumination treatment

even for an attempt to introduce 20% aluminum. Elemental analysis of the sample with 20% initially Al-content in the synthesis mixture revealed that the actual Al-loading for

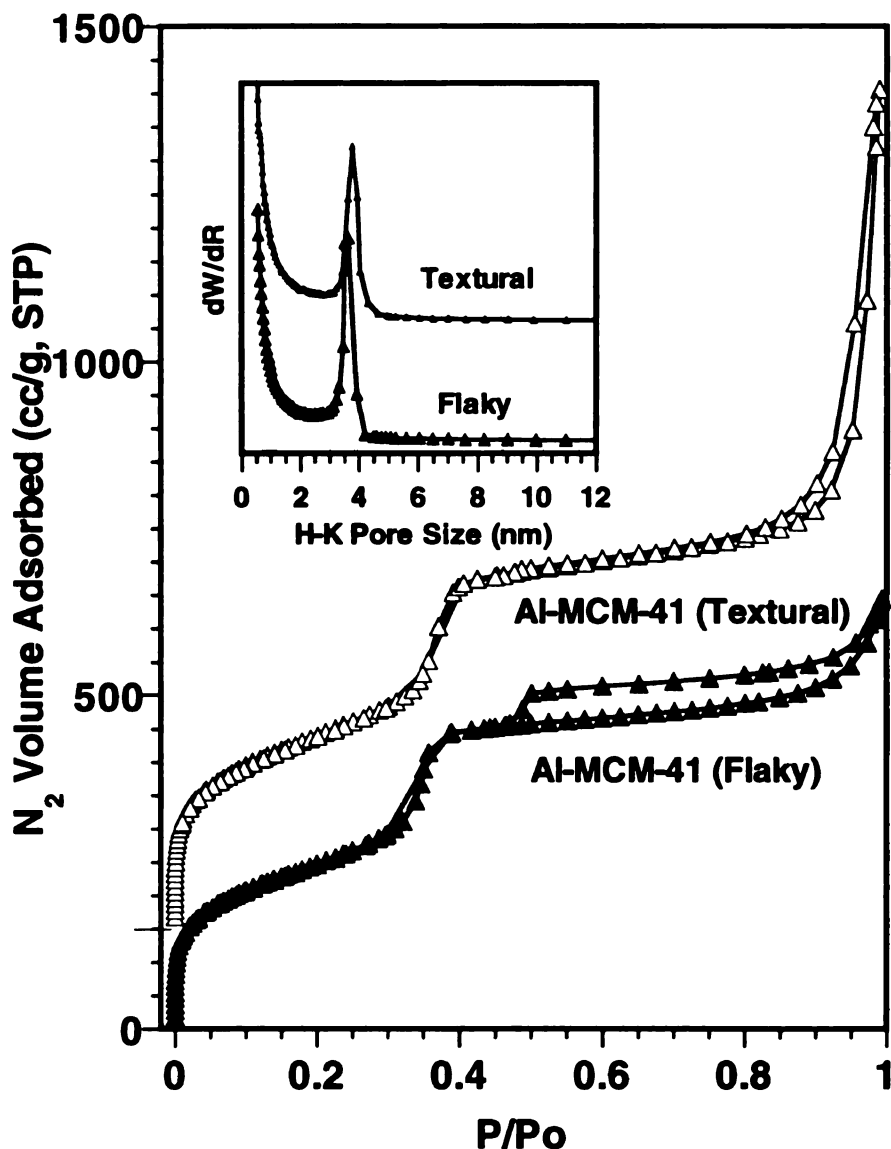


Figure 5.9. N₂ adsorption and desorption isotherms for 8.8mol%Al-substituted MCM-41 molecular sieves (calcined at 540 °C) with clay-like and HMS-like textural porosity prepared using tartaric acid as the structure promoter and aluminum nitrate as the follow-up in situ alumination reagent in the presence of surfactant micelles in the pores. (The inset is the corresponding Horvath-Kawazoe plots showing sharp narrow distribution of framework mesopores).

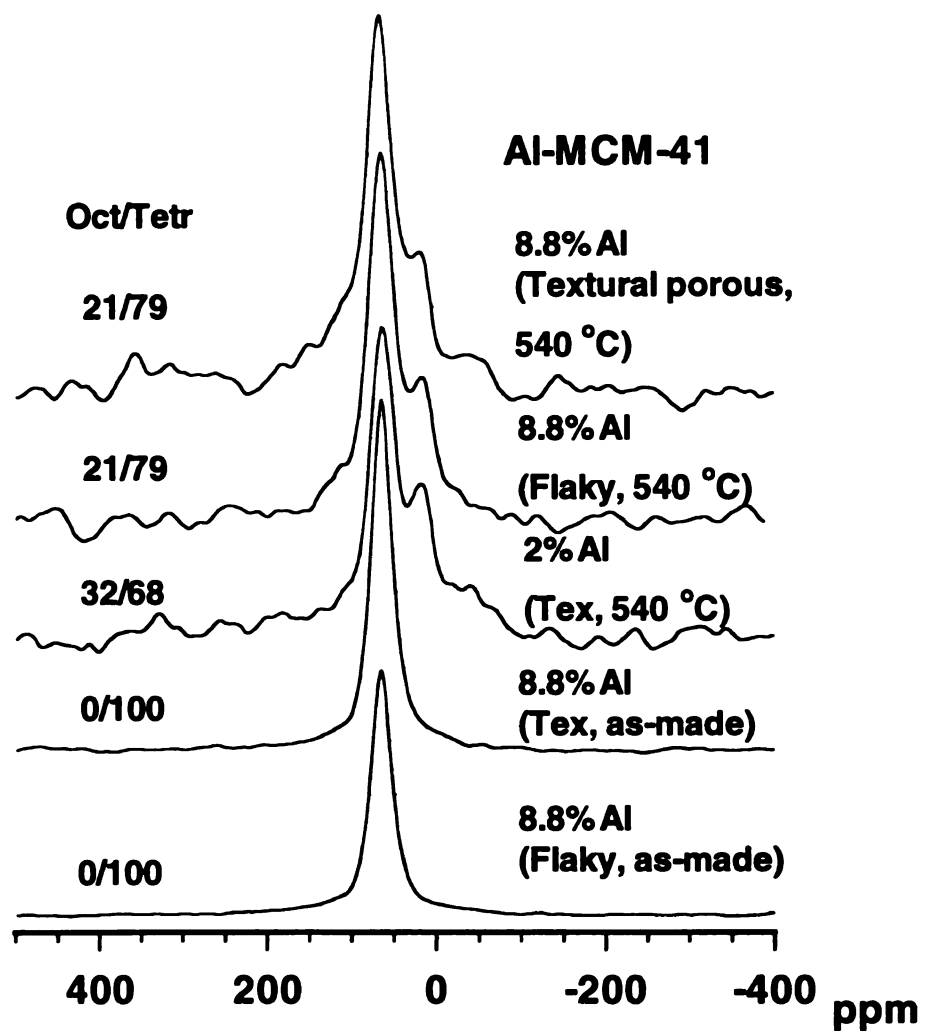


Figure 5.10. ^{27}Al -NMR spectra for as-made and calcined Al-MCM-41 molecular sieves prepared using tartaric acid as the structure promoter with HMS-like and clay-like flaky textural pores.

the final product was only 10%. In fact, the 20% aluminum introduced in the form of aluminum nitrate decreased reaction pH too much to allow the incorporation of Al into the pore walls taking place effectively. As shown in Figure 5.9, this particular Al-MCM-41 still exhibits a good textural pore volume up to 50 % of the total pore volume and well resolved hexagonal X-ray patterns. Not only did tartaric acid afford Al-MCM-41 with textural pores, but also oxalic acid, citric acid, gluconic acid and lactic acid afforded Al-MCM-41 with quite good textural pores.

²⁷Al-NMR spectra show that over 95% of total aluminum sites in the as-made samples are in tetrahedral coordination (Figure 5.10). This result indicated that the follow-up in situ alumination was as effective as in situ silicon-aluminum co-assembly and post-synthesis implantation³⁰ in the absence of surfactant. ²⁷Al-NMR spectra of our samples indicates dealumination upon calcination occurred regardless of high or low textural porosity. Approximately a third and a fifth of the total aluminum-sites were transformed from tetrahedral coordination to octahedral coordination upon calcination for 2%Al- and 8.8%Al-MCM-41, respectively. This verifies the dealumination reported by Corma³¹ and Prins³² et al. Notably, there are no observable differences in ²⁷Al-NMR spectrum for MCM-41 with and without textural porosity. In conclusion both intra-framework and extra-framework aluminum species are approximately identical from sample to sample for all calcined MCM-41 samples with the same Al-loading regardless of the textural porosity. Interestingly, the ratio of tetrahedral to octahedral Al-sites for the calcined samples increased with increasing Al-loading. This was further confirmed by temperature programmed pyridine desorption. As shown in Figure 5.11, the number of

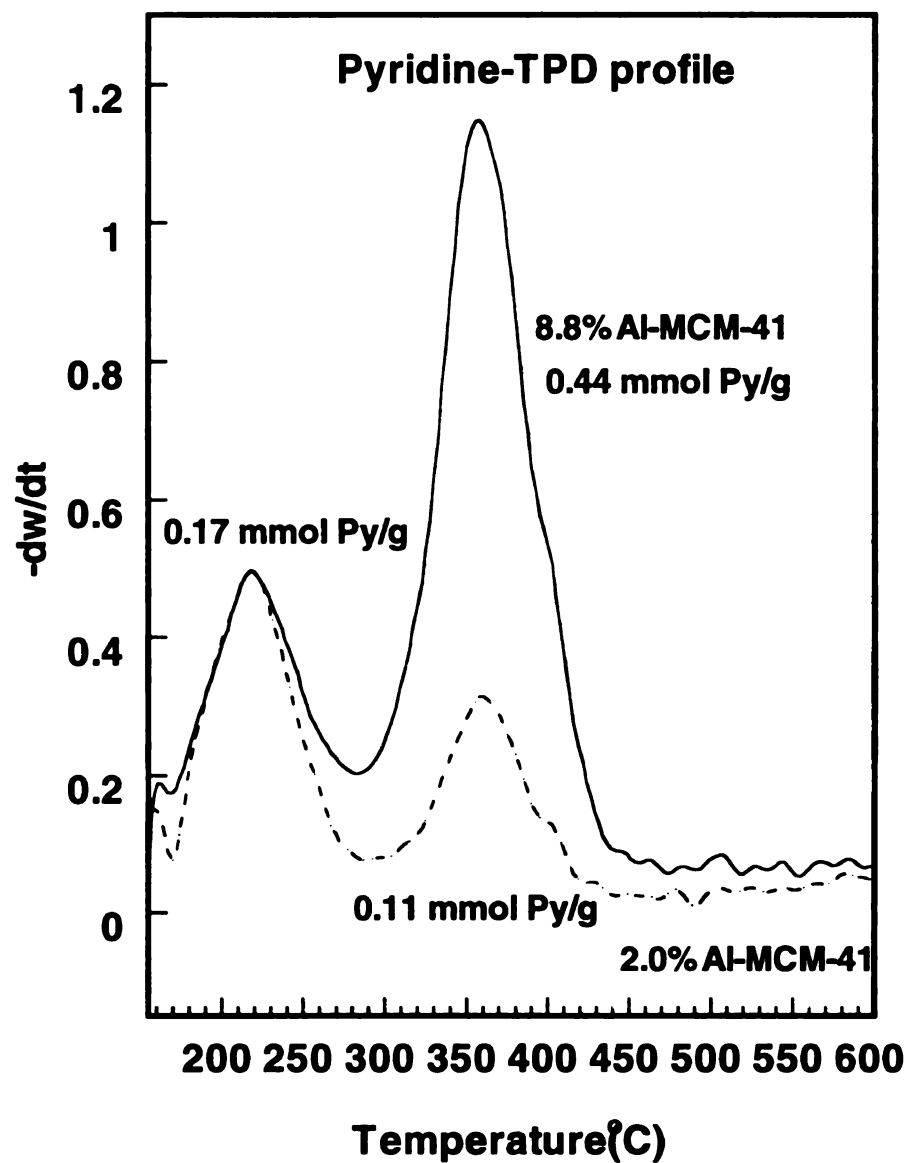


Figure 5.11. Temperature programmed desorption (TPD) of pyridine pre-adsorbed on Al-MCM-41 catalysts and purged at 150 °C in N₂ stream for 1 h before the TPD started. This TPD profile was carried out on a thermal gravity analyzer.

weaker acid sites indicated by pyridine desorption peak at 217 °C remained the same, but the number of stronger acid sites indicated by pyridine desorption peak at 350 °C increased by 4 fold when the Al-loading increased 4 times. Assuming the surfactant micelles are homogeneously distributed through the pores, the sample without prior NH_4^+ -exchangment but with higher Al-loading would require higher concentration of Na^+ cations at the pore opening to balance the negative framework charges generated by tetrahedrally incorporated Al if most of the Al-sites were at the pore opening as reported by Ryoo et al.²⁸ Hence, non-linear increase of acidity value with Al-loading would be expected. Notably, our two samples were not subjected to NH_4^+ -exchangment. A linear increase of the number of stronger acid sites with increasing Al-loading strongly suggest that aluminum was not likely just incorporated at pore openings, but rather homogeneously incorporated into the framework through the pores.

In agreement with the results of Jones et al,³³ our previous study also found that 2%Al-MCM-41 exhibited quite low acidity (0.1 mmol CHA/g, compared with 3.4 mmol CHA/g for 2%Al-HMS) possibly due to inaccessible Al-sites buried in MCM-41 framework walls.³⁴ In order to achieve an acidity for Al-MCM-41 more or less comparable to Al-HMS, aluminum-loading for most of the MCM-41 was increased to 8.8%, which gave acidity levels of 0.44 mmol CHA/g, as measured by TGA analysis (c.f. Table 5.1). This value is also comparable to that of the HY from NH_4Y available from Aldrich. As shown in Table 5.1, all Al-MCM-41 samples with similar Al-loading regardless of surface area, porous volume and textural porosity are very similar to each other in total acidity. Aluminum nitrate may provide nearly neutral aluminum hydroxylated species in the alumination medium with a pH at ~9. Therefore, the follow-

Table 5.1. Physical and chemical properties of Al-MCM-41 mesoporous molecular sieves^a

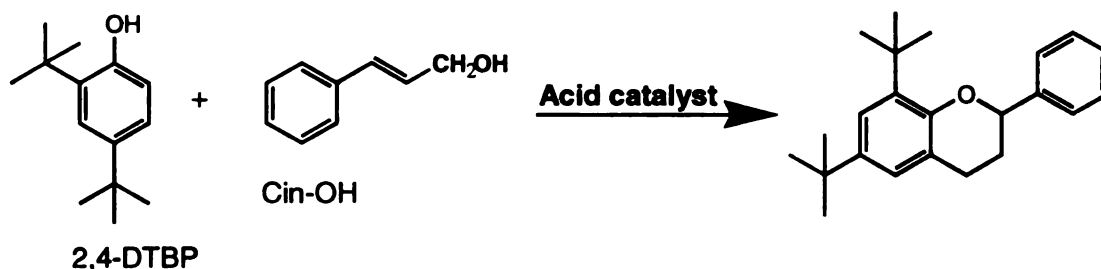
Al-MCM-41 Catalyst	Si/Al ratio	S_{BET} (m ² /g)	Pore Volume (cc/g) ^b			Pore Size (nm)	Acidity ^c (mmol /g)
			V_t	V_{fr}	V_{tex}		
H-Y zeolite ^d	2.80	670	0.30	0.30	0	0.72	0.50
Mobil	50.0	1070	0.87	0.87	0	3.3	0.10
(Sulfuric Acid)	11.1	1051	0.92	0.86	0.06	3.2	0.47
Flaky (Citric Acid)	11.1	903	0.91	0.73	0.14	3.6	0.42
Flaky (Oxalic Acid)	11.1	990	0.87	0.71	0.16	3.5	0.43
Flaky (Tartaric Acid)	11.1	922	0.87	0.71	0.16	3.5	0.44
Tex-porous (Tartaric)	50.0	927	0.89	0.72	0.17	3.5	0.14
Non-tex (Tartaric) ^e	11.1	967	0.83	0.83	0	3.5	0.44
Tex-porous (Tartaric)	11.1	1045	1.46	0.82	0.64	3.6	0.43
Tex-porous (Citric)	11.1	1011	1.38	0.72	0.66	3.5	0.43
Tex-porous (Oxalic)	11.1	1023	1.13	0.71	0.42	3.5	0.43

^a. All Al-MCM-41 samples were not NH₄⁺-exchanged except the sample prepared according to Mobil's method. ^b. The total pore volume (V_t) and the framework pore volume (V_{fr}) were calculated from the isotherm at P/Po 0.99 and 0.5, respectively. The textural pore volume (V_{tex}) is the difference between V_t and V_{fr} . ^c. The total acidity for these catalysts were obtained by means of TGA through measurement of cyclohexylamine desorption between 240 to 420 °C. ^d. This H-Y was obtained through calcination (540 °C) of a NH₄-Y with a Si/Al ratio of 2.8 and containing 2.5 wt% Na₂O, which was bought from Aldrich. ^e. This sample has no textural pores prepared using 17% less amount of tartaric acid comparable to Mobile's MCM-41.

up in situ alumination using aluminum nitrate as the reagent in the presence of surfactant molecules in the pores are likely incorporated homogeneously into the framework all the way through the pores. One more reasonable conclusion derived from the data in Table 5.1 and Figure 5.10 and 5.11 is that any differences in catalysis for those Al-MCM-41 with equivalent acidity would not be attributed to any differences in intrinsic acid siting.

5.3.4 Catalytic Alkylation of 2,4-di-tert-butylphenol with Cinnamyl Alcohol

As discussed in last section, a family of Al-MCM-41 with textural pores was prepared using various organic acids through a general method. Like the preparation of Al-HMS with textural pores, the follow-up in situ alumination of MCM-41 with textural pores using aluminum nitrate is efficient enough to incorporate tetrahedral Al into the



framework in the presence of surfactant molecules. In order to evaluate the catalytic performance for acid-sites, alkylation of 2,4-di-tert-butylphenol was conducted over Al-MCM-41 catalysts with various textural pores. The importance of accessibility to active sites in diffusion limited catalytic reaction might be manifested by these Al-MCM-41 catalysts because of their different framework pore accessibility. In the first report³⁵ of using mesoporous MCM-41 as the catalyst, this reaction was carried out at 90 °C for 24 h. As we stated,³⁴ it is not necessary for running this reaction for 24 h because one of the two reactants, cinnamyl alcohol is nearly 100% consumed after 6 h run at even 60 °C. Most of the by-products (about 10% of the total products) from this reaction were from

cinnamyl alcohol alone. Three products were identified for conversion of 2,4-di-tert-butylphenol by GC-MS analysis. These three products account up to ~90% of the consumed 2,4-di-tert-butylphenol. The major product is flavan. Two by-products were 4-tert-butylphenol and 4,6-di-tert-butyl benzofuran. Since these two by-products only account for less than 5% of consumed 2,4-di-tert-butylphenol for all Al-MCM-41 catalysts, they were not listed in Table 5.2. Interestingly, 4-tert-butylphenol, the product of dealkylation of 2,4-DTBP was barely detectable for most Al-MCM-41 catalysts, but obviously detected for HY zeolite and textural pores-free Al-MCM-41 prepared using tartaric acid that exhibited quite low flavan selectivity (normally, 11.1% and 46% for HY and textural pores-free Al-MCM-41, respectively).

As shown in Table 5.2, the traditional liquid phase alkylation catalyst, sulfuric acid was not at all effective for this reaction. Even though 2 times more protons from sulfuric acid (30 mg) was used in comparison to the acidity of 500 mg 8.8%Al-MCM-41 catalyst (~0.45 mmol/g), the conversion of 2,4-DTBP, selectivity and yield of the desired flavan were still insignificant. This may signify the importance of mild acidity observed for aluminum substituted mesoporous molecular sieve catalysts in use for this type of fine chemical alkylation. It seems that only one of those two types of acid sites on these Al-MCM-41 catalyst detected by temperature programmed pyridine desorption (c.f. Figure 5.11) is effective for this alkylation reaction. Re-use of the not-regenerated catalyst gave rise to a conversion and selectivity only ~15% lower than the values observed for the fresh catalyst. Actually, the number of weaker acid sites with a pyridine desorption peak at 217 °C still maintain the same after one cycle of the reaction. And the stronger acid sites indicated by pyridine desorption at 350 °C was no longer available for pyridine

Table 5.2. Alkylation of 2,4-di-tert-butylphenol with cinnamyl alcohol catalyzed by Al-substituted mesoporous molecular sieves

Al-MCM-41 Catalyst	Conv. (%) 2,4-DTBP	Selectivity of Flavan (%)	Yield of Flavan (%)
30 mg H ₂ SO ₄ ^a	25.5	36.9	9.4
HY	13.3	11.1	1.5
Mobil ^b (Sulfuric Acid)	47.2	71.8	33.9
Flaky (Citric Acid)	64.4	76.9	49.5
Flaky (Oxalic Acid)	61.9	71.2	44.1
Flaky (Tartaric Acid)	69.2	84.0	58.5
Tex-porous (Tartaric) ^b	69.7	79.5	55.4
Non-tex (Tartaric) ^c	46.3	45.9	21.3
Tex-porous (Tartaric)	65.8	83.5	54.9
Tex-porous (Citric)	64.4	79.5	51.0
Tex-porous (Oxalic)	63.0	79.0	50.0

*. Each catalyst contains 8.8 mol% Al except indicated samples; the reaction was carried out using 10.0 mmol of each reactant, 500 mg of catalyst, in 50 ml of isooctane at 60 °C for 6 h. a. The reaction was carried out at 90 °C for 24 h instead of 60 °C for 6 h. b. These sample contains 2.0 mol% Al. c. This sample has no textural pores (c.f, Figure 5.6).

adsorption because they were totally covered by polymeric aldehyde formed from cinnamyl alcohol condensation. Increasing the Al-loading leads to an increase of the number of stronger acid sites with tetrahedral coordination (c.f. Figure 5.10 and 5.11). However, the conversion and selectivity for alkylation does not improve with the increase of Al-loading (c.f. Table 5.2 for Tex-porous-tartaric-entries). This indicates that the Al-sites with mild acidity is crucial for this alkylation reaction in liquid phase.

The accessibility of active sites is another crucial factor for this bulky alkylation reaction. The poor performance of HY zeolite as alkylation catalyst is simply due to the inaccessibility of the active Al-sites in the micropores even though the amount of acidity for HY is approximately equivalent to that of 8.8%Al-MCM-41. In contrast to the conventional Mobil Al-MCM-41 catalyst with particle sizes of a few micrometers, the catalyst with a thin flaky particle morphology and short pore channels exhibited much higher 2,4-DTBP conversion and flavan yield (i.e. at least by 30%). Also, Al-MCM-41 prepared using sulfuric acid in the same way as the organic acid promoters to adjust the pH two times over 2 days, exhibits primarily a micrometer sized tubular particle morphology and an only slightly improved catalytic activity. However, the conversion of 2,4-DTBP, and the selectivity and yield to the flavan all increase with increasing textural porosity. The conversion of 2,4-DTBP (i.e. 66%) for texturally porous Al-MCM-41 molecular sieves was almost as good as texturally porous Al-HMS.³⁴ The selectivity to flavan was quite remarkable also (i.e. ~83%).

5.4 Conclusions

Well ordered MCM-41 molecular sieves with flaky morphology and short uni-dimensional pores orthogonal to flaky-sheet surface, as well as meso-scaled fundamental particles with high textural porosity were prepared through controlled addition of organic acids such as tartaric, citric, oxalic, gluconic, lactic and salicylic acid. Structural promotion effects of the organic acids were explicitly demonstrated by the formation of 3-d hexagonal and cubic structure at 150 °C (instead of 100 °C for MCM-41) and surfactant to silicon ratio of 0.11 (instead of 0.25 for MCM-41) and H⁺ to NaOH ratio of 0.49 (instead of 0.75 for MCM-41). Intrinsically, this is most likely a consequence of the variation of surfactant packing parameter *g*. The *g* value is likely varied through the surfactant-organic acid association to cause the phase change in formation of 3-d hexagonal and cubic meso-structures. On the other hand, slightly variation of surfactant packing parameters under conditions for MCM-41 preparations upon organic acid promotion leads to the formation of flaky as well as texturally porous silica molecular sieves. Follow-up in situ alumination of the flaky and textural porous MCM-41 in the presence of surfactant micelles in the pores afforded well incorporated Al-sites with over 95% are in tetrahedral coordination even for Al-loading up to 8.8mol%. However, up to a third of these Al-sites are transformed into octahedral sites upon removal of the surfactant by calcination. The Al-sites judged from ²⁷Al-NMR and the total acidity measured from temperature programmed desorption of cyclohexylamine are in-distinguishable for similarly loaded Al-MCM-41 regardless of particle morphology. Consequently, any differences in catalysis for these Al-MCM-41 catalysts with equivalent acidity can not be attributed to any differences in the intrinsic acid siting. The number of Al-sites with

stronger acidity indicated by desorption of pyridine at 350 °C was proportionally increased with Al-loading, but the number of Al-sites with weaker acidity indicated by desorption of pyridine at 217 °C remained the same.

The results of the studies of 2,4-DTBP alkylation with cinnamyl alcohol proves that the accessibility of the active Al-sites in flaky and textural porous Al-MCM-41 with short channel lengths is significantly facilitated. At least 30% higher conversion of 2,4-DTBP and 50% higher yield of flavan are obtained relative to Al-MCM-41 without a flaky or textural porous morphology. This alkylation reaction seems to be catalyzed by the mild acid sites since increasing the number of stronger acid sites by increasing the Al-loading does not improve the activity considerably.

5.5 References:

1. Beck, J.S.; Vartuli, J.C.; Roth, W.J.; Leonowicz, M.E.; Kresge, C.T.; Schmitt, K.D.; Chu, C.T.-W.; Olson, D.H.; Sheppard, E.W.; McCullen, S.B.; Higgins, J.B.; Schlenker, J.L. *J. Am. Chem. Soc.* **1992**, 114, 10834.
2. Corma, A. *Chem. Rev.* **1997**, 97, 2373; and Sayari, A. *Chem. Mater.* **1996**, 8, 1840.
3. Alfredsson, V.; Anderson, M.W. *Chem. Mater.* **1996**, 8, 1141.
4. Yang, R.; Pinnavaia, T.J.; Li, W.; Zhang, W. *J. Catal.* **1997**, 172, 488.
5. Monnier, A.; Schuth, F.; Huo, Q.; Kumar, D.; Margolese, D.I.; Maxwell, R.S.; Stucky, G.D.; Krishnamurty, M.; Petroff, P.; Firouzi, A.; Janicke, M.; Chmelka, B.F. *Science* **1993**, 261, 1299.
6. Anderson, M.W. *Zeolite* **1997**, 19, 220.
7. Zhang, W.; Pinnavaia, T.J. *Catal. Lett.* **1996**, 38, 261.
8. Romero, A.A.; Alba, M.D.; Klinowski, J. *J. Phys. Chem B* **1998**, 102, 123.
9. Huo, Q.; Margolese, D. I.; Ciesla, U.; Feng, P.; Gier, T. E.; Sieger, P.; Leon, R.; Petroff, P. M.; Schüth, F.; Stucky, G. D., *Nature* **1994**, 368, 317.
10. Zhang, W.; Froba, M.; Wang, J.; Tanev, P.T.; Wong, J.; Pinnavaia, T.J. *J. Am. Chem. Soc.* **1996**, 118, 9164.
11. a. Stucky, G.D.; Monnier, A.; Schuth, F.; Huo, Q.; Margolese, D.; Kumar, D.; Krishnamurty, M.; Petroff, P.; Firouzi, A.; Janicke, M.; Chmelka, B.F. *Mol. Cryst. Liq. Cryst.* **1994**, 240, 187; b. Tanev, P.T.; Pinnavaia, T.J. *Chem. Mater.* **1996**, 8, 2068.
12. a. Kloetstra, K.R.; van Bekkum, H.; Jansen, J.C. *Chem. Commun.* **1997**, 2281; b. Luan, Z.H.; Cheng, C.F.; He, H-Y.; Klinowski, J. *J. Phys. Chem.* **1995**, 99, 10590.
13. Ryoo, R.; Kim, J.M. *Chem. Commun.* **1995**, 711.
14. Edler, K.J.; White, J.W. *Chem. Mater.* **1997**, 9, 1226.
15. a. Lin, H.-P.; Mou, C.-Y. *Science* **1996**, 273, 765; b. Lin, H.-P.; Cheng, S.; Mou, C.-Y. *Chem. Mater.* **1998**, 10, 581.
16. Behrens, P. *Angew. Chem. Int. Ed. Engl.* **1996**, 35, 515.
17. Huo, Q.; Margolese, D.I.; Stucky, G.D. *Chem. Mater.* **1996**, 8, 1147.

18. Israelachvili, J.N.; Mitchell, D.J.; Ninham, B.W. *J. Chem. Soc., Faraday Trans. 2* **1976**, *72*, 1525.
19. Hyde, S.T. *Pure Appl. Chem.* **1992**, *64*, 1617.
20. Henriksson, U.; Blackmore, E.S.; Tiddy, G.J.T.; Soderman, O. *J. Phys. Chem.* **1992**, *96*, 3894.
21. Fuhhop, J-H.; Helfrich, W. *Chem. Rev.* **1993**, *93*, 1565.
22. Davis, M.E.; Chen, C.-Y.; Burkett, S.L.; Lobo, R.F. *Mater. Res. Soc. Symp. Proc.* **1994**, *346*, 831.
23. Pinnavaia, T.J.; Zhang, W. *Stud. Surf. Sci. Catal.* **1998**, *117*, 23 (Elsevier Science B.V.).
24. Armengol, E.; Corma, A.; Garcia, H.; Primo, J. *Appl. Catal. A: General* **1995**, *126*, 391.
25. Huo, Q.; Leon, R.; Petroff, P.M.; Stucky, G.D. *Science* **1995**, *268*, 1324.
26. Gallis, K.W.; Landry, C.C. *Chem. Mater.* **1997**, *9*, 2035.
27. Flegler, S.L.; Heckman, Jr., J.W.; Klomparens, K.L. "Scanning and Transmission Electron Microscopy- An Introduction" **1993**, (W.H. Freeman and Company), New York.
28. Ryoo, R.; Ko, C.H.; Howe, R.F. *Chem. Mater.* **1997**, *9*, 1607.
29. Zhang, W.; Pauly, T.R.; Pinnavaia, T.J. *Chem. Mater.* **1997**, *9*, 2491.
30. Ryoo, R.; Jun, S.; Kim, J.M.; Kim, M.J. *Chem. Commun.* **1997**, 2225.
31. Corma, A.; Fornes, V.; Navarro, M.T.; Perez-Pariente J. *Catal.* **1994**, *148*, 569.
32. Hitz, S.; Prins, R. *J. Catal.* **1997**, *168*, 194.
33. Mokaya, R.; Jones, W. *Chem. Commun.* **1996**, 983 and *J. Catal.* **1997**, *172*, 211.
34. Zhang, W.; Liu, Y.; Pinnavaia, T.J. *J. Phys. Chem.* in preparation.
35. Armengol, E.; Cano, M.L.; Corma, A.; Garcia, H.; Navarro, M. *Chem. Commun.* **1995**, 519.
36. Janicke, M.T.; Landry, C.C.; Christiansen, S.C.; Kumar, K.; Stucky, G.D.; Chmelka, B.F. *J. Am. Chem. Soc.* **1998**, *120*, 6940.

Chapter 6

Incorporation of Structural Order into Mesoporous Silica Molecular Sieves Assembled Via a Metal Salt Mediated $N^0(M^+X^-)I^0$ Pathway

Abstract

The concept of incorporating structural order into mesoporous silica molecular sieves through electrostatic interactions between electrically neutral surfactant micelle and neutral inorganic precursors has been successfully illustrated. Mesoporous silica molecular sieves with well ordered domains consisted of a hybrid 3-dimensional hexagonal and spherical cubic phases (3-d-hex-cubic), as well as an uni-dimensional hexagonal structure and a wormhole structural motif were assembled using alkyl polyethylene oxide surfactant as the structure director and tetraethyl orthosilicate as the silicon source through a new counterion mediated $N^0(M^+X^-)I^0$ pathway controlled by judicious choice of a surfactant to metal ratio, and also by choice of a metal salt from the group of $CoCl_2$, $MnCl_2$, $NiCl_2$, $CuCl_2$, $ZnCl_2$, $FeCl_2$, $FeCl_3$, $RhCl_3$, $CrCl_3$ and $LiCl$. Structural variation was strategically mediated through surfactant-metal complex formation that leads to variation of surfactant packing parameters ($g = V/a_0l$) and ultimately the inorganic meso-structures. The 3-d-hex-cubic structure is favored by “2+” metal cations such as Co^{2+} , Ni^{2+} and Mn^{2+} . Hexagonal structure is favored by both “1+” and “2+” metal cations such as Li^+ , Co^{2+} , Cu^{2+} , Zn^{2+} , and Fe^{2+} . No structural order is favored by “3+” metal cations such as Cr^{3+} , Fe^{3+} and Rh^{3+} . It seems that 3-d-hex-cubic structure formation prefers a lower interfacial charge density with a surfactant to metal ratio in the range of 4 to 12. Hexagonal structure formation is favored by a relatively higher interfacial charge density with a lower surfactant to metal ratio in the range of 1 to

3. Wormhole structure are obtained near zero interfacial charge density with a quite high surfactant to metal ratio above 17.

6.1 Introduction

Hexagonal MCM-41 and cubic MCM-48 molecular sieves have been primarily assembled via an electrostatic S^+T pathway relying on the lyotropic properties of the quaternary ammonium surfactants.¹⁻³ Analogous hexagonal and cubic silica mesostructures have been also prepared through liquid crystal templating using alkyl polyethylene oxide surfactants in the presence of significant amounts of mineral acid.⁴ Consistently, hexagonal mesoporous silica with pore size up to 300 Å was recently obtained using big triblock copolymer nonionic surfactants via an electrostatic $S^+X^+T^+$ assembly mechanism in the presence of large amount of mineral acid.⁵ Mesoporous silica and alumina molecular sieves with wormhole channel motif, however, were cooperatively assembled via an electrically neutral N^0I^0 pathway with H-bonding interactions between nonionic surfactant (N^0) and neutral inorganic reagent (I^0).⁶⁻⁸ Although the neutral assembly pathways possess environmentally benign advantages over the electrostatic assembly pathways, our previous studies only obtained disordered wormhole structures. Actually, as a consequence of weak H-bonding assembly, both S^0I^0 ^{9,10} and N^0I^0 assembly lead to silica⁶ and alumina⁷ mesoporous molecular sieves with wormhole channels. Nonetheless, chemical control of the surfactant assembly process for formation of desired mesoporous molecular sieves is still a challenge. Structurally well designed mesoporous molecular sieves are desirable for use as special sorbents, catalyst supports and catalysts, functional ceramics, sensors and separation-membrane precursors.

Therefore, it would be chemically significant and scientifically interesting to produce ordered meso-structures from neutral assembly by a facile method.

It has been known that the interfacial interactions between surfactant micelles and inorganic precursors play an important role in directing the formation of meso-structures.¹¹ Longer ranged electrostatic interaction usually affords relatively higher order of mesostructures in comparison with the shorter ranged H-bonding interaction that leads to X-ray disordered but uniformly porous meso-structures.¹² Our strategy to incorporate higher structural order into mesoporous silica molecular sieves assembled using nonionic surfactant and neutral inorganic precursors is based on partial coulomb interactions at the interface between surfactant micelles and inorganic precursors without altering the fundamental feature of H-bonding assembly. Polyethylene oxide has been known to form helical complexes with Li^+ , Cu^{2+} and Zn^{2+} .¹³⁻¹⁵ In this work we examine the capability of alkyl polyethylene oxide surfactants to complex metal cations as an effective approach to incorporate coulomb forces at the interfaces between surfactant and hydroxylated neutral silicon species to form relatively well ordered mesoporous silica molecular sieves.

Here we report a versatile novel method to prepare mesoporous silica molecular sieves. Mesostructures such as a hybrid structure consisted of 3-d hexagonal and spherically cubic (3-d-hex-cubic), an uni-dimensional hexagonal, and a wormhole-like meso-structures were synthesized through judicious choice of metal cations and control of the surfactant to metal ratio. We also purposely allow the assembly to take place in a neutral medium to maintain the H-bonding feature through a metal salt mediated neutral assembly pathway ($\text{N}^0(\text{M}^+\text{X}^-)\text{I}^0$). The strategy involves variation of surfactant molecular

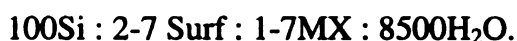
packing parameter g (i.e. $g = V/a_0l$)¹⁶ through formation of metal complex which varies the effective head group area of the surfactant substantially to cause a phase change of the assembled products.

6.2 Experimental

Structurally ordered mesoporous silica molecular sieves were synthesized using tetraethylorthosilicate (TEOS) as the silicon source and nonionic surfactant including Brij 56 ($C_{16}H_{33}(EO)_{10}H$), Tergitol ($C_{12-16}H_{25-33}(EO)_{8-10}H$) and Triton X-100 ($C_8H_{17}Ph(EO)_{10}OH$) as the structure directors in the presence of metal salts such as $CoCl_2$, $NiCl_2$, $MnCl_2$ and $LiCl$. The reactions were carried out at a neutral pH and a temperature between 35 to 60 °C in a reciprocal thermal bath under very gently shaking for 40 h. The product was filtered and dried in air. The obtained 3-d-hex-cubic and uni-dimensional hexagonal mesoporous silicas were denoted as MSU-C and MSU-H, respectively. The molar composition for MSU-C synthesis was



MSU-C was only formed in the presence of “2+” metal salts especially in favor of $CoCl_2$, $NiCl_2$ and $MnCl_2$. The molar composition for MSU-H preparation was



MSU-H was assembled using the same reagents, under the same reaction conditions for MSU-C, except for the surfactant to metal ratio. MSU-H was also formed using $LiCl$, $CuCl_2$ and $ZnCl_2$ in place of $CoCl_2$. As-made material was either refluxed in ethanol for 2 h or calcined at 600 °C for 6 h to remove the surfactant from their mesopores.

The powder X-ray diffraction pattern of the samples was recorded on a Rigaku Rotaflex Diffractometer using Cu K_{α} radiation ($\lambda = 1.542 \text{ \AA}$). N_2 adsorption and desorption isotherms were measured on an ASAP 2000 sorptometer at $-196 \text{ }^{\circ}\text{C}$. The sample was evacuated under 10^{-5} torr at $150 \text{ }^{\circ}\text{C}$ over night before the measurement. ^{29}Si NMR spectra were recorded on a Varian VXR-400S spectrometer with a 7-mm zirconia rotor, at a spin frequency of 4.2 kHz. TEM images were taken on a JEOL 100CX with a CeB_6 gun that was operating at an acceleration voltage of 120 kV. The specimen was loaded onto a holey carbon film that was supported on a copper grid by dipping the grid into a suspension of the solid sample in ethanol.

6.3 Results and Discussion

6.3.1 Materials Characterization

Figure 6.1 shows TEM images of MSU-C and MSU-H. MSU-C (top image) exhibits cavity type pores with an entrance pore diameter of $\sim 5.5 \text{ nm}$ and inter-pore distance of $\sim 13.7 \text{ nm}$. MSU-H exhibits MCM-41-like uni-dimensional channels with a diameter of about 4.0 nm . Selected area electron diffraction patterns (insets) confirms uni-dimensional hexagonal structure for MSU-H. However, the diffraction patterns for MSU-C is complicated. No explicit structure assignment could be achieved for this diffraction pattern. To assign this diffraction pattern more accurately, a series of patterns were generated using an image-processing program, NIH Image.

For the sake of comparison, the TEM image of MSU-C and its electron diffraction pattern are shown in Figure 6.2a and 6.2b, respectively. The optic diffraction pattern 2c obtained through Fourier-transformation of the image 2a shows two interdigitated

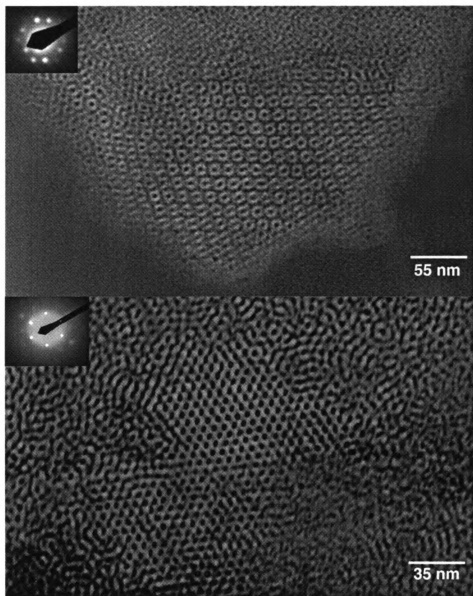


Figure 6.1. TEM images of calcined ($600\text{ }^{\circ}\text{C}$) mesoporous silica molecular sieves prepared in water using the alkyl polyethylene oxide type surfactant Brij 56 ($\text{C}_{16}\text{H}_{33}(\text{EO})_{10}\text{H}$) as the structure director and TEOS as the silicon source in the presence of CoCl_2 salt as the structure promoter under the same reaction conditions ($45\text{ }^{\circ}\text{C}$, 40 h reaction time) except that the surfactant to Co^{2+} ratios are different. The surfactant to silicon ratio was 1 to 24 for both samples, but the surfactant to metal ratio was 8.5 for the sample denoted as MSU-C (top photo) and 2.0 for the sample denoted as MSU-H (bottom photo). These images are provided as negatives for easier viewing of the pores as black spots. Pore to pore distance is constantly $\sim 13.7\text{ nm}$ through the specimen for MSU-C. The insets are the electron diffraction patterns for areas imaged.

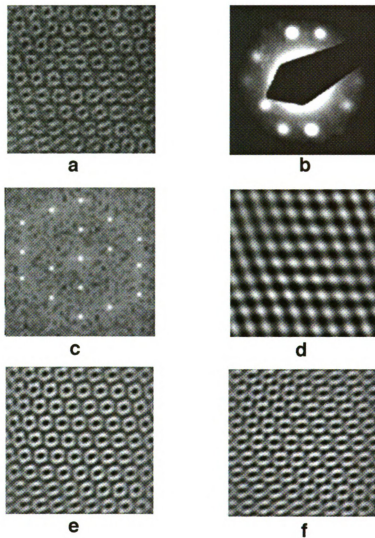


Figure 6.2. (a). Selected area TEM image of MSU-C; (b). Electron diffraction pattern of MSU-C; (c). Optic diffraction pattern obtained from the Fourier-transformation of image (a); (d). Image obtained by reverse-Fourier-transformation of the center tetragonal pattern in the optic diffraction pattern (c); (e). Image obtained from the total reverse-Fourier-transformation of optic diffraction pattern (c); (f). Image obtained from the reverse-Fourier-transformation of 7 diffraction spots selected from pattern (c) in such a way that these 7 spots resembling 7 spots in the real electron diffraction pattern (b).



Figure 6.3. A TEM segment for MSU-C showing a different orientation of the structure. The optic diffraction pattern (obtained by Fourier-transformation of arrow indicated area in the image) is attributable to both a (01-10)-3-d-hexagonal orientation and a (210) cubic orientation. These patterns are very similar to the diffraction pattern for meso-structured silica films with pores running orthogonal to the film surface, as reported by Brinker et al.¹⁷ Notably, the pore to pore distance is ~ 13.7 nm.

hexagonal patterns and a central tetragonal pattern. This is indicative of a faulted hybrid structure that combines both 3-dimensional hexagonal and cubic structural symmetries. Reverse Fourier-transformation of the center tetragonal pattern gave rise to image 2d, which is obviously different from original image 2a, but it shows the same inter-pore-distance of 13.7nm as for cavity pores. Reverse Fourier-transformation of the whole optic pattern 2c generated a nice cavity image 2e with cylindrical pores around the cavity-shaped pores. This image is more like the observed image as shown in 2a. Surprisingly, if we just reverse-fourier-transform 7 reflection spots chosen from the pattern in 2c in such a way that they are arranged similar to the observed electron diffraction pattern 2b, the resulted image (2f) clearly show 6 cylindrical pores in a distorted hexagon around the cavity-shaped pores. This is very much like the observed image 2a. Since only ideal 3-d hexagonal and cubic hybrids can generate diffraction pattern as shown in 2c, image 2f suggests that the obtained MSU-C is more like a distorted structural hybrid than a pure phase. These TEM images are similar to those of a meso-structured silica film reported by Brinker et al.¹⁷ It seems that the hybrid meso-structure is dynamically evolving under certain assembly conditions. Actually, we also observed a segment of our MSU-C sample by TEM (Figure 6.3), which shows cavity pores arranged in distorted cubic fashion. The optic diffraction pattern (from Fourier-transformation of the image section pointed by an arrow) is consistent with either a (210)-cubic orientation or a (01-10)-3-d-hexagonal orientation.

In addition to the hybrid ordering, there are disordered wormhole structural domains that co-exist with the well ordered structural domains within the same particle for both MSU-H and MSU-C. The disordered domains presumably resemble the ordered

counterparts in porous connectivity. Three-dimensional porous connectivity for the 3-d-hex-cubic structure and uni-dimensional porous conductivity for the hexagonal structure should be retained through the whole particle for MSU-C and MSU-H, respectively.

The X-ray powder diffraction patterns of MSU-H further confirms the hexagonal feature by showing (100), (110) and (200) reflections (Figure 6.4). The XRD pattern for MSU-C only exhibits a single reflection peak. The intense peak at low 2Θ angle exhibits a d-spacing of 6.1 nm. By assuming this peak to be a cubic (210) reflection, the calculated unit cell parameter is 13.7 nm which is consistent with the inter-pore-distance observed by TEM for this sample (c.f. Figure 6.1). Lacking higher order reflections in the X-ray, the diffraction pattern also is in consistent with the presence of disordered 3-d wormhole pores.

N_2 adsorption and desorption isotherms of MSU-C (Figure 6.5) indeed exhibit a characteristic hysteresis loop for necked cavity pores. In reasonable agreement with the TEM measurement, the effective pore size calculated using the Horvath-Kawazoe model is 6.0 and 4.3 nm for MSU-C and MSU-H, respectively. The pore size for MSU-C is about 2 times larger than the pore diameter of a MCM-48 (i.e. 2.5 nm)¹⁸ assembled using cetyltrimethyl ammonium bromide which has the same alkyl chain length as Brij 56. A high surface area of 1103 m²/g and a pore volume of 1.06 cc/g for MSU-C strongly suggest that the over-all quality of this silica molecular sieve is comparable to a bicontinuous cubic MCM-48.¹⁸ Similar to that of MCM-41, the isotherm for MSU-H showing no hysteresis loop is consistent with uni-dimensional hexagonal pores.

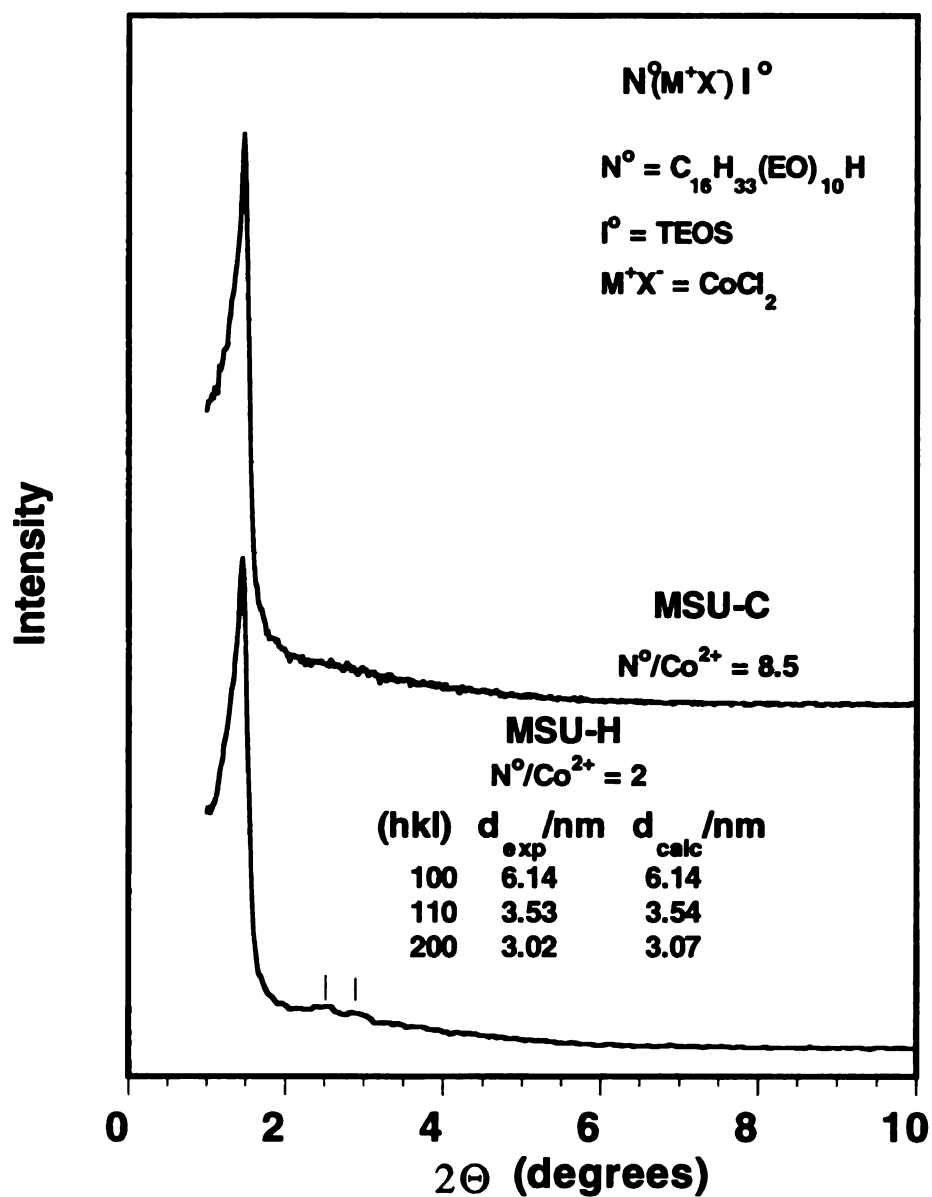


Figure 6.4. X-ray diffraction patterns for the calcined MSU-C and MSU-H samples that were used to obtain the TEM images shown in Figure 6.1. Both d-spacings, observed and calculated according to a uni-dimensional hexagonal phase for MSU-H, are provided for comparison.

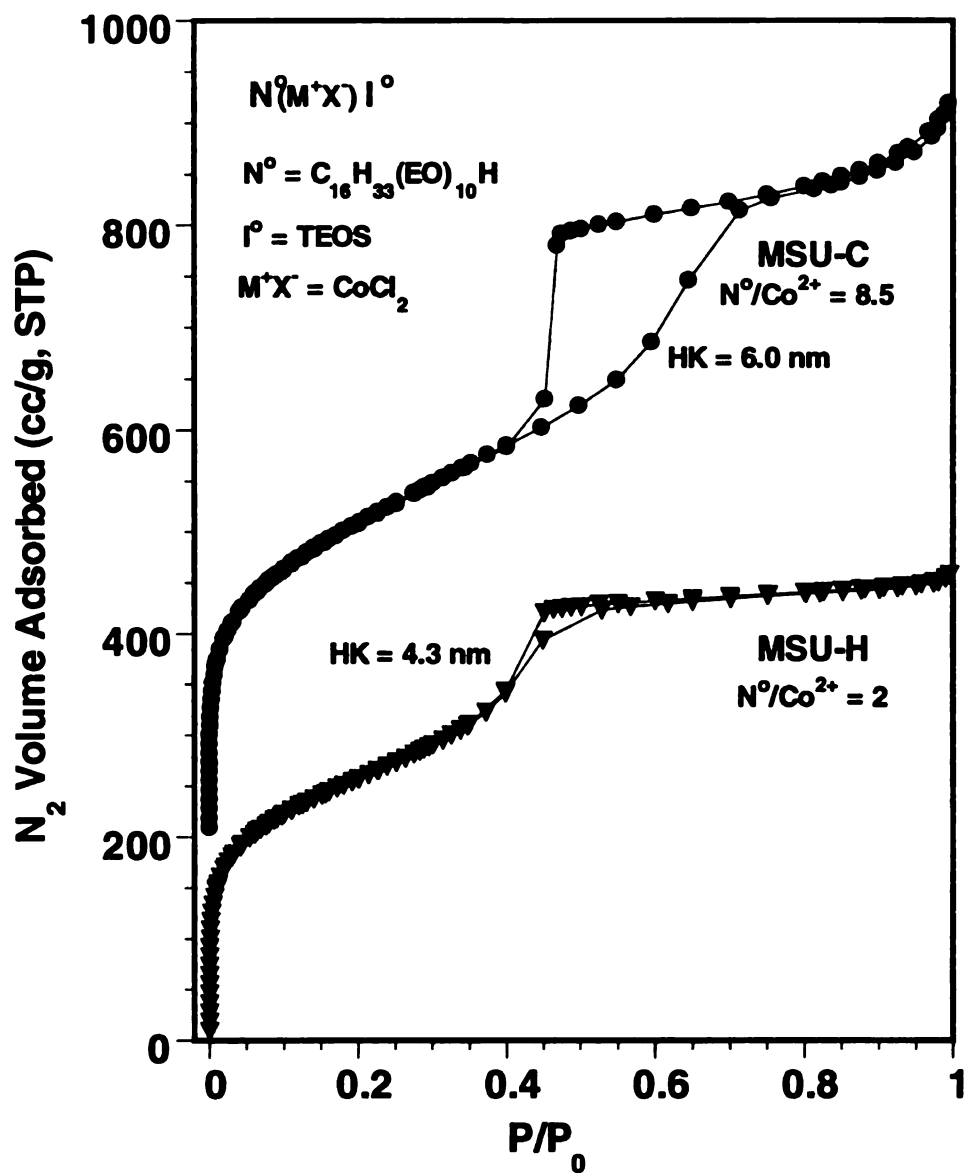


Figure 6.5. N_2 adsorption and desorption isotherms for calcined MSU-C and MSU-H. Pore necking hysteresis loop for MSU-C is indicated by the step at desorption branch, which is ~ 0.2 unit of relative pressure behind the adsorption branch. MSU-H exhibits almost identical adsorption and desorption branches signify the uniformity of uni-dimensional pores.

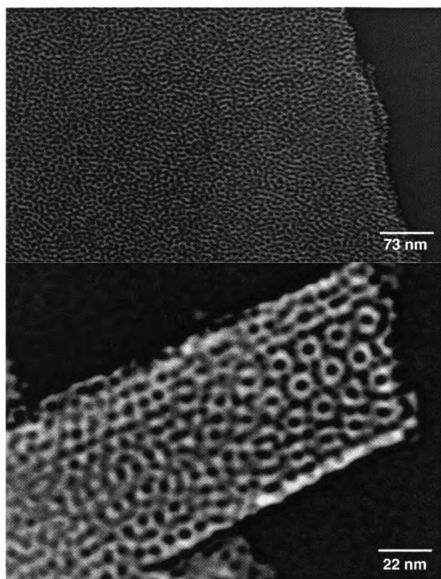


Figure 6.6. TEM images showing the wormhole (top) and 3-d-hex-cubic (lower) meso-structures assembled at Co^{2+} : Brij56 molar ratios of 1:13 and 1 : 8.5 respectively. TEOS was the silicon source and the silicon to surfactant ratio was 17 to 1.

In accordance with previously reported MSU-X silicas, only a wormhole structural motif was formed when little or no metal salt was used to assemble a mesostructure at a quite high surfactant to metal ratio of 17 (Figure 6.6, top). However, when this ratio was reduced to 8.5, a nice 3-d-hex-cubic structure was reproduced (Figure 6.6, bottom). The details of this marvelous image reveals a very high resemblance to a spherical cubic surfactant meso-phase in space group of $Im\bar{3}m$ showing cavity type linkages which has been observed previously.¹⁹

Figure 6.7 shows X-ray diffraction patterns of mesostructures formed at various surfactant to Li^+ ratios. Li^+ was chosen because there are many reports on Li^+ -polyethylene oxide complexes.^{20,21} Relatively well ordered hexagonal silica with higher 2θ angle reflections was formed at a $Li^+/Surf$ ratio of 1 to 2. Disordered silicas with single reflection were formed at $Li^+/Surf$ ratio of 0 or greater than 3. Interestingly, no cubic or hybrid meso-structure was obtained under any circumstances for Li^+ , K^+ and Na^+ . The N_2 adsorption and desorption isotherms (Figure 6.8) without hysteresis loops confirm the presence of uni-dimensional hexagonal pores for the silica with hexagonal reflections. In contrast, the N_2 isotherms for the disordered silicas that exhibit a single X-ray reflection show hysteresis loops indicating significant pore necking (cavity-shaped wormholes), and probably 3-dimensional pore connectivity.

As expected, the effect of polyethylene oxide complex formation with “3+” metal cations are different from those observed for complexes with “1+” and “2+” metal ions. The experiment performed for Fe^{3+} , Cr^{3+} and Rh^{3+} indeed showed very different results from those with Fe^{2+} and Co^{2+} . All of the silicas prepared in the presence of “3+” metal cations exhibit wormhole structure regardless of the surfactant to metal ratio. Also, their

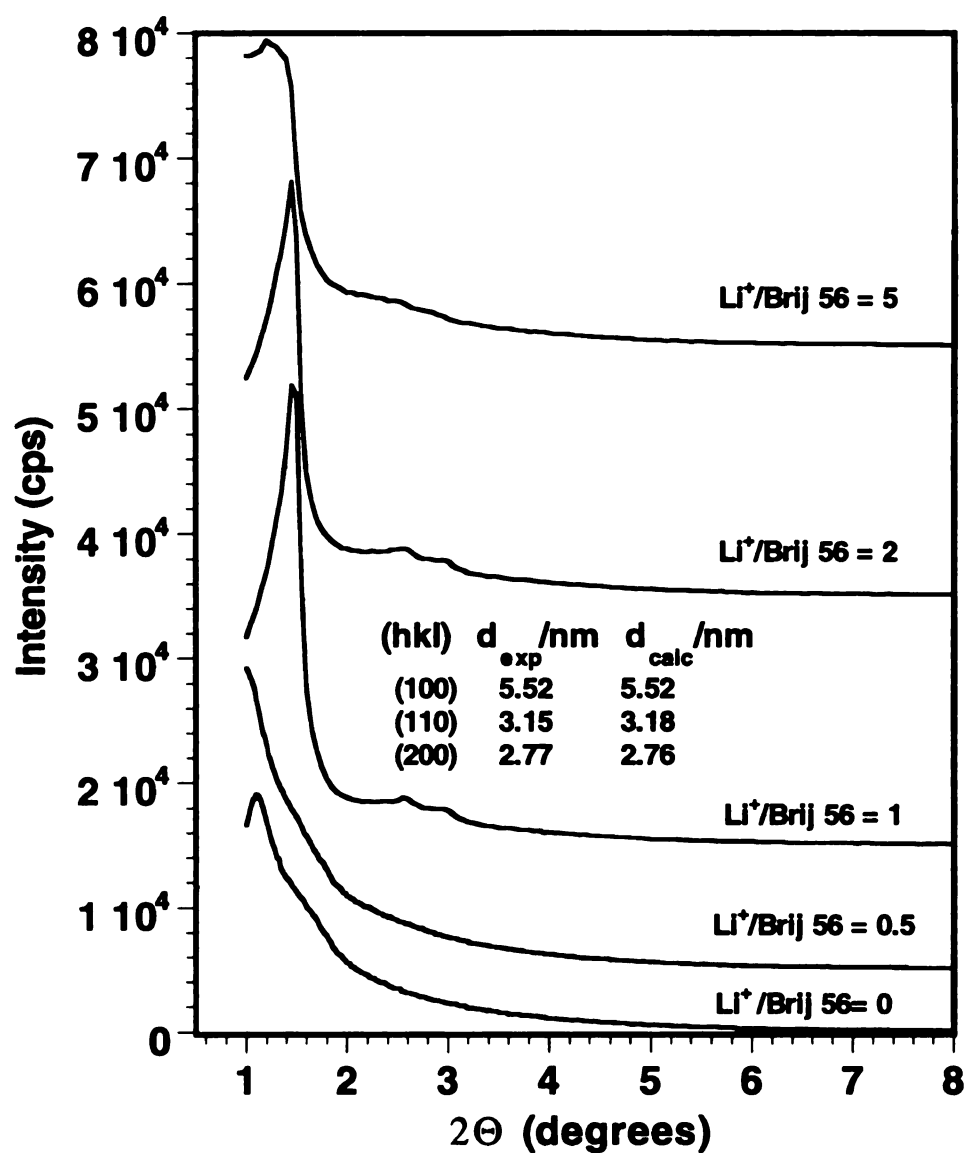


Figure 6.7. X-ray diffraction pattern of the calcined (600 °C) meso-structured silica molecular sieves assembled using Brij 56 as the structure director and TEOS as the silicon source at a silicon to surfactant ratio of 15 to 1 under the same reaction conditions (45 °C, 40 h reaction time), except that the surfactant to Li^+ ratio was varied as shown.

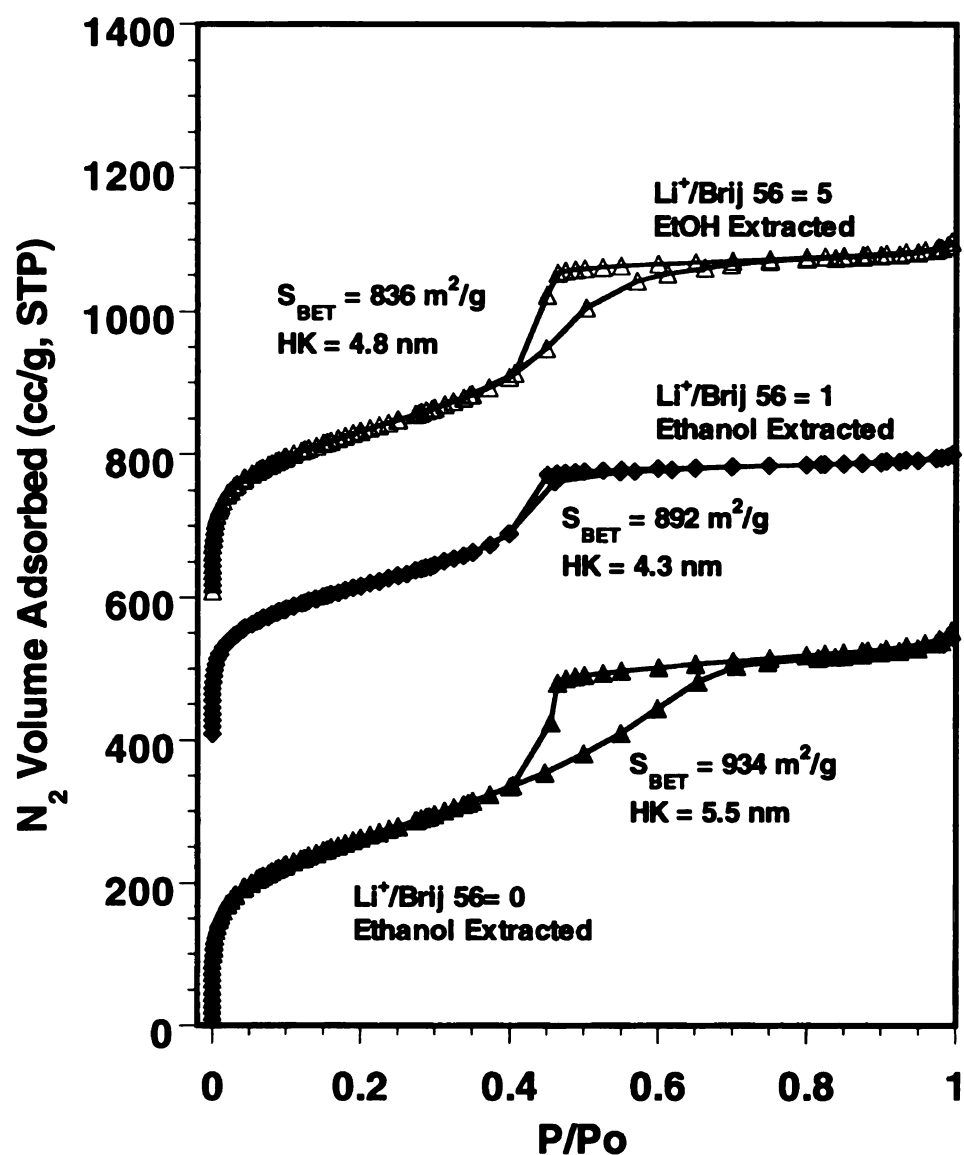


Figure 6.8. N_2 adsorption and desorption isotherms of as-made meso-structured silica molecular sieves as described in Figure 6.7. The surfactant in the mesopores was removed by ethanol extraction (i.e. refluxing in ethanol for 2 h) prior to the adsorption measurement. Again, the hexagonal silica exhibits no hysteresis loop, as expected for uniform uni-dimensional pores, whereas the wormhole silicas show pore necking hysteresis loops.

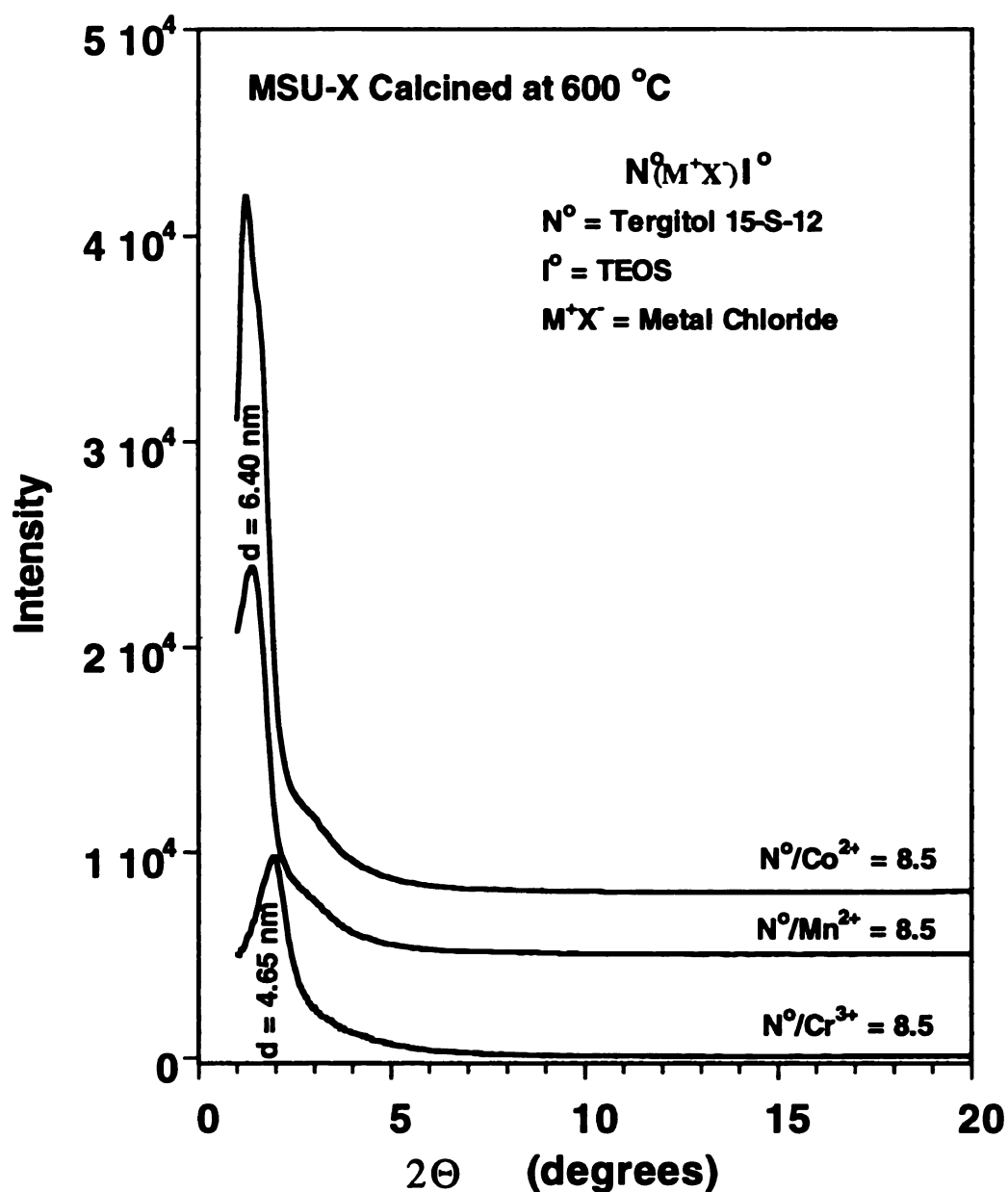


Figure 6.9. X-ray diffraction patterns for calcined (600 °C) mesoporous silica molecular sieves prepared using the mixed alkyl polyethylene oxide surfactant Tergitol 15-S-12 ($C_{12-16}H_{25-33}(EO)_{8-10}H$) as the structure director and TEOS as the silicon source under the same reaction conditions (45 °C, 40 h reaction time and a surfactant to metal cation ratio of approximately 24 to 1), but different cation valences for the promotional metal salts. The X-ray patterns show a decrease of d-spacing from 6.4 to 4.65 nm upon replacing Co^{2+} and Mn^{2+} with Cr^{3+} .

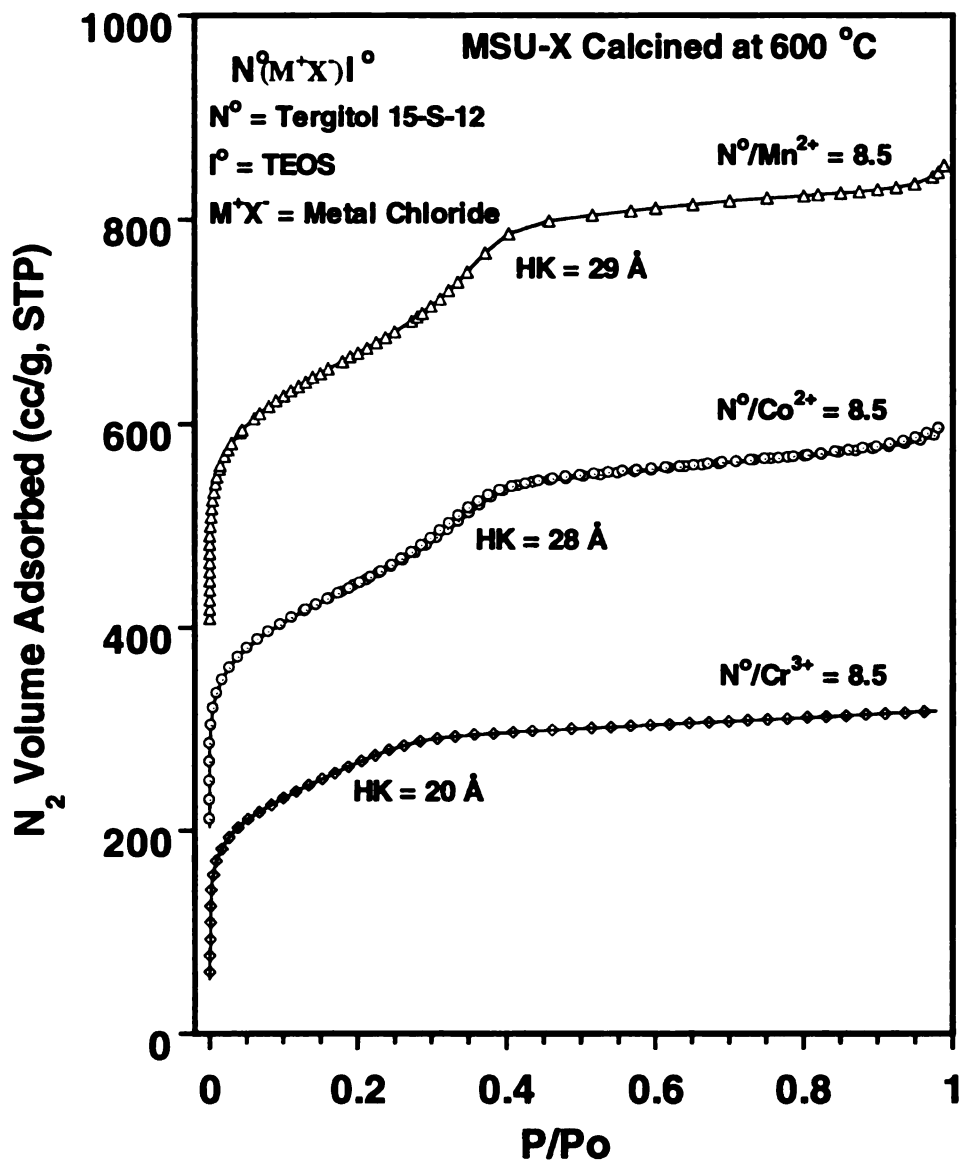


Figure 6.10. N_2 adsorption and desorption isotherms for mesoporous molecular sieves described in Figure 6.9. The Cr^{3+} mediated structure shows a pore size 2.0 nm in comparison with a pore size of 3.3 nm for the structures mediated by Co^{2+} and Mn^{2+} .

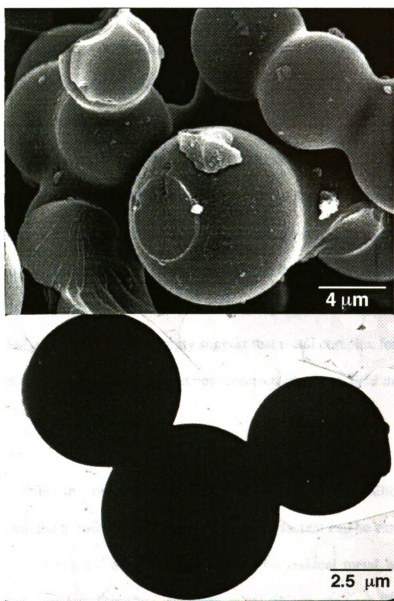


Figure 6.11. SEM (top) and TEM (bottom) images of mesoporous silica prepared using Tergitol 15-S-12 in the presence of Cr^{3+} as a structure promoter, showing micrometer sized intergrown spherical particles with flattened surfaces on the spheres.

pore size is at least 7 Å smaller than the silicas prepared in the presence of “1+” or “2+” metal cations. For example, the mesoporous silica formed in the presence of Cr³⁺ exhibits a much smaller d-spacing (i.e. 4.6 nm), in addition to smaller mesopores (~2.0 nm), in comparison with the materials promoted by Mn²⁺ and Co²⁺ (Figure 6.9 and 6.10). Actually, all of the mesoporous molecular sieves formed with Rh³⁺, Fe³⁺, and Cr³⁺ as promoters exhibit smaller pores (~2.0 nm). These same metal cations promote the formation of intergrown spherical particles, many with flatten surfaces (Figure 6.11). Notably, these mesoporous molecular sieves were synthesized under the same reaction conditions using Tergitol 15-S-12 (a mixture of C₁₂ to C₁₆ alkyl polyethylene oxide surfactant) as the structure director. The different pore structure and morphologies obtained for “3+” and “2+” cations strongly suggest that metal complex formation play an essential role in determining the phase and pore connectivity in the final meso-structure.

6.3.2 Discussion

The possibility that metal cations may be incorporated into the silica framework is excluded, because the transition metal along with the surfactant can be easily removed by ethanol extraction. Chemical analysis confirms that no residual metal is detectable for ethanol extracted samples. Therefore, first, the metal cations are very likely complexed by surfactant head groups. Second, the assembly process in the presence of metal salt maintains neutral H-bonding interfacial interactions that are weak enough to allow removal of surfactant by solvent extraction. Consequently, MSU-C and MSU-H are very likely assembled through a new metal complex mediated N⁰(M⁺X⁻)I⁰ mechanism.

Figure 6.12 shows ^{29}Si NMR spectrum for as-made MSU-H, a representative silica mesostructure prepared by a metal-salt mediated pathway. Typical ^{29}Si NMR spectra for HMS obtained by $\text{S}^{\circ}\text{T}^{\circ}$ assembly and two MCM-41 samples obtained by S^+T and $\text{S}^+\text{X}^+\text{T}^+$ pathways are also included for comparison. The spectra for both MSU-H and

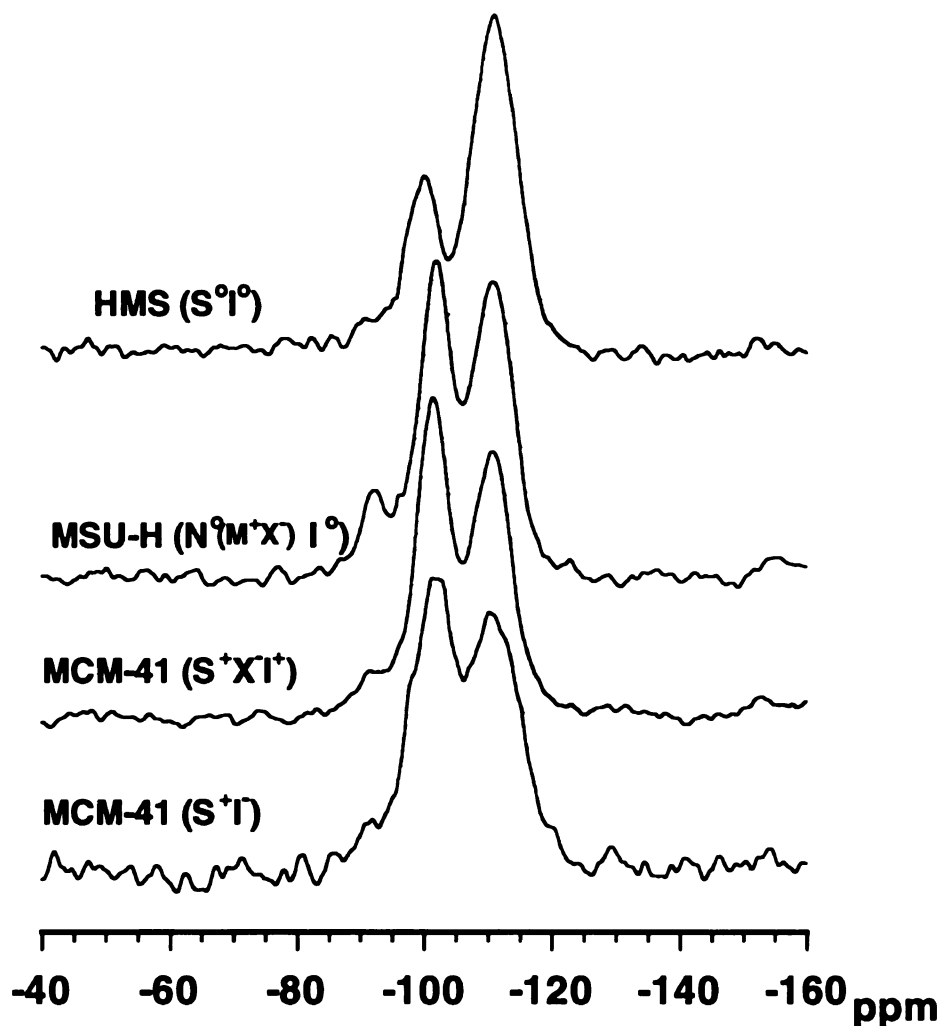
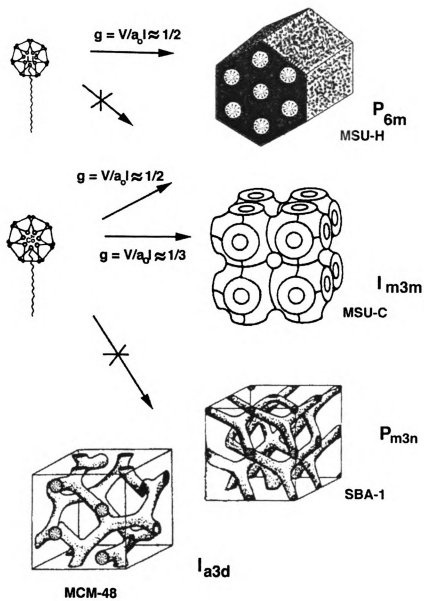


Figure 6.12. ^{29}Si NMR spectra for as-made HMS($\text{S}^{\circ}\text{T}^{\circ}$), MSU-H, MCM-41($\text{S}^+\text{X}^+\text{T}^+$) and MCM-41(S^+T). MSU-H was synthesized using Brij 56 as the structure director in the presence of CoCl_2 . HMS and MCM-41s were prepared as reported.^{9,24}



Scheme 1

MCM-41 ($S^+X^-T^+$) exhibit three well resolved resonance bands at -92, -100, and -110 ppm representing 2Q , 3Q and 4Q silicon cross-linking connectivity. Apparently, the spectrum for MSU-H is very much like the spectrum for MCM-41 formed through the counterion mediated $S^+X^-T^+$ pathway, but different from either HMS (S^0T^0) or MCM-41(S^+T). This resemblance strongly supports that MSU-H was assembled through a new counterion-mediated $N^0(M^+X^-)I^0$ pathway.

By forming complexes with metal cations, we incorporate longer ranged coulomb interactions into the surfactant micelles that cooperatively assemble with silica species to form either ordered uni-dimensional hexagonal or 3-d-hex-cubic structures. As illustrated in Scheme 1, small Li^+ likely form intra-molecular complex with polyethylene oxide head group in a helical conformation.¹³ The rod-like micelles formed from this surfactant-metal complex should be more rigid and easily aligned into a long-range hexagonal inorganic-organic mesophase with the help of interfacial coulomb interactions between the micelles and inorganic precursors. However, for larger Co^{2+} , which is well-known for adopting versatile coordination numbers, intra- or inter-surfactant molecular complexes are likely to form upon changing the surfactant to metal ratio (S/M). The formation of helical intra-molecular surfactant-metal complex may be more favorable as a result of positive charge repulsion at a lower S/M ratio (i.e. 1/1). As a consequence of competitive complexation, inter-molecular surfactant-metal complex may be more favorable at a higher S/M ratios (i.e. 8.5/1). In the case of inter-molecular complex formation, a larger effective head group area (a_0) would result a significant decrease in surfactant micelle packing parameter g to about 1/3 ($g = V/a_0l$). Therefore, in forming a thermodynamically

favoured product, spherical micelles (at low surfactant concentration, i.e. 0.027 M) could pack into a body centered Im3m cubic meso-structure.^{22,23} Noticeably, an ideal Im3m cubic structure is fundamentally different (c.f. Scheme 1) from bicontinuous Ia3d cubic MCM-48 and Pm3n cubic SBA-1 assembled using cetyltriethyl ammonium bromide via electrostatic S⁺X⁻T⁺ pathway.²³ In the case of intra-molecular complex formation, surfactant micelles with a relatively smaller head group area and larger micelle packing parameter g at about 1/2, rod-like surfactant-complex micelles may pack cooperatively into hexagonal meso-structures.

Meso-structure formation is known to be driven by non-polar and polar interactions in a medium with suitable polarity. Previous work has revealed that meso-structure phases depended on the lyotropic properties of the surfactant.³ Under the cooperative assembly conditions used in the present work, the initial surfactant concentration was far less than needed to form liquid crystal phases.²⁴ However, the surfactant molecules were eventually occluded in the framework pores as if they were in liquid crystal phases. The structure of the assembled product was primarily determined by the surfactant structure and reaction conditions.^{3,23} For example, cubic MCM-48 was synthesized at higher surfactant concentrations than hexagonal MCM-41.³ 3-d hexagonal SBA-2 was synthesized using double headed quaternary ammonium gemini surfactant rather than single headed surfactant.²⁵ Similarly, hexagonal, 3-d hexagonal and cubic mesoporous silicas were made using different polyethylene and polypropylene oxides block copolymer surfactants in the presence of concentrated mineral acids.²⁶ And worm-hole like mesoporous silicas were made using nonionic surfactant in neutral medium.⁶⁻⁸ Obviously, these strategies focused on changes of surfactant structure or surfactant

concentration or co-surfactant^{27,28} to change the packing parameter (g) and this effectively varied the phase of inorganic meso-structure. Our approach by changing the surfactant packing parameter through chemical complex formation between surfactant head group and metal cations that ultimately change the assembled meso-structure is new. Although the possibility of forming complexes between polyethylene oxide surfactant and transition metal salt has been demonstrated for the formation of meso-structured transition metal oxides,²⁹ the metal salt has not been found to be influential in affecting the structure of the final product. In our synthesis approach, however, the metal cations were used just as structure promoters rather than a framework precursor. In addition, none of the reported meso-structures prepared using nonionic surfactants have exhibited a TEM image similar to ours for the hybrid 3-d-hex-cubic structure.

6.4 Conclusion

Modification of polyethylene oxide surfactant head groups through complexation with transition and alkaline metal cations was carried out for silica mesoporous molecular sieve synthesis. The variation in meso-structure upon variation of the valence of metal cations was quite dramatic. Mesoporous silica molecular sieves with either ordered 3-d-hex-cubic or uni-dimensional hexagonal domains were synthesized by judicious choice of metal cations. The 3-d-hex-cubic structure was favored by “2+” metal cations such as Co^{2+} , Ni^{2+} and Mn^{2+} . The uni-dimensional hexagonal structure were favored by both “1+” and “2+” metal cations such as Li^+ , Co^{2+} , Cu^{2+} , Zn^{2+} , and Fe^{2+} . Wormhole structure were favored by “3+” metal cations such as Cr^{3+} , Fe^{3+} and Rh^{3+} . It seems that the 3-d-hex-cubic structure prefers a lower interfacial charge density with a surfactant to metal ratio in the range of 4 to 12. The uni-dimensional hexagonal structure favors a relatively

higher interfacial charge density with a lower surfactant to metal ratio in the range of 1 to 3. The wormhole structure favors a zero or low interfacial charge density with a quite high surfactant to metal ratio, above 17.

6.5 Reference

1. Kresge, C.T.; Leonowicz, M.E.; Roth, W.J.; Vartuli, J.C.; Beck, J.S. *Nature* **1992**, *359*, 710.
2. Beck, J.S.; Vartuli, J.C.; Roth, W.J.; Leonowicz, M.E.; Kresge, C.T.; Schmitt, K.D.; Chu, C. T.-W.; Olson, D.H.; Sheppard, E.W. *J. Am. Chem. Soc.* **1992**, *114*, 10834.
3. Vartuli, J.C.; Schitt, K.D.; Kresge, C.T.; Roth, W.J.; Leonowicz, M.E.; McCullen, S.B.; Hellring, S.D.; Beck, J.S.; Schlenker, J.L; Olson, D.H.; Sheppard, E.W. *Chem. Mater.* **1994**, *6*, 2317.
4. Attard, G.S.; Glyde, J.C.; Goltner, C.G. *Nature* **1995**, *378*, 366.
5. Zhao, D.; Feng, J.; Huo, Q.; Melosh, N.; Fredrickson, G.H.; Chmelka, B.F.; Stucky, G.D. *Science* **1998**, *279*, 548.
6. Bagshaw, S.A.; Prouzet, E.; Pinnavaia, T.J. *Science* **1995**, *269*, 1242.
7. a. Bagshaw, S.A.; Pinnavaia, T.J. *Angew. Chem.* **1996**, *108*, 1108; *Angew. Chem. Int. Ed. Engl.* **1996**, *35*, 1106. b. Zhang, W.; Pinnavaia, T.J. *Chem. Commun.* **1998**, 1185.
8. Prouzet, E.; Pinnavaia, T.J. *Angew. Chem.* **1997**, *109*, 533; *Angew. Chem. Int. Ed. Engl.* **1997**, *36*, 516.
9. Tanev, P.T.; Pinnavaia, T.J. *Science* **1995**, *267*, 865.
10. Zhang, W.; Pauly, T.R.; Pinnavaia, T.J. *Chem. Mater.* **1997**, *9*, 2491.
11. Behrens, P. *Angew. Chem. Int. Ed. Engl.* **1996**, *35*, 515.
12. Zhang, W. "Ph.D. Dissertation in Michigan State University", Chapter 1, **1999**.
13. Armand, M.B. in *Polymer Electrolyte Review - 1* (Eds.: J.R. MacCallum, C.A. Vincent), Elsevier Applied Science, London and New York, **1987**, p 1.

14. Jr. Bailey, F.E.; Koleske, J.V. in *Alkylene Oxides and Their Polymers*, Marcel Dekker, New York, **1990**.
15. McBreen, J.M.; Yang, X.-Q.; Lee, H.-S. *J. Electrochem. Soc.* **1996**, *143*, 3198.
16. Israelachvili, J.N.; Mitchell, D.J.; Ninham, B.W. *J. Chem. Soc., Faraday Trans. 2* **1976**, *72*, 1525.
17. Lu, Y.; Ganguli, R.; Drewien, C.A.; Anderson, M.T.; Brinker, C.J.; Gong, W.; Guo, Y.; Soyey, H.; Dunn, B.; Huang, M.H.; Zink, J.I. *Nature* **1997**, *389*, 364.
18. Zhang, w.; Pinnavaia, T.J. *Catal. Lett.* **1996**, *38*, 261.
19. Ober, C.K.; Wegner, G. *Adv. Mater.* **1997**, *9*, 17.
20. Striebel, K.A.; Wen, S.J.; Ghantous, D.I. *J. Electrochem. Soc.* **1997**, *144*, 1680.
21. Tajitsu, Y. *J. Mater. Sci.* **1996**, *31*, 2081.
22. Hyde, S.T. *Pure & Appl. Chem.* **1992**, *64*, 1617.
23. Huo, Q.; Margolese, D.I.; Stucky, G.D. *Chem. Mater.* **1996**, *8*, 1147.
24. Huo, Q.; Margolese, D. I.; Ciesla, U.; Demuth, D. G.; Feng, P.; Gier, T. E.; Sieger, P.; Firouzi, A.; Chmelka, B. F.; Schüth, F.; Stucky, G. D. *Chem. Mater.* **1994**, *6*, 1176.
25. Huo, Q.; Leon, R.; Petroff, P.M.; Stucky, G.D. *Science* **1995**, *268*, 1324.
26. Zhao, D.; Huo, Q.; Feng, J.; Chmelka, B.F.; Stucky, G.D. *J. Am. Chem. Soc.* **1998**, *120*, 6024.
27. Gallis, K.W.; Landry, C.C. *Chem. Mater.* **1997**, *9*, 2035.
28. Chen, H.; Huang, L.; Li, Q. *Chem. Mater.* **1997**, *9*, 2685.
29. Yang, P.; Zhao, D.; Margolese, D.I.; Chmelka, B.F.; Stucky, G.D. *Nature*, **1998**, *396*, 152.